



**University of
Nottingham**

UK | CHINA | MALAYSIA

Design and Development of a Wearable Device for Real-Time Detection and Monitoring of Obstructive Sleep Apnoea

Thesis submitted to the University of Nottingham for the degree of Master of Science

Sep 2025

Satya Sai Manikanta Varma Penmatsa
20714521

Supervisor: Dr. Ricardo Correia

Department of Electrical and Electronic Engineering
Faculty of Engineering
University of Nottingham

Table of Contents

Chapter 1 - Introduction.....	1
1.1 Project Context.....	1
1.2 Background Review.....	4
1.3 Case for Project.....	8
1.4 Project Proposal	10
Chapter 2 – System Overview, Design, and Development.....	16
2.1 Target Sleep Events and Scoring Standards.....	16
2.2 Signal Type Selection and Design Considerations	20
2.3 Component Selection and System Integration.....	26
2.4 Event Detection Algorithms.....	37
2.5 Events to Signal features mapping.....	50
2.6 Microcontroller Process Outline	52
2.7 Wearable Design	53
Chapter 3 – System Validation and Results	55
3.1 Pre-Validation	55
3.2 Test Setup.....	57
3.3 Results.....	59
3.4 Specification Validation	65
Chapter 4 – Conclusion.....	68
4.1 Future Work	69
4.2 Societal Fit	70
4.3 Reflection.....	71
Reference List	73

Chapter 1 - Introduction

Wonder why everything feels so much better after a well-rested sleep, your thoughts are clearer, and your mood is lighter. Our waking life's quality is anchored in the hours we spend asleep. Sleep is a vital biological process supporting many essential activities in the human body, not only rest. From memory consolidation, detoxification and hormone control to tissue healing, sleep is the internal maintenance cycle of the body [1]. Though we spend almost a third of our life asleep, which is about 25 years over the average lifespan, we sometimes forget its actual importance.

However, millions of people often without realising it have sleep disorders that interfere with this essential function. Obstructive Sleep Apnoea (OSA) is the most common respiratory disorder affecting sleep quality and continuity, characterised repeated interruptions in breathing during sleep. These interruptions interfere with the natural progression of the sleep cycle, depriving the body of the restorative processes necessary for maintaining both physical health and cognitive function. If left untreated, OSA has been linked to a wide range of health consequences, including an elevated risk of cardiovascular disease, impaired cognitive performance, reduced quality of life, cancer, depression, and an increased likelihood of motor vehicle accidents [2]. However, a lot of cases go undiagnosed for years because of the discomfort, expense, and inconvenience associated with standard sleep studies carried out in clinical settings.

The ability to monitor sleep at home offers a convincing substitute for conventional clinical approaches as the demand for easily available and proactive healthcare keeps growing. Conventional diagnostic tools for sleep apnoea can be intrusive and may themselves interfere with natural sleep patterns. In-home and remote monitoring systems offer promising solutions, not only for detecting disorders like OSA but helps people to keep track of their sleep health, also for alerting individuals in real-time and enabling timely intervention in severe cases.

This thesis focuses on the detection and notification of sleep apnoea, with an emphasis on minimising discomfort to preserve sleep quality. By exploring how unintrusive methods can reliably detect sleep disturbances and notify users in real time, this work aims to advance early awareness and promote a more seamless integration of sleep health monitoring into everyday life. It investigates how a combination of remote monitoring technologies such as chest straps for movement, heart rate tracking, SpO₂, temperature sensors, and microphones for acoustic analysis can be integrated into a user-friendly system that provides real-time alerts and allows users to view, save, and analyse their sleep data, thereby enabling effective yet unobtrusive detection of sleep-related disruptions.

1.1 Project Context

Motivation Global Prevalence and Public Health Concern

Obstructive sleep apnoea is a growing global health concern with almost 1 billion adults aged 30–69 years estimated to be affected globally, 425 million of which suffer from moderate to severe forms of the condition [3], OSA is underdiagnosed and untreated despite its frequency, even in highly developed countries, mostly due to the limits of traditional clinical diagnostic techniques such as in-lab polysomnography (PSG). If left untreated, OSA can have serious consequences, including increased healthcare expenses, cognitive impairment, cardiovascular problems, and reduced quality of life. One of the first studies Benjafield and colleagues [3] to fully estimate the worldwide prevalence of this condition, this emphasises the pressing need of easily available and scalable diagnostic techniques. Early identification with non-intrusive,

home-based devices is increasingly regarded as a critical step in enhancing sleep health at the public level, as OSA often develops without obvious symptoms. The importance and limits of the gold standard, in-lab polysomnography (PSG), must be examined first to understand the present diagnostic situation.

Limitations of Polysomnography (PSG)

The gold standard for diagnosing obstructive sleep apnoea (OSA) is polysomnography (PSG), which records several physiological signals simultaneously, such as oxygen saturation, respiratory effort, airflow, EEG, EOG, EMG, and ECG, to provide comprehensive data [4], [5]. However, PSG has several drawbacks that make it less practical for routine use or extensive screening, even with its high diagnostic accuracy. The process necessitates spending the night in a specialised sleep lab, where the strange surroundings and several wired electrodes and sensors as shown in figure.1 and might disrupt normal sleep cycles and cause the "first-night effect" [4], [5]. According to the patient, this may make the procedure unpleasant and even stressful, which could lower the calibre and precision of the information gathered [4].

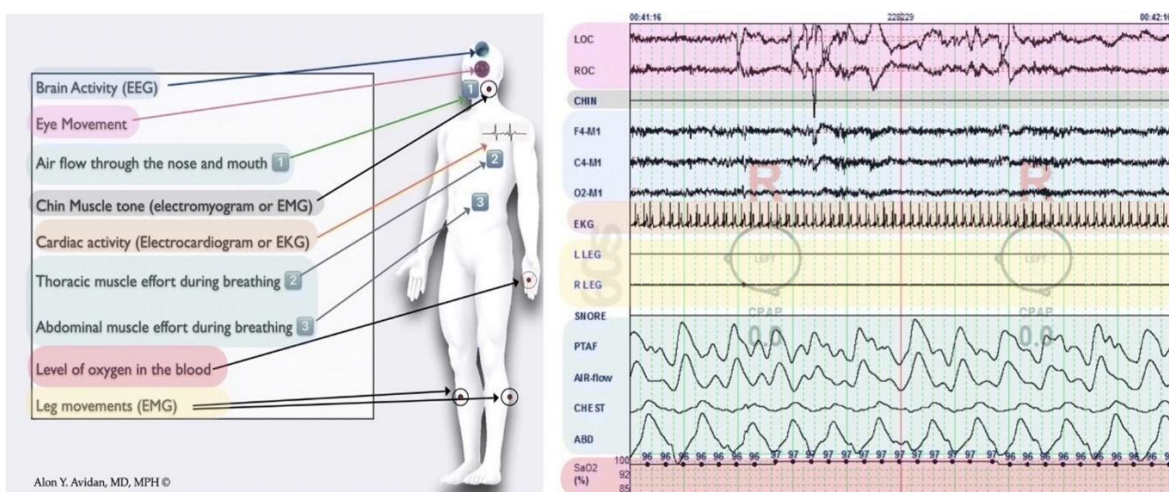


Figure 1. Illustration of Polysomnographic Channels and Physiological Signals Monitored During Sleep. The right panel shows corresponding waveform outputs. Adapted from "Clinician-Focused Overview and Developments in Polysomnography" by Alon Y. Avidan, MD, MPH [5].

Cost, Access, and Resource Burden

Beyond discomfort, PSG presents substantial financial and accessibility challenges. A complete in-lab diagnostic and titration PSG, for example, can cost up to CAD 908 per patient in Canada if it is done over two separate nights [6]. Depending on the diagnostic route used, even single-night split investigations might cost anywhere from CAD 384 to CAD 660 [6], these prices were reported in 2014. Healthcare systems and patients are both financially burdened by these costs, particularly in areas with lengthy waitlists or little public funding. Wait times for PSG can range from a few weeks to more than six months in publicly financed systems like those in UK, Canada and Australia, especially for patients with milder symptoms [6], [7]. In addition to delaying diagnosis and treatment, these delays may deter patients from seeking care altogether, which eventually leads to worse results.

The burden on sleep clinics and healthcare professionals is further increased by issues such as the requirement for specialists, the scarcity of labs, and the high cost of equipment [5], [7]. Because of this, PSG is still necessary in the high-risk patients, but its drawbacks underscore the urgent need for more accessible, scalable, and patient-friendly options. This has led to a rise in interest in home-based sleep diagnostics, which seek to reproduce the clinical insights of PSG in a more convenient and economical way.

Current Scalable Alternatives

Actigraphy is another popular technique for tracking sleep-wake patterns over long periods of time. It is especially helpful in detecting insufficient sleep syndrome, and circadian rhythm sleep-wake disorder. This wearable gadget uses limb movement (wrist or ankle) to assess important sleep metrics, like sleep latency (SL), and total sleep time (TST) [8]. A systematic study by the American Academy of Sleep Medicine found that actigraphy performs quite well compared to PSG, particularly for TST and SL, but often overestimates TST and underestimates SL when compared to sleep logs [8]. In situations where clinical investigations may not be practical, actigraphy provides a low-cost, non-invasive alternative that is perfect for long term monitoring, even though it lacks the detail of PSG, such as breathing data or sleep stages.

With the ability to track sleep in the convenience at home, consumer sleep technologies (CSTs) and Home Sleep Apnoea Tests (HSATs) have grown in popularity in recent years and present an attractive substitute for clinical sleep evaluations. These wearables employ accelerometers, temperature sensors, and photoplethysmography (PPG) and other parameters to predict sleep patterns and categorise sleep stages. Although accuracy in recognising sleep stages is still inconsistent validation studies have demonstrated that several of the newest commercial devices, like the Fitbit Alta HR, Sleepscore Max and EarlySense Live (CSTs), operate on par with or better than traditional actigraphy in detecting sleep and wake states [9]. A comprehensive comparison between PSG and seven consumer sleep-tracking devices revealed a poorer specificity (0.18–0.54), especially on nights when sleep was disturbed, but a high sleep detection sensitivity (≥ 0.93) [9]. Both CSTs and HSATs are significant milestones towards increasing access to sleep diagnostics, with each weighing trade-offs between comfort, accuracy, and clinical utility.

Growing Adoption and Caution in Clinical Use

Public interest in CSTs is growing quickly despite these drawbacks. About 25% of American adults reported using a wearable gadget or a smartphone app to measure their sleep as of 2019, and nearly 30% of them owned one. A broader societal shift towards proactive personal health management is reflected in the forecast that the global wearable sleep tracking industry will reach \$7 billion by 2026 [9]. Experts warn against relying too much on unregulated tools in clinical practice due to data privacy concerns and proprietary algorithms that are not independently validated [10].

Societal and Economic Impact

Obstructive sleep apnoea (OSA) is a common but often neglected health problem with major societal and economic consequences. Nearly 29.4 million adults in the United States alone suffer from it, but up to 80% go untreated, which results in an estimated \$149.6 billion in yearly expenses linked to higher accident risk, decreased employment productivity, and increased healthcare use. Among those diagnosed, treatment modalities include CPAP, oral appliances, and surgery as shown in figure 2. Lifestyle interventions are assumed for all diagnosed individuals [11]. Beyond economics, untreated OSA raises the risk of cardiovascular events. Men with severe, untreated OSA are approximately three times as likely to have a fatal heart attack or stroke than those without the disorder [12]. Despite the risks, low awareness and discomfort with standard diagnostics postpone OSA detection. But with telemedicine 38 times more popular than it was before the pandemic [13], there is an opportunity to make sleep monitoring more widely available, making OSA a public health priority.

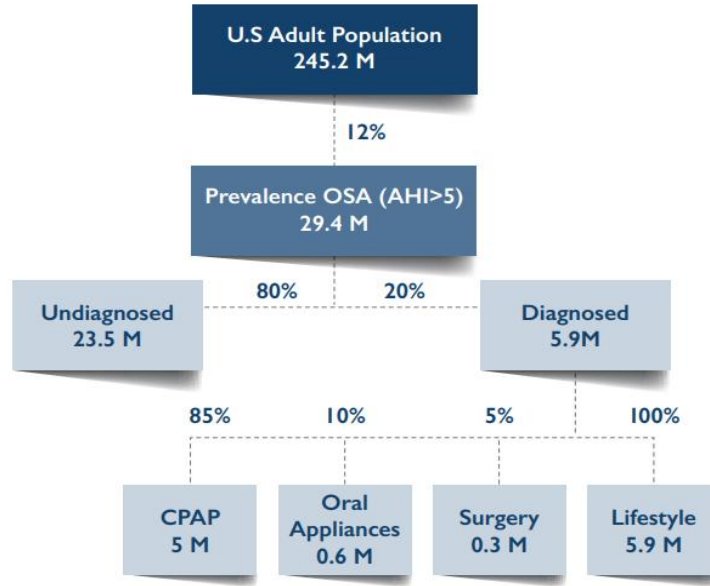


Figure 2 Frost & Sullivan estimates Prevalence, Diagnosis and Treatment of OSA in the United States [11].

Engineering Challenges

The limits of polysomnography (PSG) pose several difficulties in the development of practical sleep apnoea (SA) detection systems. To overcome these challenges, designers must give top priority to a few essential qualities in their systems, including cost-effectiveness, minimal disruption to the user's natural sleep schedule, ease of use, and reliable detection and prediction ability. Ideally, the system should allow for unrestricted movement by utilising wireless data transmission rather than wired connections. It must also provide high diagnostic accuracy while staying small, portable, and energy-efficient [14], making it suited for use in long term home-based applications.

1.2 Background Review

Overview of Sleep Apnoea

Sleep apnoea is a common sleep disorder characterised by frequent breathing pauses during sleep, resulting in interrupted sleep and low oxygen levels. Obstructive sleep apnoea (OSA) and central sleep apnoea (CSA) are the two primary types.

- OSA is characterised by a physical blockage of the upper airway despite persistent effort to breathe, and it is frequently associated with obesity and weak airway muscles.
- CSA, which is frequently observed in patients with heart failure or those using opioids, happens when the brain is unable to communicate with the breathing muscles.

Despite having different causes, both kinds can result in low oxygen levels, poor sleep, and a higher chance of cardiovascular problems such as high blood pressure, heart failure, and stroke [15].

Polysomnography (PSG) is the gold standard for detecting Obstructive Sleep Apnoea (OSA). However, its disadvantages are well known, discomfort from electrodes and cabling, the first-night effect, need for specialist supervision, and expensive [16]. PSG assessments are closely related to the Apnoea-Hypopnea Index (AHI), which counts the number of apnoeic (in total cessation) and hypopnea (partial blocking) breathing events per hour of sleep. OSA is categorised into the following severity levels based on AHI values [17]:

OSA Severity	AHI (events/hour)
Normal	< 5
Mild	5 to < 15
Moderate	15 to < 30
Severe	≥ 30

Table 1. Classification of Obstructive Sleep Apnoea (OSA) Severity Based on Apnoea-Hypopnea Index (AHI).

Limitations of AHI and the Need for New Diagnostics

Although AHI offers a consistent method for categorising OSA, it ignores the disorder's larger physiological effects, which includes metabolic effects, sleep disturbances, and cardiovascular effects. Research indicates that AHI has a weak correlation with patient-reported outcomes and long-term health hazards, especially in patients with complicated medical illnesses or unusual symptom profiles [16]. These drawbacks have sparked interest in more straightforward, diagnostic options. At the same time, home sleep apnoea tests (HSATs) and wearable technology are aimed at maintaining diagnostic accuracy while enhancing use and comfort. Recent research has investigated a variety of physiological signals, including SpO₂, airflow, acceleration, body temperature and heart-related measures to create small, non-invasive detection devices with simple hardware architecture that can be used for remote monitoring or at home.

Review of Wearable and Consumer-Grade Technologies

Numerous sensors have been used in wearable technology to track physiological indicators linked to sleep apnoea. Chyad et al. [18] present the Sleep Apnoea System, with 2 units, one for measurement and other for monitoring as shown in figure 3. It uses a chest-mounted flex sensor to track breathing movements and a MAX30101 pulse oximeter to detect heart rate (HR) and peripheral oxygen saturation (SpO₂) using photoplethysmography (PPG). The device processes data using an Arduino Uno microcontroller and wirelessly transmits to a PC via Bluetooth, ensuring real-time monitoring in a lightweight, portable design. Validation against the Alice PDx HSAT device showed 99.94% agreement for HR and SpO₂, supported by Bland-Altman plots (95.4% HR and 95.6% SpO₂ within $\pm 2\sigma$ limits). However, the small sample size (six participants) and potential sensor movement artefacts limit its generalisability, with future work focussing on device miniaturisation and broader testing.

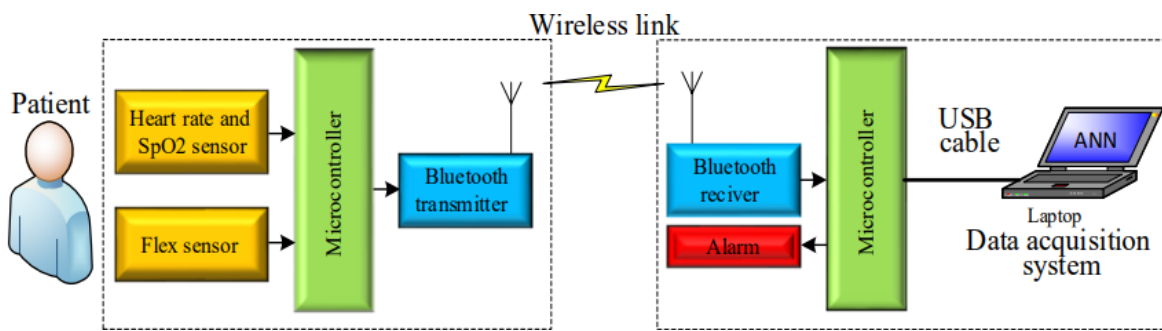


Figure 3 Illustration of the Sleep Apnoea Detection and Prediction System Proposed by Chyad et al. [18].

Tiwari et al. [19] introduced a flexible wearable 3D-printed device that combines force-sensitive sensors, heart rate, and SpO₂ to automatically detect sleep apnoea. The prototype comprises a MAX30102 pulse oximeter for measuring SpO₂ and heart rate via photoplethysmography (PPG), as well as a custom force-sensitive resistor made using spray-

coated silver ink (97.6% Ag) on a glass epoxy substrate and verified by COMSOL simulations for a linear pressure-voltage response in the 0–40 N range. The device's lightweight, ergonomic 3D-printed housing implies patient comfort and portability, and its ESP32 microcontroller processes data and wirelessly sends it to a web interface for real-time monitoring. To detect apnoea events, the software uses signal processing algorithms to extract respiratory rate, filter noise, and synchronise SpO₂ and force sensor data. High conductivity and uniform silver deposition were confirmed by SEM (scanning electron microscopy) as part of the sensor validation process, and COMSOL models matched experimental findings under applied stress. Future studies will focus on human trials, environmental durability, and further size reduction.

Alhamad et al. [20] developed the Sleep Apnoea Detecting and Monitoring System, which detects breathing patterns using a nasal temperature sensor and an Arduino Mega2560 processor. It has a vibration motor on a bracelet to wake patients during extreme occurrences, a Wi-Fi shield to transmit data to ThingSpeak, and a GSM shield for SMS notifications. The mobile application enables users to save and share data with healthcare providers. Ranjitha BS's system [21] uses a thermistor to measure breathing rate through exhaled air temperature and an LM35 sensor for body temperature, processed by an Arduino Uno. It includes a SIM900 GSM module for SMS alerts, an LCD for status display, and a vibration motor for patient alerts. Functionality testing confirmed operational success; Further testing is necessary because detection validation was not included in any of these studies.

Sangeetha et al. [22] present a smart mattress system that track sleep posture and identify obstructive sleep apnoea. It had a respiratory microphone sensor near the nose to measure breathing rate and pressure sensors set up in a 2x3 grid beneath the mattress to identify sleeping postures (left, right, and centre). A Real-Time Clock (RTC) timestamps the sensor readings. Arduino UNO processes sensor data, interfaces with an LCD for real-time display, and sounds a buzzer for abnormal conditions like low or high breathing rates. Data is sent to a web application for remote monitoring, that shows graphs of respiration rates and sleep positions over time. The system uses pressure thresholds to identify sleep posture and uses the microphone to calculate breathing rate. If the breathing rate is less than 12 breaths per minute or more than 20 breaths per minute, apnoea is flagged. Tested on five participants, the results demonstrated an accuracy of 84.80% with standard training.

The Sleepcare Kit and S-Pillow (SKP), a self-x based closed loop wearable IoT system, was developed by Jeon et al. [23] to detect and treat sleep apnoea in real time without the need for external servers or human assistance. It continuously measures heart rate, acceleration, SpO₂, and respiration with sensors and their positions as shown in figure 4. To correct posture and stop apnoea episodes, the S-Pillow senses the patient's head position and inflates internal air pads. With just wearable technology and no external infrastructure, SKP carries out self-setup, self-monitoring, self-analysis, self-control, self-adaptation, and self-recovery. This enables the system to detect sleep, track breathing, spot anomalies, and take appropriate action on its own. The Risky Abnormal Breathing Detection Algorithm (RADA) scores the severity and continuity of events to determine whether intervention is necessary. It does this by analysing breathing, SpO₂, and acceleration signals to separate actual sleep apnoea events from false alarms caused by motion or minor disruptions. While Long-Term Closed Loop Control accumulates successful previous reactions and applies them in advance under comparable future circumstances, Short-Term Closed Loop Control dynamically modifies the air-pads during apnoea episodes. According to evaluation results, SKP considerably decreased control frequency and apnoea length when compared to existing approaches, while RADA achieved 97.4% accuracy in identifying dangerous breathing occurrences.

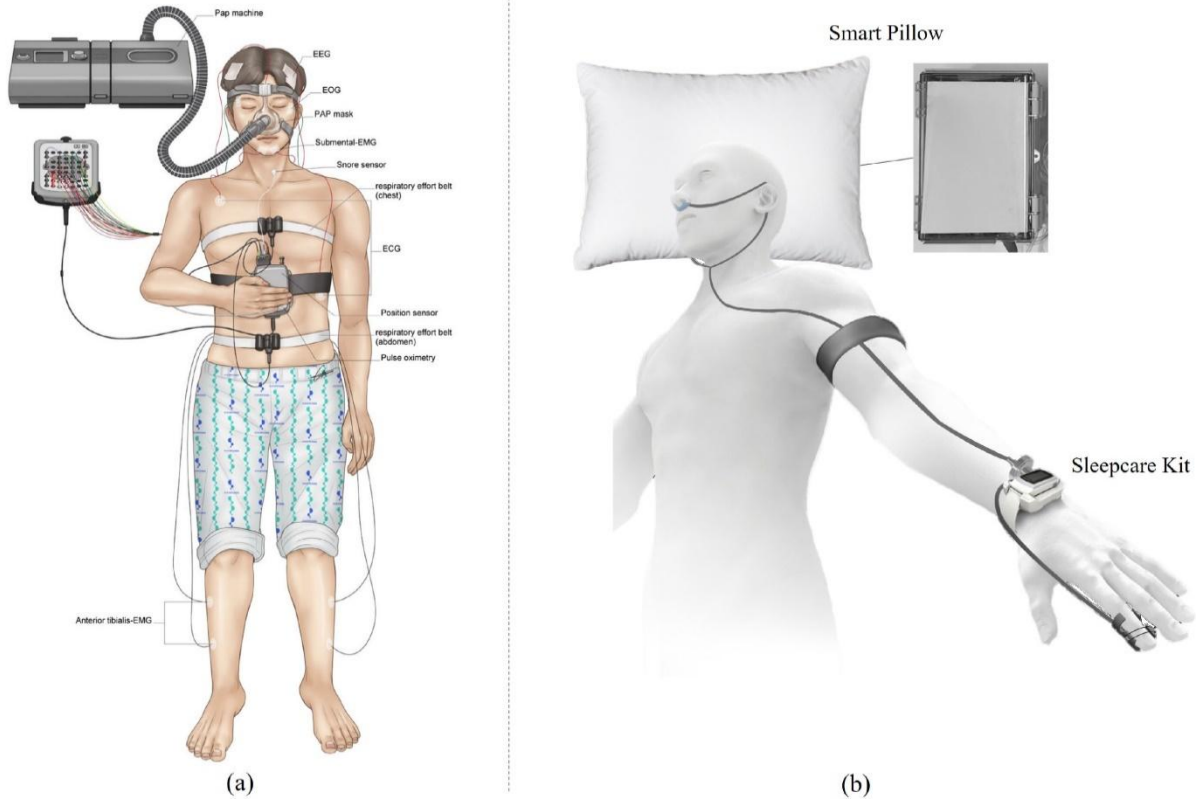


Figure 4 (a) Conventional in-lab polysomnography (PSG) setup with continuous positive airway pressure (CPAP) therapy, (b) Proposed wearable Internet of Things (IoT)-based Sleepcare Kit and Smart Pillow system by Jeon et al..

A wearable, real-time sleep apnoea detection system was developed by Yüzer et al. [24]. To identify breathing patterns, the device uses a MEMS-based ADXL345 accelerometer that is put on the diaphragm. An Arduino Mega 2560 microprocessor processes the data and activates a vibration motor on a bracelet to notify patients when apnoea episodes occur. Additionally, it logs laying positions, apnoea timestamps, and breathing signals onto an SD card for subsequent review. The device uses accelerometer data to recognise four different lying positions and diagnoses central sleep apnoea (CSA) by detecting decreases in diaphragm movement. It then provides adjustable vibration alerts in real time to restart breathing. Ten patients with different levels of apnoea were utilised for validation; all apnoea events were identified, alarms effectively induced breathing to resume, and the longest period without breathing was 42 seconds. Further research is necessary to address potential vibration adverse effects like sleep disruption.

Commercial wearable devices like Apple and Samsung smartwatches are increasingly focusing on integrating sleep apnoea risk detection into consumer health monitoring. The Sleep Apnoea Notification Feature [25] on the Apple Watch Series 9 and Ultra 2 detects moderate to severe sleep apnoea ($AHI \geq 15$) by analysing breathing abnormalities during sleep. To estimate breathing patterns and identify brief disruptions, the system uses triaxial accelerometer data. It combines nightly measurements over a 30-day period (with at least 10 nights of data) and notifies users if 50% or more of the nights exhibit elevated disturbances. Training on 11,156 nights of data from 4,702 persons with varying ages, sexes, BMIs, races, and ethnicities was necessary for development and validation. In-lab PSG and home HSAT recordings assessed in accordance with AASM standards (using the 4% desaturation rule for hypopneas) supplied ground truth. With 1,499 participants, clinical validation revealed a sensitivity of 66.3% and a specificity of 98.5%. The specificity was high throughout normal and mild apnoea levels, but the sensitivity was higher for severe cases (89.1%) than moderate instances (43.4%). The

feature is not designed for users who have already been diagnosed with sleep apnoea, and it focusses on risk alerting rather than diagnosis, recommending users to consult their healthcare professionals if indicated. The reviewed literature point to lack of comprehensive validation, and few studies focus primarily on single isolated physiological parameters like SpO₂ or accelerometer. A comparative summary of studies is presented below in table-2.

Study	Signals Used	System Components and Methods	Validation Method	Limitations
Chyad et al. [18]	HR, SpO ₂ , Chest movements	Arduino Uno, Bluetooth, MAX30101, Flex sensor	Compared to Philips Alice PDx HSAT for HR and SpO ₂ measurements	Small sample (6), sensor artifacts
Tiwari et al. [19]	HR, SpO ₂ , Chest movements	MAX30101, force-sensitive sensor (silver ink on epoxy), ESP32, Web interface, COMSOL simulations	Simulation	No clinical trials, durability issues
Alhamad et al. [20]	Breathing rate from Nasal temperature	Nasal temperature sensor, Arduino Mega2560, GSM, Wi-Fi, ThingSpeak, vibration motor	Functionality testing (detection, alerts)	No clinical validation
Ranjitha BS [21]	Breathing rate from Nasal temperature, Body temperature	LM35(Body temperature), Thermistor, Arduino Uno, SIM900 GSM, LCD, vibration motor	Functionality testing (detection, alerts)	No clinical validation, false alarm risk
Sangeetha et al. [22]	Pressure sensors, Microphone	Arduino UNO, RTC, Microphone, Pressure sensor, Shallow CNN,	Tested on 5 participants.	Small sample (5)
Jeon et al. [23]	Respiration, SpO ₂ , HR, acceleration	Smart Pillow, RADA algorithm, autonomous operation	RADA algorithm	Needs broader testing, posture refinement
Yüzer et al. [24]	ADXL345 accelerometer	Arduino Mega 2560, SD card, vibration motor	Tested on 10 patients; all events detected	Vibration side effects, needs hospital trials
Apple [25]	Triaxial accelerometer (Apple Watch)	Health app, 30-day data analysis	Clinical study (1,499 participants) vs. PSG/HSAT	Not for diagnosed users, notification-focused

Table 2. Summary of literature review of Wearable-Based Sleep Apnoea Detection Systems using different physiological signals and detection architectures.

1.3 Case for Project

Drawing back from the project context, OSA affects nearly 1 billion adults globally, yet 80% of cases remain undiagnosed. Undiagnosed OSA contributes to annual economic losses exceeding hundreds of billion dollars in healthcare costs, accidents, and reduced productivity. Conventional diagnostic methods like polysomnography (PSG) are intrusive, expensive, and

not suitable for routine and widespread screening. This project aims to bridge these gaps by combining clinical-grade sensing with user-centric design, empowering individuals to proactively manage sleep health.

Uniqueness and Approach

The project's uniqueness lies in the combination of multiple, complementary physiological signals without stressing users with invasive setups.

- Multiple operating modes tailored for screening and monitoring sleep apnoea.
- Novel adaptive algorithms for real-time data processing and alerting.
- Prioritisation of low-cost components, minimal setup time, and home usability while striving for performance comparable to research-grade solutions.
- A mobile interface for viewing data and sharing it with clinicians will make the system suitable for long-term, at-home use.
- Minimise discomfort, disruptions to natural sleep patterns by using a non-invasive, wireless design.
- Facilitating the early detection of severe apnoea episodes by real-time alerts.

The developed framework will emphasise clear algorithm design, precise signal acquisition, and robust artefact removal methods to ensure that the collected physiological data is accurate, meaningful, and clinically valuable. It lays a strong foundation for future AI or machine learning extensions. This focus directly addresses a major gap in the current field, where poor signal quality can reduce classifier performance, accurate and clean waveforms are essential for extracting meaningful patterns necessary for reliable diagnosis [26]. Moreover, many existing deep learning models for sleep apnoea detection were trained and validated on limited public datasets, such as PhysioNet [26], restricting their generalisability. Broader validation across diverse settings including clinical and home environments, as well as varied demographics is needed to improve robustness. Without this, models trained on small or biased datasets risk overfitting and failing in real-world applications.

Feasibility and Constraints

The project is ambitious yet realistic, focusing on developing a functional proof-of-concept rather than a fully commercialised product.

Constraints include:

- Limited resources and time for clinical validation.
- Challenges in achieving PSG-level accuracy with non-intrusive sensors.

However, feasibility is supported by:

- The use of validated sensor technologies (e.g., MAX30101 validated by Chyad et al. [18]).
- Focus on real-time functionality to tackle engineering challenges such as multi sensor data integration, processing efficiency, and detection accuracy.

The project also plans to validate core functionalities under controlled conditions, using phantoms, motion simulators and test detection algorithms with manually scored data.

Impact and Value

The project promises significant scientific and commercial impact:

- Scientific Advancement: By developing a reliable, non-intrusive diagnostic tool, this work contributes to sleep medicine, enabling researchers to study OSA in natural settings with greater fidelity than PSG allows.
- Commercial Potential: With the wearable sleep tracking market projected to reach \$7 billion by 2026 [9], this cost-effective system targets a growing consumer base, offering a viable alternative to both PSG and less accurate CSTs.
- Public Health Benefits: Early detection facilitated by this system could reduce the societal burden of untreated OSA, lowering healthcare costs and mitigating risks like cardiovascular events and accidents [11], [12].

1.4 Project Proposal

Aims and Objectives

The aim of this project is to design and develop a compact, reliable, and non-intrusive wearable device for the continuous monitoring and real-time detection of obstructive sleep apnoea (OSA) in adults that overcomes the drawbacks of conventional polysomnography (PSG), suitable for long-term use in both home and hospital environments. By prototyping a multi-sensor system including SpO₂, heart rate, inertial measurement unit (IMU) for chest movements, microphone for snoring detection, and temperature sensors for airflow analysis, the project seeks to deliver accurate apnoea event detection and user notifications while prioritising comfort, with minimal setup and preserving natural sleep patterns. With a scalable, affordable solution, this project seeks to give people the ability to proactively manage their sleep health and a tool for early sleep apnoea screening.

To realise this aim, the project outlines the following objectives:

- Design a User-Centric Wearable System: Develop a lightweight and compact wearable integrating SpO₂, Heart rate, IMU, temperature and audio sensors, optimised for adult use with minimal sleep disruption.
- Implement Dual Operating Modes:
 - Mode 1 (Comprehensive Screening Mode): Operate all sensors (SpO₂, Heart rate, IMU, microphone, and temperature) continuously to enable detailed multi-parameter data collection. This mode is designed for early-stage screening, trend identification, and clinical correlation.
 - Mode 2 (Targeted Monitoring Mode): Prioritise IMU-driven SpO₂ activation to optimise battery life while maintaining reliable detection of apnoea events. This is intended for individuals already diagnosed with sleep apnoea, focusing on tracking the frequency and severity of apnoea episodes during long-term home monitoring.
- Develop Robust Firmware and Algorithms: Create embedded software for real-time sensor data integration, apnoea event detection artifact elimination, data logging, and alerts, targeting decent detection accuracy and minimal false positives.
- Enable Comprehensive Data Logging: Record SpO₂, chest movement, posture, temperature, and audio data with timestamps for post-analysis and correlation studies.
- Develop a Real-Time Dashboard: Create a user-friendly mobile interface for near real-time visualisation of sensor data, posture, and apnoea alerts.
- Facilitate Data Export: Enable users and clinicians to export data in CSV format for offline review or advanced analysis.

- Eliminate Movement Artifacts: Implement signal processing techniques to filter out noise and movement artifacts from SpO₂ and IMU data, during natural sleep movements.
- Validate System Performance: Test the device using phantoms (SpO₂ and motion simulators) and detection accuracy of algorithms with sleep apnoea datasets.

Specifications

The project will adhere to the following specifications, each aligned with the aim and objectives:

1. Wearable Design and Comfort:
 - Requirement: Device must be compact, minimal wiring, lightweight (within 300g), and comfortable for overnight wear with adjustable straps.
 - Testing and Success Criteria: Verify weight meet the requirements, ensure straps maintain sensor placement during simulated overnight wear using motion simulation.
 - Justification: Lightweight and compact design ensures stability and usability, mitigates the "first-night effect" seen in PSG [5].
2. Dual Operating Modes:
 - Requirement: Mode 1 logs all sensor data at 1 Hz; Mode 2 logs IMU data at 1 Hz and activates SpO₂ only on IMU-detected events.
 - Testing and Success Criteria: Verify detection accuracy in both modes against marked events from datasets.
 - Justification: Balances power efficiency and performance for extended monitoring.
3. Real-Time Detection and Alerts:
 - Requirement: Detect apnoea events with >80% accuracy and <10% false positives; alert within 10 seconds.
 - Testing and Success Criteria: Use sleep apnoea datasets with labelled events to evaluate algorithm detection performance; measure alert latency during simulated events.
 - Justification: Ensures timely and accurate detection in a controlled environment.
4. Artifact Elimination:
 - Requirement: Reduce movement artifacts in SpO₂ and IMU data by using signal filtering.
 - Testing and Success Criteria: Introduce controlled artifacts via motion phantoms and measure signal-to-noise ratio improvement post-filtering and processing.
 - Justification: Clean signals are critical for accurate apnoea detection.
5. Data Logging and Export:
 - Requirement: Log all sensor data with timestamps; export in CSV format. Data logging interval adjustable by user.
 - Testing and Success Criteria: Sample data export and analysis on PC.
 - Justification: Facilitates post-test analysis and validation.
6. User Interface:
 - Requirement: Real-time dashboard displaying sensor data, and alerts. Clear event markers for detected apnoea incidents.
 - Testing and Success Criteria: Confirm dashboard updates within 10 seconds of data acquisition; verify event markers, alert notifications trigger correctly during simulated events.
 - Justification: Ensures monitoring functionality during testing.

7. Power Consumption:

- Requirement: Battery life of ≥ 7 hours in Mode 2 and ≥ 4 hours in Mode 2 (2000 mAh battery).
- Testing and Success Criteria: Measure and compare runtime in both modes under identical phantom testing conditions.
- Justification: Validates power efficiency for overnight use.

8. Validation:

- Requirement: Achieve $>80\%$ apnoea event detection accuracy against datasets.
- Testing and Success Criteria: Evaluate detection algorithms against labelled apnoea events in datasets.
- Justification: Ensures the device's performance is rigorously assessed using controlled and standardised methods.

Risks and Mitigations

The table 3 provides a concise summary of key risks, their implications, and how to address them, all tailored to the project's objectives and timeline.

Risk	Severity	Likelihood	Potential Impact	Mitigation Strategy
Battery Life Below Specification	High	Medium	Device may not support overnight monitoring.	Optimise the algorithm, try different sampling rates for each sensor instead of 1Hz for all sensors. Test and calibrate power consumption during early stages.
Movement Artifacts Impact Data Quality	High	Medium	False positives or undetected apnoea events; reduces detection accuracy.	Implement, test and tune artifact rejection filters (e.g., moving average, Kalman filters). Validate during motion simulation tests.
Inexperienced with mobile/web dev	Medium	Medium	Real-time visualisation feature could be delayed.	Prioritise simple web-based dashboard initially. Optionally upgrade to mobile app if time permits.
Phantom and Dataset Availability for Validation	Medium	Low	Validation delayed or limited if phantoms/datasets are not accessible.	Pre-identify open datasets and other alternatives (programmable motor setups for chest motion).
Multi-sensor data handling issues	Medium	Medium	Could delay firmware development and compromise device reliability.	Early prototyping with individual sensor modules. Integration tests to ensure progressive compatibility.

Hardware Component Failure or Delivery Delays	High	Low	Project timeline impacted if critical components are unavailable or defective.	Order components early; maintain backup of critical parts.
Signal Processing Complexity	Medium	Medium	Risk of scope expansion and delays in achieving clean signals.	Focus on basic, validated filtering techniques first (bandpass, thresholding). Add complexity only if time permits.
Lack of Clinical validation	Medium	High	Limits the final validation accuracy.	Clarify from the beginning that the project scope focuses on proof-of-concept performance under simulated and dataset-based validation, not clinical trials.
Low Detection Accuracy	High	Medium	Algorithm accuracy may drop below >80%, compromises core functionality and validation.	Test multiple signal processing methods, refine and adapt algorithms.
Prototype Discomfort During Use	High	Medium	Device too bulky, misalignment of sensors. User may feel irritated during sleep, can cause data loss.	Try to evenly distribute the weight. Use lightweight materials, adjustable elastic straps, rounded edges on casing. Adjust design iteratively.

Table 3. Identification, severity, likelihood, and mitigation strategies for risks associated with the development of the sleep apnoea detection wearable device.

Milestones and Deliverables

Below are the milestones and deliverables designed to meet the project's aims, objectives, and specifications.

Milestone 1: Design and Component Selection (Week 2)

- Deliverable:
 - Bill of materials (BOM) with costs and suppliers, Order the components.
 - Start working on algorithms and decision logic.
- Selecting components (e.g., sensors, processor) ensuring the wearable meets specifications like weight (<300g).

Milestone 2: Prototype Assembly and Basic Firmware (Week 4)

- Deliverable:
 - Assembled hardware prototype with sensors (SpO₂, IMU, microphone, temperature) and processor.
 - Basic firmware for sensor data acquisition and logging.

- Create an initial prototype to test hardware integration and basic data collection functionality.

Milestone 3: Dual Mode Implementation (Week 6)

- Deliverable:
 - Firmware update enabling Mode 1 (comprehensive logging) and Mode 2 (IMU-triggered SpO₂ activation).
 - Initial Power consumption measurements for both modes.

Milestone 4: Apnoea Detection Algorithm and Artifact Elimination (Week 8)

- Deliverable:
 - Apnoea detection algorithm integrated into firmware.
 - Signal processing code for artifact reduction.
- Develop the core detection algorithm, reducing artifacts by >90% for reliable performance.

Milestone 5: Real-Time Dashboard and Alerts (Week 9)

- Deliverable:
 - Functional mobile or web dashboard displaying real-time sensor data and apnoea alerts.
 - Final Power consumption measurements for both modes.
- Provides a user interface for real-time monitoring, with alerts triggering and dashboards updated within 10 seconds of an apnoea event.

Milestone 6: Validation with Phantoms and Datasets (Week 10)

- Deliverable:
 - Validation with accuracy metrics from phantom tests and dataset evaluations.
- Validates system performance, targeting >80% detection accuracy.

Milestone 7: Final Integration and Testing (Week 11)

- Deliverable:
 - Fully integrated device with all features (dual modes, detection, dashboard, data export).
- Combine all components and features, tested for overnight functionality and usability.

Milestone 8: Project Completion and Documentation (Week 12)

- Deliverable:
 - Final project report (design, development, testing, validation results).
 - Presentation of findings and demonstration.

Conclude the project with thesis and a demonstration of the system.

Time plan

The Gantt chart below in figure 5 depicts the project's detailed timeline. The plan divides the project into clearly defined tasks and subtasks, each with their own start and end dates, durations, and dependencies. Major milestones and supervision meetings are scheduled at critical stages to review progress, address risks early, and stay on track with project objectives. The timeline also includes some buffer periods for risk mitigation and iterative improvements.

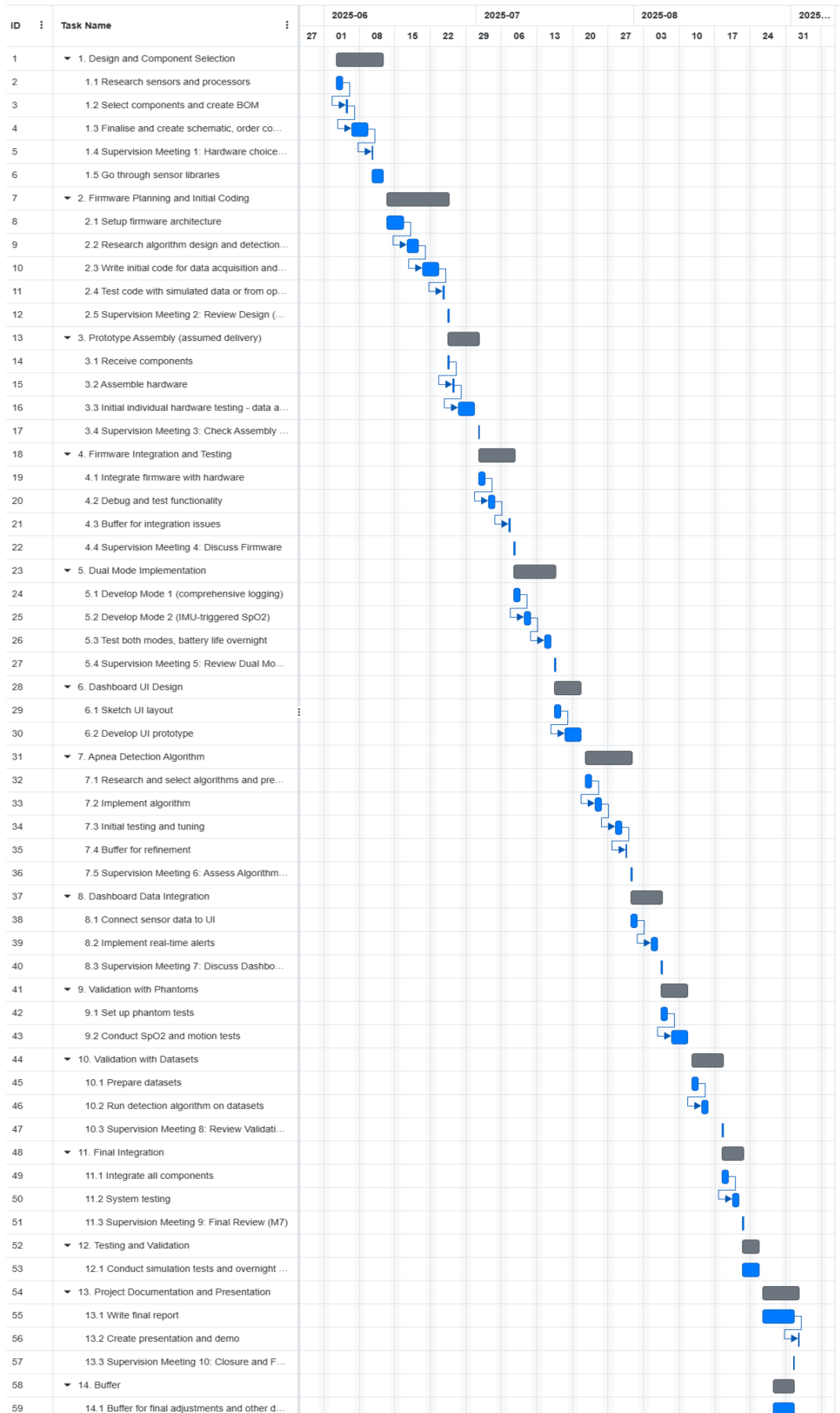


Fig 5: Project Timeline Gantt Chart

Chapter 2 – System Overview, Design, and Development

2.1 Target Sleep Events and Scoring Standards

Sleep Events of Interest

While classifying respiratory events as obstructive or central apnoea may appear straightforward, it can be difficult in practice. Physiologically, obstruction is indicated when airflow is reduced despite maintained respiratory effort, or when increased effort is observed for an existing amount of airflow indicating airway narrowing or blockage. On the other hand, the lack of both airflow and respiratory effort characterises central apnoea. A hypopnea as shown in figure 6 is a partial reduction in airflow during sleep that leads to a drop in oxygen saturation and/or an arousal from sleep. In sleep studies, it can be difficult to accurately differentiate between obstructive and central hypopnea subtypes [27]. Hypopneas are scored as obstructive by default, due to the difficulty in distinguishing between types.

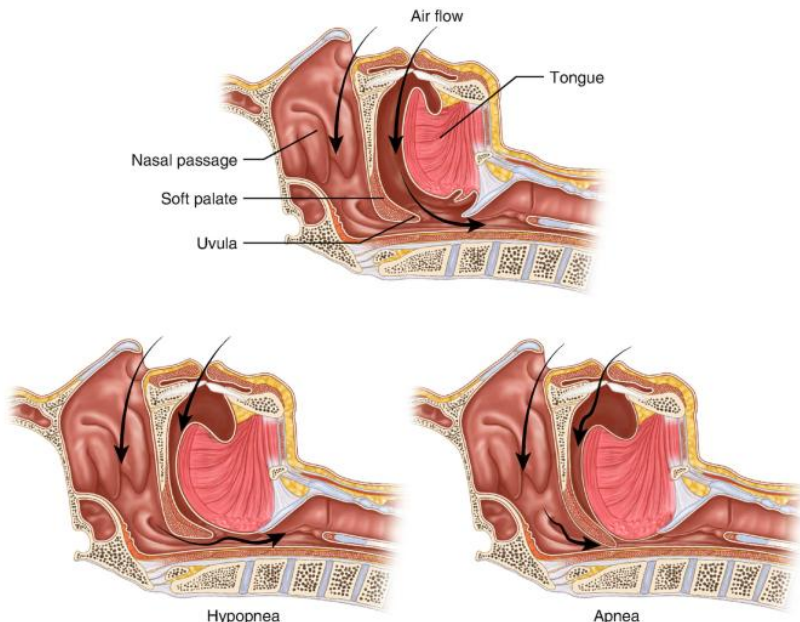


Figure 6: Illustration of Normal Breathing, Hypopnea, and Obstructive Apnoea This diagram shows the upper airway anatomy during sleep, comparing normal airflow (top), partial obstruction resulting in hypopnea (bottom left), and complete airway collapse causing obstructive apnoea (bottom right). In hypopnea, airflow is partially reduced due to narrowing of the airway, whereas in apnoea, the airway is fully blocked, stopping airflow entirely [28].

Given the complexities and ambiguities involved in distinguishing hypopnea subtypes, and considering the primary goal of this thesis, the wearable system developed in this thesis makes no attempt to classify hypopneas as obstructive or central. Instead, it focusses on detecting both apnoea and hypopnea events, categorising only apnoea events based on signal characteristics, and counting hypopnea events. These detections then can be used to calculate the Apnoea-Hypopnea Index (AHI), a clinically accepted measure for determining the severity of sleep apnoea (refer table-1) that avoids the added complexity of subtype differentiation for hypopneas.

To classify respiratory events from the PSG data, if there are thoracoabdominal (Thorax/Chest, abdomen) movements and steadily rising pressure swings in oesophageal pressure, and

concludes with arousal and breathing resumes [27], it can be confirmed as obstructive apnoea as shown in figure 7.

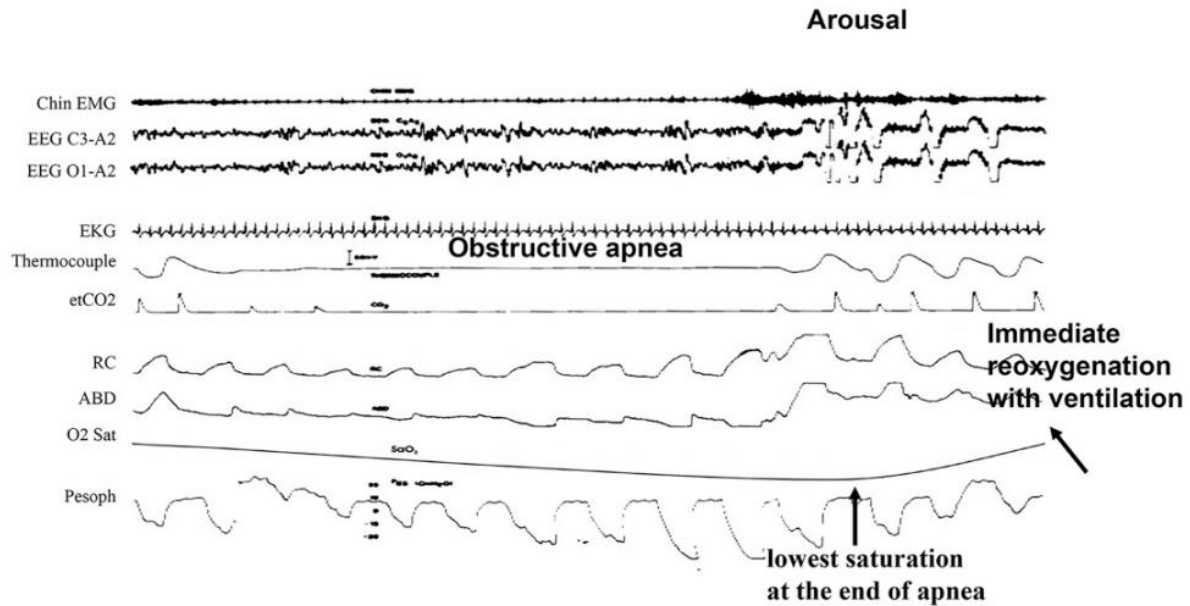


Figure 7: Example of an obstructive apnoea event from polysomnography, showing absence of airflow despite continued respiratory effort (Rib Cage - RC, Abdomen - ABD, oesophageal - Pesoph), leading to oxygen desaturation (O₂ Sat) and followed by arousal-induced reoxygenation, thoracoabdominal movement and increasing oesophageal pressure confirming airway obstruction [27].

In contrast, there was no thoracoabdominal movement or change in oesophageal pressure, confirms central apnoea as shown in figure 8. These concepts about airflow and thoracoabdominal efforts form the foundation of the guidelines established by the American Academy of Sleep Medicine (AASM) to differentiate between different apnoea types [27].

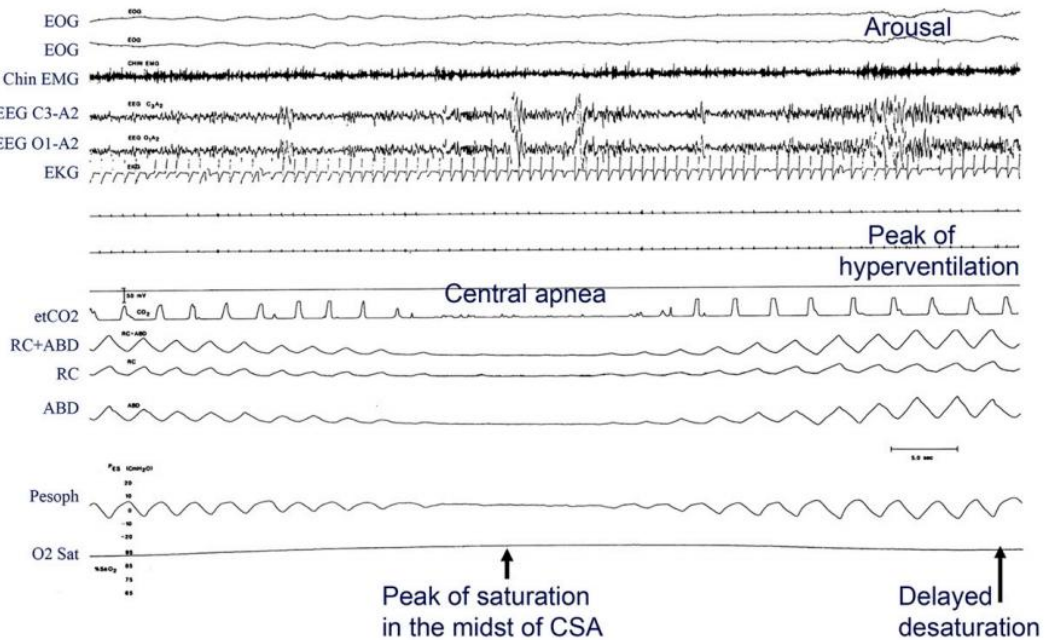


Figure 8: Polysomnographic tracing of a central sleep apnea (CSA) event. This chart illustrates a central apnea episode where both airflow and respiratory effort (rib cage and abdominal effort) are absent, indicating lack of neural respiratory drive [27].

For OSA, Oxygen saturation remains relatively stable during the initial part of the apnoea and then a notable desaturation (drop in SpO₂) towards the end of the apnoea episode, reaching the lowest saturation just before reoxygenation. Rapid reoxygenation is observed following the arousal and resumption of ventilation. For CSA, there is no sharp desaturation at the start of apnoea. Instead, there's a peak in SpO₂ mid-apnoea, followed by delayed desaturation post-apnoea, due to delayed circulation and oxygen exchange dynamics. Reoxygenation happens slowly, aligned with gradual return of ventilation.

When a CSA patient experiences an obstructive episode, Mixed sleep apnoea is said to be present. During CSA, patients experiencing apnoea may experience an obstructive event, such as a blockage of the airway due to various reasons (OSA). A secondary occurrence of OSA in a CSA patient is typically observed 10 seconds after the CSA event begins [29]. The figure 9 below compares airflow and respiratory effort patterns in various types of Sleep Apnoea targeted for classification after scoring an apnoea event as per scoring criteria mentioned in the following section. Hypopneas that meet these criteria are automatically classified as obstructive hypopnea, as previously stated.

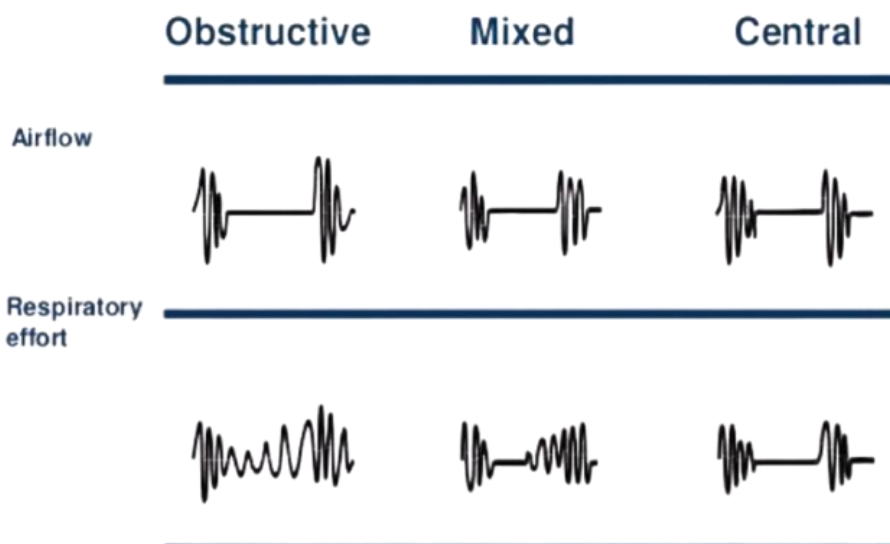


Figure 9 depicts the differentiation of sleep apnoea subtypes based on airflow and respiratory effort. It depicts the airflow and respiratory effort traces used to differentiate between obstructive, mixed, and central sleep apnoea events during sleep studies [29]. In obstructive sleep apnoea, airflow stops despite persistent or increasing respiratory effort, indicating upper airway collapse. Mixed sleep apnoea starts with no respiratory effort (central), then resumes effort without airflow (obstructive). Central sleep apnoea is distinguished by the absence of both airflow and respiratory effort, indicating a weakened central respiratory drive. These waveform patterns are important diagnostic indicators for accurate subtype classification.

Scoring Criteria from AASM Standards

The AASM Manual for the Scoring of Sleep and Associated Events is an internationally recognised framework for classifying and quantifying sleep stages, respiratory disturbances, arousals, and other physiological events. Standardising definitions, scoring rules, and technical specifications ensures consistency and reliability in polysomnography and home sleep apnoea testing in clinical settings. Its structured criteria for airflow, respiratory effort, and oxygen desaturation can act as the foundation for accurate diagnosis of sleep disordered breathing, making it a good guide for the development of the home sleep apnoea testing system in this study.

The 2017 edition (Version 2.4) [30] Scoring Guidelines were consulted while designing the prototype for this study. It includes home sleep apnoea testing specific adaptations that explain

how to score respiratory events and arousals in settings without complete EEG coverage. These are used in designing and selecting the device's sensors and scoring algorithms.

According to the guidelines in Section IX of the AASM Sleep Scoring Manual, the home sleep apnoea testing, which uses respiratory flow and/or effort parameters, requires the reporting of specific physiological and technical parameters to ensure data completeness and diagnostic reliability. The AASM recommends reporting the device type, airflow sensor type, respiratory effort sensor type, oxygen saturation, and heart rate (as determined by ECG or pulse oximetry). Body position, sleep/wake or monitoring time, and snoring detection are all optional parameters that the investigator can include at their discretion. In this thesis, the prototype employs a wearable band for device type, an oronasal thermistor for airflow detection, an abdominal movement IMU sensor for respiratory effort, and a pulse oximeter for oxygen saturation and heart rate (via PPG). The optional features include body position monitoring which is done in this study via IMU and snoring detection using microphone, while sleep and wake time estimation has been omitted due to the absence of EEG/EOG/EMG-based measurements.

The Scoring Manual also specifies the sensor requirements for identification of respiratory events during home sleep apnoea testing, which were slightly deviated in this study. The guidelines require the use of at least one airflow sensor, with an oronasal thermal airflow sensor and a nasal pressure transducer being the most effective combination for detecting apnoea and hypopnea. In this thesis, an oronasal temperature sensor (thermistor) is used to detect airflow reductions associated with obstructive and central events, while an abdominal movement sensor (IMU) is used to estimate respiratory effort in a manner like standard recommended respiratory inductance plethysmography (RIP) belts.

The manual defined that an apnoea event should be scored when a $\geq 90\%$ reduction in peak signal excursion from the pre-event baseline, as measured by a recommended or alternative airflow sensor, lasting at least 10 seconds. Apnoea is further classified based on the presence or absence of respiratory effort in line with previously mentioned in figure 9. Notably, the AASM states that apnoea identification does not require a minimum oxygen desaturation, and any respiratory event that meets apnoea criteria is scored as such. Hypopneas are scored by the magnitude and duration of airflow reduction, which is accompanied by oxygen desaturation, with criteria varying depending on whether sleep is documented. In the absence of EEG-based sleep staging, as in this study, a respiratory event is scored as hypopnea if there is a $\geq 30\%$ reduction in peak signal excursion from the pre-event baseline, lasting at least 10 seconds and associated with a $\geq 3\%$ oxygen desaturation. Table 4 summarises scoring rules for the respiratory events of interest for this study.

Event Type	Flow Limitation Criteria (Duration & Magnitude)	Respiratory Effort (Abdominal Motion)	Oxygen Desaturation (SpO_2)	Snoring (Additional Indicator)
Obstructive Apnoea	Absent airflow ($\geq 90\%$ drop) for ≥ 10 s	Present (continued or increased effort)	Not applicable	Often present
Central Apnoea	Absent airflow ($\geq 90\%$ drop) for ≥ 10 s	Absent (no inspiratory effort)	Not applicable	No
Mixed Apnoea	Absent airflow ($\geq 90\%$ drop) for ≥ 10 s	Absent to Present effort transition	Not applicable	No
Hypopnea	Reduced airflow ($\geq 30\%$ drop) for ≥ 10 s	Minimal effort	$\geq 3\%$ drop	Not applicable

Table 4. Criteria being used for scoring and differentiating respiratory events based on AASM Scoring Rules for home sleep apnoea testing

The sensor types mentioned in this subsection are briefly outlined to allow a direct comparison between the AASM standard requirements and the specific types used in this study, as well as the corresponding reported parameters. This overview focusses on both the parameters covered and the few rules from the standards that were not implemented in the current prototype. The following section explores deeply into each type, including technical reasoning, design trade-offs, and justifications for inclusion or exclusion.

2.2 Signal Type Selection and Design Considerations

The next step is to look at the several ways to sense each parameter needed for home sleep apnoea testing now that the AASM's requirements, recommendations, and technology guidelines clearly defined. This subsection will investigate various sensor technologies and measurement methods for measuring airflow, respiratory effort, oxygen saturation, body position, and snoring, with a focus on weighing the trade-offs between user comfort, wearability, and measurement accuracy. Each technology is evaluated in terms of its suitability for long-term, unattended use in a home environment, potential integration into a compact wearable form factor, and reliability of event detection. Based on this analysis, the final set of signals for the proposed wearable home sleep apnoea testing device is chosen.

Signals and Comfort-Accuracy Trade-offs

Accurate airflow estimation is necessary to improve the detection accuracy of apnoea and hypopnea. Airflow measurement can detect these events, and flow limitation as a flattening of the inspiratory flow waveform due to airway narrowing. Because invasive airflow measurement is impracticable in everyday situations, non-invasive approaches for providing flow signals have been developed.

The pneumotachograph is the gold standard [31], however it is not practical for routine home sleep testing. It measures the airflow accurately, and therefore precise waveform analysis. It is a flow sensor that operates on the principle that airflow is proportional to the pressure drop across a resistance when the flow is laminar. However, it requires a nose or face mask attached to the sensor, which will interfere with natural sleep, and is therefore mostly used in studies or monitored lab settings. Because the pneumotachograph is bulky and uncomfortable, qualitative airflow measurements, are a more widely accepted alternative. Qualitative airflow measures include monitoring changes in airway pressure and temperature at the user's nose and mouth.

Thermistors and thermocouples are simple and tolerable, but they are a rough estimate and not entirely a quantitative or a direct airflow measure. They are tiny sensors positioned at the airway passage, either mouth or nostrils or both to measure temperature variations between inspired surrounding air and expired air at around 37°C which is the internal body temperature. They produce an electrical signal corresponding to resistance change in thermistors and voltage change in thermocouples proportional to temperature changes between inhaled and exhaled air. While these devices are good fit because to their ease of use, small size, and high user tolerance, they have inherent limits. Their dynamic response is comparatively slow, the thermal time constant is a measure of how quickly a temperature sensor responds to a change in temperature, for thermistors its around 5 to 10 seconds and the relation between electrical output and actual airflow is nonlinear, therefore difficult to identify and quantify partial obstructions and their readings are heavily reliant on precise sensor location. If placed too close to nostril it might miss mouth breathing and vice versa. To rule this out, two thermistors simultaneous may be used to cover both types of breathing. As a result, they cannot accurately quantify flow magnitude or waveform shape, but they are effective at detecting full airflow cessation and hence useful for recognising apnoea [31].

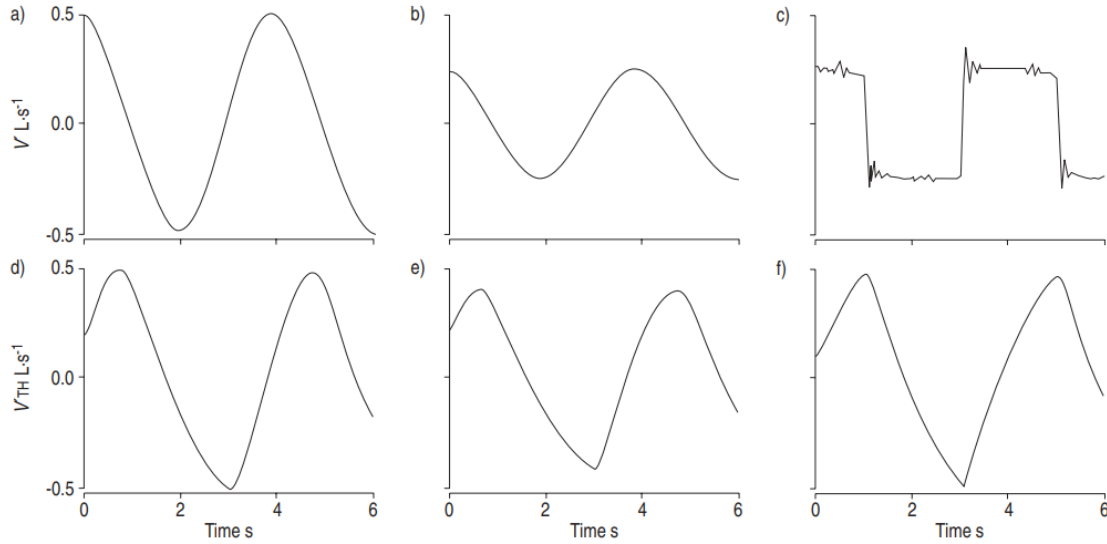


Figure 10: Comparison of actual airflow waveforms measured by a reference pneumotachograph (a–c) with corresponding signals from a thermistor (d–f) under controlled bench test conditions. (a) and (d), (b) and (e), and (c) and (f) represent matched flow conditions, demonstrating that while thermistors can detect the presence or absence of airflow, they provide limited accuracy in reproducing waveform shape and magnitude, particularly during rapid or irregular flow changes, a slight delay in response is also noticeable reflecting its slower response time [31].

Nasal air pressure transducer is other commonly used and accepted alternative, connected to a sensitive pressure transducer measure pressure changes in the nostrils generated by inspiratory and expiratory airflow. This pressure signal is directly proportional to flow magnitude. However, the relation is nonlinear and has a quadratic pattern. Linearisation approaches, such as using the square root of the recorded pressure, can increase waveform accuracy and enable more reliable diagnosis of hypopneas and flow limitation as shown in figure 11 [31]. Nasal air pressure transducers have a high dynamic response, allowing them to catch the smallest details of inspiratory waveforms. However, their readings can be lost during mouth breathing, partially lost during mixed breathing, and influenced by prong location or different sizing, which can potentially increase nasal resistance in certain situations. It has a medium user tolerance and is more discomforting than thermistors specially during longer studies. Despite these limitations, they are widely employed in clinical polysomnography as an additive or alternative for thermistors, particularly when hypopnea and flow limitation score are important.

Respiratory inductive plethysmography (RIP), like thermistors which does not detect airflow directly, estimates ventilation by recording cross-sectional changes in the thorax and abdomen with inductive bands [31]. Calibrated ribcage and abdominal data can be combined to produce a derived flow signal. This method is reliable in controlled conditions, but it is prone to errors if the bands shift over the night.

No one airflow measuring technique is ideal for all situations, particularly in unsupervised home sleep testing, when simplicity, patient tolerance, and robustness to movement artefacts are important. Pneumotachographs, while accurate, are not ideal for home use due to their bulky nature. Thermistors and thermocouples are useful and well tolerated, although they are limited to qualitative identification of airflow cessation, making them better suited for apnoea detection than hypopnea scoring. Nasal air pressure transducers provide better waveforms and can detect slight flow limitation and hypopnea, although their effectiveness is limited by mouth breathing and prong displacement. For home sleep apnoea testing, combining complementing sensors such as a thermistor for accurate apnoea detection and nasal pressure for hypopnea and flow limitation scoring would be the ideal case as it provides the optimum accuracy, as redundancy helps eliminate deviations inherent in each approach. This is in line with the AASM

Sleep Scoring Manual, which states that at least one airflow sensor must be used, with the optimum setup including an oronasal temperature sensor and a nasal pressure transducer.

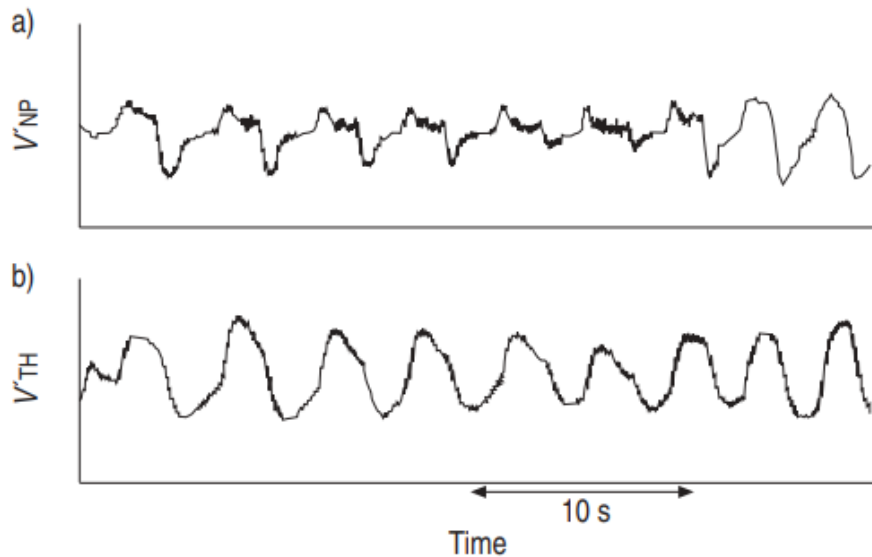


Figure 11: Comparison of airflow signals obtained simultaneously from nasal air pressure transducer (a) and from temperature changes using a thermistor (b) in a patient. The nasal prong signal preserves waveform detail suitable for detecting flow limitation, whereas the thermistor signal provides less accurate waveform representation [31].

Airflow signals are a must for recognising the event and extent of breathing disruptions, but they do not differentiate between obstructive and central events. To accurately classify apnoea, respiratory effort must be measured to identify whether breathing stoppage is followed by inspiratory muscle activity. There are multiple techniques for evaluating respiratory effort during sleep, from invasive gold standard to non-invasive options, each with trade-offs in accuracy, comfort, and applicability for home usage.

The gold standard for evaluating respiratory effort in sleep studies is oesophageal pressure monitoring [32] using a small catheter with an intraluminal balloon. It detects intrathoracic pressure swings, allowing for accurate classification between obstructive, central, and mixed events. However, its intrusive nature results in poor patient tolerance, possible sleep disturbance, making oesophageal pressure highly accurate but impractical alternative for routine home-based testing.

The previously mentioned Respiratory inductive plethysmography (RIP) can also be used for measuring respiratory effort. RIP measures cross-sectional area changes around the thorax and abdomen using elastic bands with inductive coils, which are then transformed into estimates of volume. It is the AASM's suggested non-invasive alternative to oesophageal pressure for detecting respiratory effort and is used in polysomnography [33]. RIP is simple to use, but its accuracy is strongly dependent on precise belt positioning and stability during sleep. Belt movement, posture changes, or a lack of calibration can reduce the effort signal quality.

Suprasternal Pressure (SSP) measured by sensor, inserted above the sternal notch (between the collarbones), measures low-frequency pressure fluctuations from the throat during inspiratory exertion, as well as tracheal and snoring noises [32, 33]. It is non-invasive, stable across body postures, and less sensitive to movement artefacts than RIP and comfortable for patients, therefore a great alternative.

Inertial measurement units (IMUs) offer a cheap and non-invasive way to record the small chest and abdominal movements that occur during sleep. The study by S. Kontaxis et al [34] found that a single waist-mounted IMU that comes in a small package containing both the accelerometer and gyroscope could track respiratory rate with excellent precision, with a correlation of more than 0.95 with polysomnography standards and an average error of less than one breath per minute. The sensor detects the modest rise and falls of the abdomen as the lungs expand and collapse, converting those mechanical motions into a clear, analysable signal. Making it easy to track the respiratory effort.

Once airflow and effort are determined, the next objective is how to interpret the impact of those breathing changes and pauses on the body and can be picked up any further signs. Oxygen saturation and snoring tests are the go-to options. SpO₂ identifies whether dips in airflow are lowering oxygen levels, allowing to distinguish between insignificant and significant events. Overnight oximetry alone isn't perfect as it can't distinguish between obstructive and central events, and it's not very good at detecting mild disease, but study by Yassin et al show it's reliable for moderate to severe OSA [35]. Snoring, on the other hand, can be noisy yet informative signal. The pitch and rhythm of a person's snores can indicate where the blockage is occurring in the airway. Both are high user tolerable additions.

Pulse oximetry is a common, non-invasive method for monitoring oxygen saturation and pulse rate during sleep. In the referenced study [35], overnight recordings utilising a wrist-mounted oximeter revealed oxygen desaturations of $\geq 4\%$ from baseline and reached sensitivities of 66.7%, 80%, and 100% for mild, moderate, and severe OSA, respectively, but has low specificity therefore some false positives are expected for mild and moderate cases. While this restricts its usefulness as a single diagnostic tool, especially for milder diseases, it adds essential physiological information when paired with airflow and effort data. For a home-based wearable device, its unobtrusive nature, ease of use, and ability to detect large desaturation episodes make it a useful and supporting signal.

Snoring is an audio indicator of upper airway vibration and disruption, and its features can reveal information about the obstruction site. In the study [35], recordings made with a fixed-position microphone were looked for pitch, frequency range, harmonic content, and waveform structure. Palatal snoring was characterised by low-pitched, repetitive bursts, whereas tongue base snoring had a higher pitch, larger frequency range, and less regular patterns, combined obstruction shown characteristics of both. Although acoustic analysis alone cannot consistently distinguish sleep apnoea from simple snoring, it can discriminate between palatal and tongue base snoring and, when paired with airflow and effort data, adds to a more comprehensive event profile. A small microphone is a viable addition to a wearable system due to its low intrusion level.

Airflow, respiratory effort, oxygen saturation, and acoustic signals together provide a holistic picture of sleep-disordered breathing. Each signal type presents a distinct balance between comfort, accuracy, and diagnostic value. The system design challenge lies in selecting and integrating these sensing types to maximise diagnostic capability while maintaining wearability. The next section maps each selected signal to the targeted sleep events and outlines the reasoning behind the final sensor configuration.

Selected Signals for Wearable Design

The practical limits of a wearable device meant for home use had to be balanced with adherence to AASM standards during the prototype design. Four primary sensing types are used in the final configuration, a nasal thermistor for airflow, an IMU for respiratory effort and body

position, pulse oximetry for heart rate and oxygen saturation, and a microphone for snoring sound analysis as shown in figure 12 (c). Airflow, respiration effort, oxygenation, and at least one optional feature are the minimum suggested criteria for at-home sleep apnoea testing that these signals together cover while preserving a high degree of comfort and use.

This design excluded several standard signals. Despite being recommended by AASM guidelines for identifying hypopneas and mild flow limitation, the nasal pressure transducer was not included because to the discomfort and low tolerance that are linked to using nasal cannulas in unsupervised home settings. Even though RIP is still the preferred method for detecting paradoxical movement, the thoracoabdominal RIP belts, which are commonly used in PSG and HSAT to measure effort, have been substituted with a waist-mounted IMU.

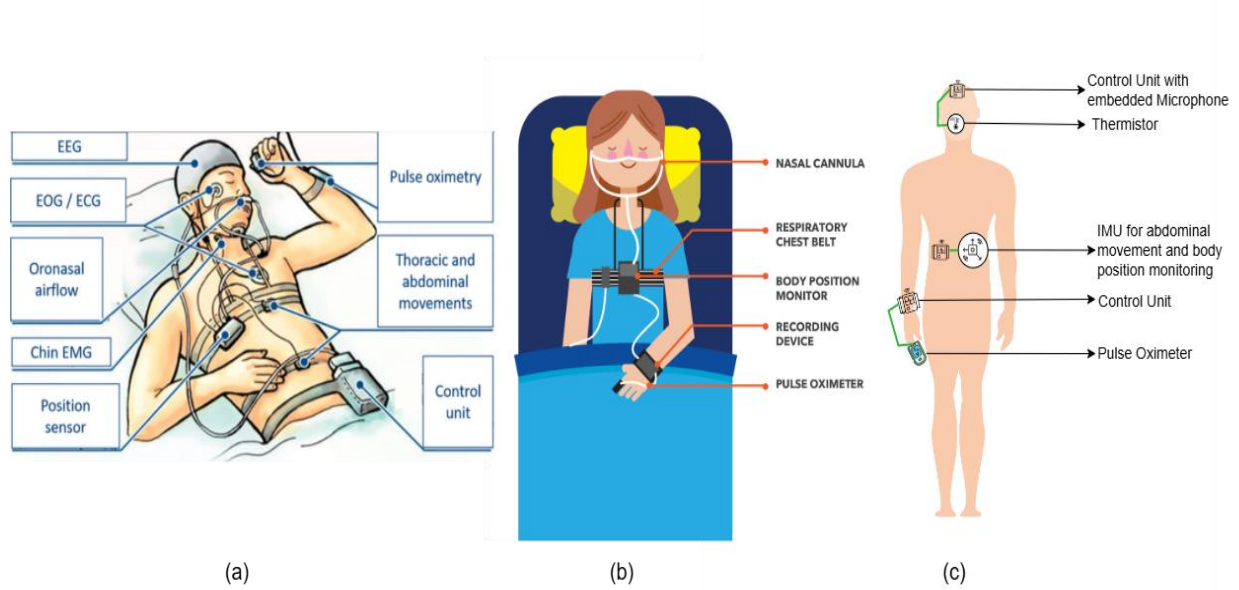


Figure 12: Comparison of monitoring setups for sleep apnoea assessment. (a) Full polysomnography (PSG) with comprehensive neurophysiological and cardiorespiratory channels [36]. (b) A typical home sleep apnoea test (HSAT) configuration using a nasal cannula, respiratory belts, body position monitor, recording device, and pulse oximeter [37]. (c) The proposed prototype system, incorporating a thermistor for airflow, IMU for respiratory effort and body position, pulse oximeter for SpO₂ and heart rate, and a control unit with embedded microphone for snoring detection.

Furthermore, because EEG, EOG, and chin EMG need numerous electrodes on the face and scalp, which is not suitable for the targeted form factor, they were excluded from the design although they are very common in PSG. Because of their omission, total recording time (TRT) is used instead of total sleep time (TST), but this restricts the capacity to evaluate sleep staging or arousals. IMU can catch an arousal if associated with a significant movement. Leg EMG and ECG were also not included to maintain a basic and wire-free design, both would have resulted in more electrodes and connections.

Common Signals in PSG and HSATs	AASM Guideline / Standard Use [30]	Diagnostic Value	Inclusion in Prototype Design	Reason for Inclusion / Exclusion
Oronasal Thermistor	Recommended airflow sensor (apnoea detection)	Reliable for detecting apnoea events, less sensitive to	Included	Comfortable, simple to integrate, fulfils AASM

		hypopnoea or flow limitation		minimum airflow requirement
Nasal Pressure Transducer	Preferred airflow sensor (hypopnoea, flow limitation)	High sensitivity for hypopnoea and flow limitation	Excluded	Cannula uncomfortable, poor tolerance at home, trade-off for comfort and sensitivity
Thoracoabdominal RIP Belts	Standard for respiratory effort	Detects paradoxical movement, Semi-quantitative tidal volume (the amount of air inhaled or exhaled during a breath)	Excluded	Replaced by IMU. RIP belts, need additional unit for body position sensing.
IMU (Abdomen)	Not standard, studies [34], proved it to be reliable alternative	Tracks abdomen motion for effort, also captures body position	Included	Compact, reusable, easy integration and cost effective. No need of additional body position sensing unit
Pulse Oximetry (SpO ₂ , HR)	Essential in HSAT and PSG for hypopnoea	Detects desaturations, estimates AHI severity, monitors HR	Included	Non-invasive, user tolerable, strong physiological marker
Microphone (Snoring)	Optional in HSAT, often included in PSG	Provides obstruction site clues, screens for upper airway resistance	Included	Minimal user burden, complements airflow, effort signals. An additional confirmatory signal for OSA.
EEG / EOG / Chin EMG	Optional in HSAT, Essential in PSG (sleep staging, arousals, REM detection)	Required for sleep/wake scoring, staging, and arousal detection	Excluded	Too many electrodes, intrusive for wearable design, focus kept on breathing-related parameters
Leg EMG	Standard in PSG, for periodic limb movement detection	Identifies limb movements, relevant in differential diagnosis	Excluded	Additional electrodes, excluded to reduce wires and complexity

ECG	Standard in PSG	Enables to check for HR variability, and other parameters related to heart.	Excluded	Would add electrodes, excluded to minimise sensors and maintain wireless design
-----	-----------------	---	----------	---

Table 5. Summary of Standard signals used in PSG and HSATs, AASM-recommended signals and their implementation in the prototype design, highlighting diagnostic roles, inclusion/exclusion decisions, and rationale based on comfort–accuracy trade-offs.

In conclusion, the comparison table 5 and the figure 12 demonstrate how the suggested prototype reduces the wide range of signals utilised in PSG and HSAT to a more wearable and convenient form. The design prioritises patient comfort and convenience of use while maintaining the criteria required for accurate detection of sleep-disordered breathing by reducing the usage of cables, and invasive sensing techniques. The fundamental logic behind the signal selection procedure is reflected in this balance between diagnostic function and ease of use for regular monitoring.

2.3 Component Selection and System Integration

The next step after defining the signal types is to translate them into a functioning system by selecting hardware components and integrating them into a unified prototype. This section describes the sensors, processing units, and supporting modules used to obtain the desired signals, as well as the methods utilised to combine them into a compact and wearable form factor. The objective is to ensure reliable data collecting while maintaining ease of use, battery life, and efficient communication between components.

Sensor Module Evaluation

To detect respiratory effort and body position, this prototype uses the MPU6050, a commonly used MEMS (microelectromechanical systems) six-axis inertial measurement unit that combines a 3-axis accelerometer and a 3-axis gyroscope on a single silicon die. The accelerometer has linear acceleration range from $\pm 2g$ to $\pm 16g$, and the gyroscope have angular velocity range from $\pm 250^\circ/\text{s}$ to $\pm 2000^\circ/\text{s}$ [38]. This allows the accurate monitoring of both translational and rotational movement. The sensor unit can perform sensor fusion internally by using an embedded digital motion processor, which reduces computational load on the microcontroller.

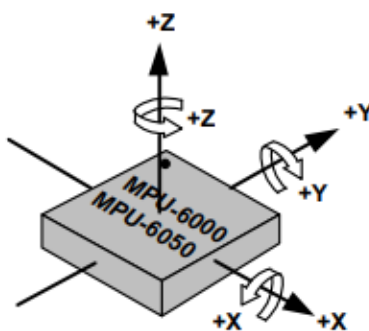


Figure 13: Orientation of the three-axis accelerometer and gyroscope sensing axes in the MPU-6050 IMU, showing the positive directions of linear acceleration ($+X$, $+Y$, $+Z$) and angular velocity (rotation about X , Y , and Z) [38].

For this application, linear acceleration range was set to the lowest available $\pm 2g$ and gyroscope angular velocity range to $\pm 250^\circ/\text{s}$. The sensor communicates via I2C, making it easily integrated with low-power microcontrollers used in wearable devices. The MPU6050 uses microelectromechanical systems (MEMS) technology for its operation. Microscopic proof masses mounted on springs inside a silicon substrate form the accelerometer. These masses deflect when the sensor accelerates, changing the capacitance between stationary and mobile plates as shown in figure 14. This variation is then translated into an electrical signal that is proportionate.

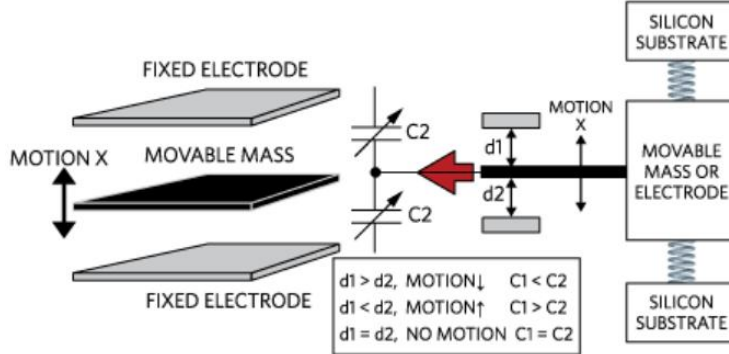


Figure 14: Working principle of a MEMS accelerometer. A movable proof mass is suspended between fixed electrodes, forming a variable capacitor. Displacement of the mass under acceleration alters capacitance (C_1 , C_2), which is measured to determine the direction and magnitude of motion [39].

The Coriolis effect is the working principle in gyroscope as shown in figure 15, it is a vibrating MEMS structure undergoing a secondary displacement when there is an angular movement. The device can measure rotational motion because this displacement is similarly interpreted as a change in capacitance. The inbuilt digital motion processor processes the six-degree-of-freedom data produced by the combination of these two sensing elements to produce stable orientation and motion estimations appropriate for tracking both fine respiratory-induced abdominal movements during breathing cycles and sleep posture.

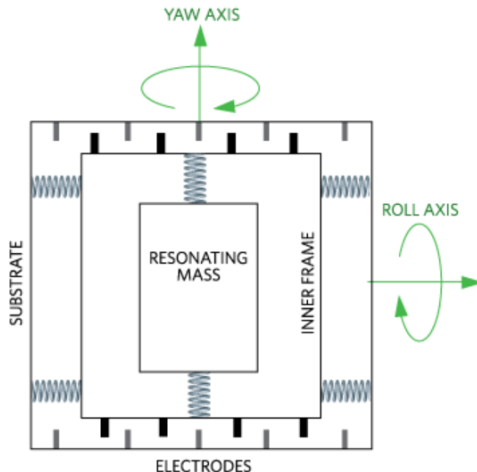


Figure 15: Working principle of a MEMS gyroscope. A vibrating resonating mass mounted on springs experiences Coriolis forces when subjected to angular velocity, causing measurable displacements along the roll and yaw axes, which are detected by surrounding electrodes [39].

To detect blood oxygen saturation and heart rate, the prototype uses a MAX30102 sensor module from Analog devices, a combined pulse oximeter and heart rate monitoring module. The sensor has a photodetector, high-resolution analogue front end, and digital signal processing, as well as two LEDs (660 nm red and 880 nm infrared) as shown in figure 16 [40].

The primary operating mechanism is based on photoplethysmography (PPG), in which light emitted into the tissue is absorbed or scattered as blood volume varies during the cardiac cycle. Oxyhaemoglobin (HbO_2) and deoxyhaemoglobin (Hb) absorb light differently at red and infrared wavelengths, allowing the relative ratio of absorption to be used for determining oxygen saturation (SpO_2).

The I²C supported digital interface enables easy communication with low-power microcontrollers. The power requirements are a 1.8 V core supply and 3.3 V for the LED driver, making it good for nightly sleep monitoring.

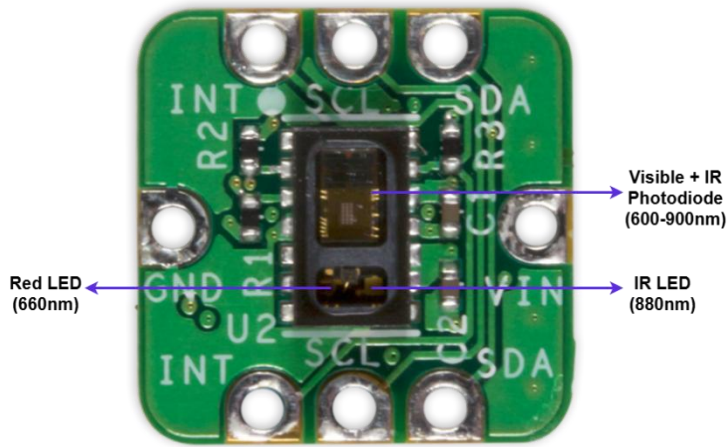


Figure 16. MAX30102 pulse oximeter breakout module showing the integrated red/IR LEDs and photodiode in the centre, with surrounding pads for power (VIN, GND), communication (SCL, SDA), and interrupt (INT) connections. The reflective optical path is aligned perpendicular to the sensor surface, enabling PPG acquisition from finger placement.

The MAX30102 works on the reflected pulse oximetry principle, using red (660 nm) and infrared (880 nm) LEDs to illuminate the finger. A photodiode (PD) detects reflected light that has both an AC component, which indicates pulsatile blood flow, and a DC component, which represents non-pulsatile absorption from tissues and venous blood. Analysing the AC to DC ratio for both wavelengths yield a measure ratio (R) as shown in the equation below, that correlates with oxygen saturation. The SpO_2 value is estimated by an empirically derived linear relationship with R as shown in the equation with constants $C1 = 110$ and $C2 = -25$, this configuration also allows for heart rate extraction from the IR AC signal.

$$R = \frac{(AC/DC)_{Red}}{(AC/DC)_{IR}}$$

$$\text{SpO}_2 = C1 + C2 \times R = 110 - 25R$$

The MAX30102 includes a low-noise charge-sensitive photodiode amplifier and a 19-bit sigma-delta ADC with adjustable sample rates (50-3200 samples per second), providing good sensitivity for this application. The analogue front end allows for changeable LED current drivers (0-50 mA, programmable in 0.2 mA steps) [40] to balance signal quality and power consumption. The device supports both SpO_2 mode (using red and IR wavelengths) and HR-only mode (using IR wavelength).

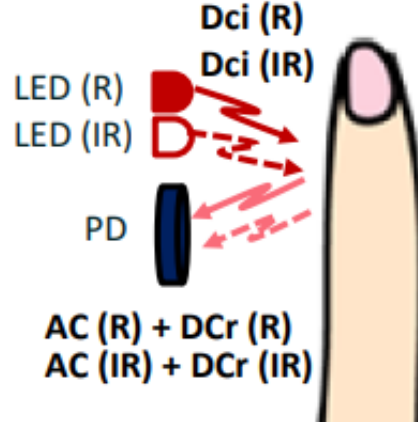


Figure 17. Working principle of the MAX30102 reflective pulse oximeter. Red (660 nm) and infrared (880 nm) LEDs illuminate the finger, and the reflected light is detected by the photodiode (PD). The detected signal contains both a pulsatile AC component, corresponding to arterial blood volume changes, and a DC component, representing static tissue and venous absorption. These signals are used to compute SpO₂ and heart rate. Image taken from [41].

This prototype places the pulse oximeter module on the finger, ensuring accurate SpO₂ and HR signals during sleep. The raw PPG (photoplethysmography) waveforms are processed to find oxygen desaturation episodes ($\geq 3\%$ reduction in SpO₂), which are then classified as respiratory disturbances. By combining optical and electrical components in a single package, the MAX30102 minimises circuit complexity, power consumption, and form factor, which is ideal for building a wearable, home-based monitoring system.

The prototype uses a negative temperature coefficient (NTC) thermistor, an extremely tiny, temperature-sensitive resistor whose resistance gradually drops as the temperature rises, to monitor airflow. The chosen thermistor is a 2.4 mm diameter bead-type thermistor as shown in figure 18 with a resistance of 10 k Ω at 25 °C and good sensitivity (4%/°C at 25°C) [42] within the interested temperature range. The sensor, which is positioned close to airstream at the nostrils, records variations in the temperature of the airflow with relation to the surrounding air, it gets warmer during expiration and cooler during inspiration and creates a waveform that depicts the breathing cycle. A halt in airflow causes a flat thermistor signal, this technique can be used to identify apnoea.



Figure 18. Bead-type NTC thermistor (10 k Ω at 25 °C) used for nasal airflow measurement [42]. The compact epoxy-coated bead provides fast thermal response, enabling detection of inspiratory and expiratory temperature changes during breathing.

The thermistor is connected to V_{CC} and creates a voltage divider with a 10 k Ω fixed resistor to ground for signal conditioning, the MCU ADC can then sample the junction. V_{out} increases on inspiration and decreases on expiration. Choosing 10 k Ω matches the thermistor's resistance as room temperature, maximising sensitivity near the body-air temperatures. The output with this setup is,

$$V_{out} = V_{cc} \times \frac{10 \text{ k}\Omega}{10 \text{ k}\Omega + R_{Thermistor}}$$

So, if the ADC returns a value X from range $(0, X_{\max})$, then,

$$V_{out} = V_{cc} \left(\frac{X}{X_{\max}} \right)$$

$$R_{Thermistor} = 10 \text{ k}\Omega \left(\frac{V_{cc}}{V_{out}} - 1 \right)$$

By using the material constant, β (~ 3900 K) and a reference temperature ($T_0 = 25$ °C = 298.15K) and resistance (10 kΩ),

$$\frac{1}{T} = \frac{1}{T_0} + \frac{1}{\beta} \ln \left(\frac{R_{Thermistor}}{10 \text{ k}\Omega} \right)$$

$$T = \frac{1}{\frac{1}{T_0} + \frac{1}{\beta} \ln \left(\frac{R_{Thermistor}}{10 \text{ k}\Omega} \right)}$$

$$T(\text{°C}) = T - 273.15$$

The prototype also uses a digital MEMS microphone (SPH0645) on an Adafruit I2S breakout board to record any upper airway sounds, including snoring. This device combines a capacitive MEMS transducer paired with a low-noise preamplifier and a sigma-delta modulator to provide direct digital audio output in I2S format, avoiding the need for an external ADC [43]. By integrating the analogue-to-digital conversion inside the sensor, the microphone greatly lowers noise pickup and gives a clean digital interface with the microcontroller.



Figure 19. Adafruit I2S MEMS microphone breakout (SPH0645LM4H-B). The front side (left) shows the MEMS microphone port and supporting circuitry, while the rear side (right) provides labelled pins for power (3.3 V, GND), I2S digital interface (DOUT, BCLK, LRCL) [44].

The transducer element is a small diaphragm hanging above a fixed backplate as shown in figure 19, forming a variable capacitor. The surrounding acoustic pressure induces diaphragm displacement, which modulates capacitance and produces a corresponding electrical signal. The internal amplifier first conditions the signal, which is then digitised by the sigma-delta modulator. The breakout board offers clock, word select, and data lines for direct connection to conventional I2S peripherals on microcontrollers. The microphone breakout board needs a supply voltage of 3.3 V and a current demand of about ~0.6 mA [43,44], making it acceptable for continuous overnight use.

The microphone is placed at the forehead, embedded in the control unit, close to the airway. Its purpose is to capture snoring occurrences, which are then evaluated for temporal and spectral properties. The detailed snoring detection algorithm is discussed in next section, providing valuable information in addition to airflow and effort signals.

A 1.54-inch LCD panel with an integrated microSD card slot (DFR0649) [45] is used for local data presentation and onboard storage. The monitor has a 240×240 -pixel resolution and a full RGB colour interface for clear visualisation, system status, and summary metrics. The module communicates with low-power microcontrollers using an SPI bus (Serial Peripheral Interface). The working voltage is 3.3 V, with current consumption based on lighting intensity. The onboard LED backlight is changeable.

In addition to screen, the breakout features a microSD card slot for data storage. The SD card interface also uses SPI and supports conventional FAT file system formatting. In the context of this project, the LCD serves as a small interface for confirming device status and sensor connections, while the microSD card ensures continuous, logging of multi-sensor data during the sleep study.

Accurate timestamping of signals is important in sleep study, especially when synchronising several data streams or computing event durations like apnoea length, oxygen desaturation, and recovery times. The prototype uses the DS3231 Real-Time Clock (RTC), a temperature-compensated crystal oscillator-based device. The DS3231 RTC achieves long-term accuracy of ± 2 ppm (± 1 minute per year) [46, 47] by integrating the crystal and temperature compensating circuitry on-chip. The module's ultra-low-power backup, is supplied by a coin-cell battery (CR1220), ensures that timekeeping continues even when the main system is turned off. It operates from a 3.3–5 V supply. Typical battery current drain is less than 1 μA , providing couple of years of uninterrupted operation. RTC time is appended to data written to the SD card.

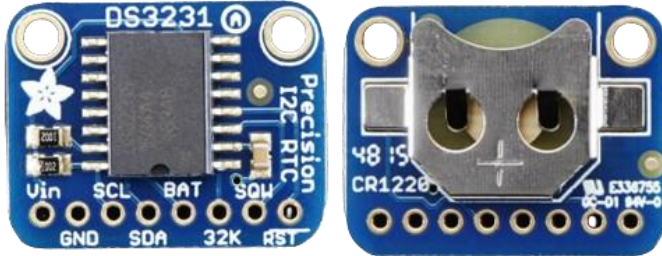


Figure 20. DS3231 precision real-time clock (RTC) breakout board. The front side (left) shows the DS3231 IC with I2C interface pins (SDA, SCL), power inputs, while the rear side (right) houses the CR1220 coin-cell holder for battery backup, ensuring continuous timekeeping even during power loss [46].

Microcontroller Selection

This prototype's main processing and control unit is the ESP32-WROOM-32 module, which combines all sensing, storing, and communication capabilities into a small, low-power platform. It contains Espressif's dual-core Xtensa 32-bit LX6 CPU, which can run at up to 240 MHz. With currents ranging from ~ 240 mA peak (Wi-Fi Tx) to < 10 μA in deep-sleep, there are several power modes supported, including active, modem-sleep, light-sleep, and deep-sleep. It supports dual-mode Wi-Fi (802.11 b/g/n) and Bluetooth 4.2 [48] enabling wireless data transfer and low-power peripheral connectivity. For this prototype, Wi-Fi is used for data transmission, with a 2000mAh rechargeable battery pack, this enables continuous monitoring for whole night while still offering Wi-Fi bursts for data transfer.

The ESP32-WROOM-32 has extensive peripheral set, which complements the sensor suite in this project without the need for additional controllers. The I2C bus links to the MPU6050 IMU (respiratory effort and body position) and the DS3231 RTC for timestamping. The SPI bus powers the 1.54" TFT LCD display and microSD card module, providing real-time data visualisation and data logging. The I2S interface streams audio directly from the digital MEMS

microphone (SPH0645), and with help of Analogue pins, the junction voltage can be detected and then digitises the thermistor voltage divider output for airflow measurement.

The ESP32-WROOM-32 is placed on a DFRobot FireBeetle ESP32 I/O Expansion Board – DFR0654 [49, 50] to make it easier to integrate sensor, storage, and display modules. The breakout includes onboard power regulation (5 V to 3.3 V), allowing direct connection to USB or battery packs without the need for external regulators. This is very beneficial in portable sleep monitoring devices, where both rechargeable Li-ion cells and USB-based charging and logging can be used interchangeably. The board also incorporates a USB-to-UART converter (CP2104), which enables simple programming and debugging over a normal micro-USB connector while providing serial connectivity for data monitoring throughout the build [49, 50].

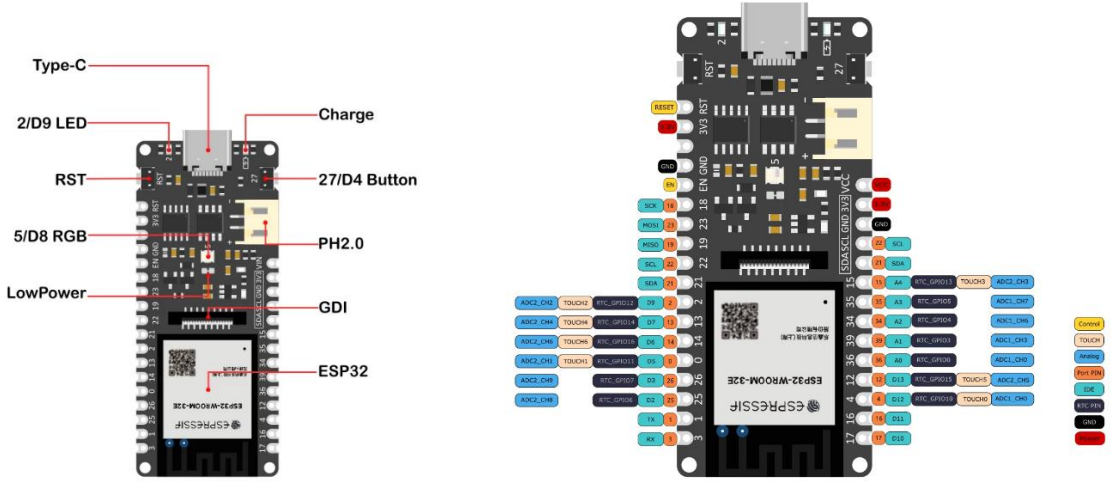


Figure 21. Pinout diagram of the DFRobot FireBeetle ESP32 breakout board. The left image highlights the major onboard features such as USB Type-C port, reset and user buttons, GDI, PH connection, power management, and the ESP32 module. The right image shows detailed mapping of GPIOs with support for ADC, UART, I2C, SPI, and PWM functions, providing flexible interfacing for multiple sensors and peripherals in the prototype [49].

The FireBeetle ESP32 board also includes two additional hardware features, that are helpful for this project setup. The first is the GDI interface as shown in figure 21 (18-pin FPC connector), which allows the chosen screen and microSD module to be directly plugged in via a flat flexible connection. The second type is the PH2.0 connector, which is intended for direct connection of a single-cell Li-ion or Li-poly battery. The board's inbuilt charging circuitry and power management allow it to effortlessly handle both USB Type-C charging and Li-ion battery operation. The board also has on board charging circuit with a red charging LED as status indicator, with three states, off when fully charged or disconnected, steady on while charging, and fast blinking when powered via USB without a battery connected. This eliminates the need for external battery management circuits, simplify wiring, and no need to remove the battery out of enclosure every time for charging.

The arrangement of the sensors would necessitate lengthy cabling harnesses if a single microprocessor served as the central control unit and a single battery might not last for whole night with all sensors and other modules (RTC, Screen, SD card writing, Wi-Fi transmission) continuously running overnight. For instance, the IMU should be placed around the abdomen, the thermistor near the nose, and the pulse oximeter on the finger. These wires would need to be long enough to allow for free movement to accommodate users with varying body sizes and sleeping positions. This would result in a configuration that is not all that different from the

current commercial HSAT devices, except for the IMU and thermistor being used in place of belts and cannulas.

Wireless System Architecture

Therefore, system design separates the sensors into three groups as shown in figure 22 according to where they are located on the body to get around this restriction and lessen the wiring. Short, body-worn connections are possible instead of lengthy wires since each group is controlled by a separate local microcontroller with a separate battery. The ESP32 microcontrollers' built-in Wi-Fi allows for wireless group communication, allowing all data to be recorded without the inconvenience of wires.

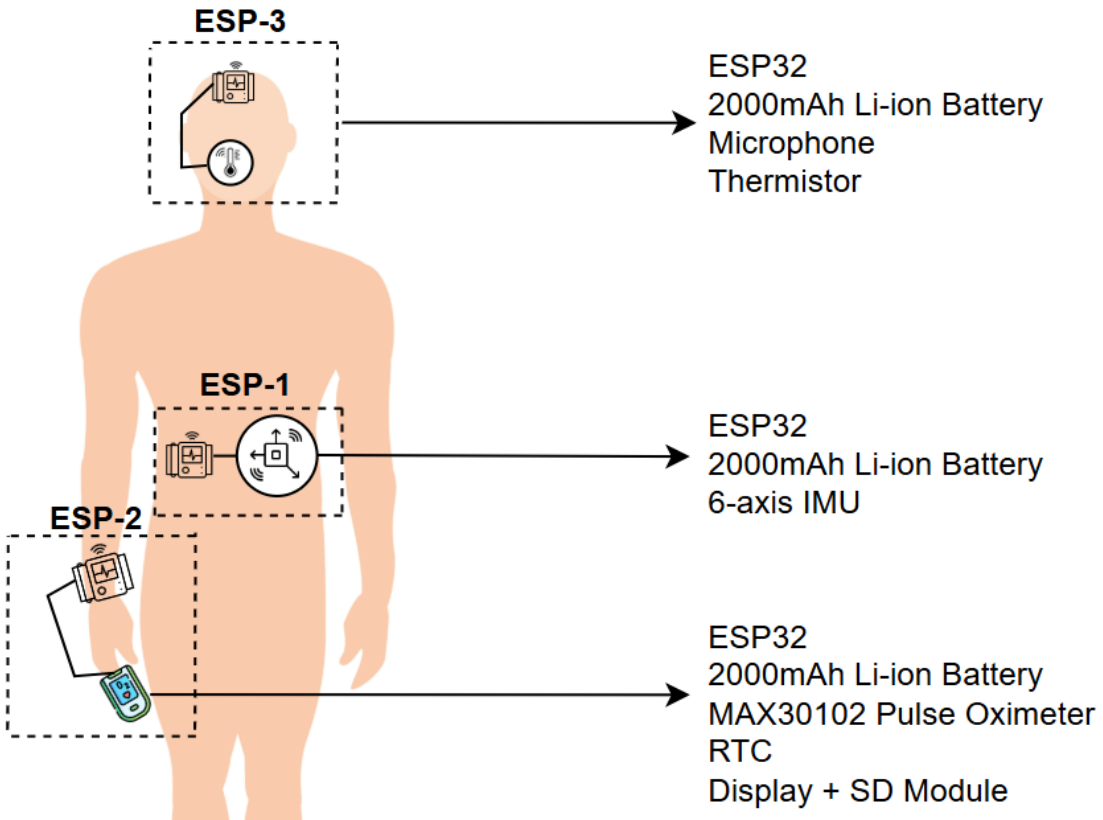


Figure 22. System architecture showing the division of sensors into three body-mounted groups, each managed by a dedicated ESP32 microcontroller with independent Li-ion battery supply. ESP-3 (head) manages the thermometer and microphone; ESP-1 (abdomen) manages the IMU; and ESP-2 (arm) manages the pulse oximeter, RTC, and display/SD storage module. Wireless communication between units is achieved using the ESP32's integrated Wi-Fi.

This distributed architecture as shown in figure 22 eliminates the need for lengthy connection between sensors and the control unit. By combining each microprocessor with its corresponding sensors, the system ensures short, robust connections and can accommodate users of various body sizes without requiring extensive wiring. Each ESP32 acquires signals locally and wirelessly streams them, with data centrally aligned and transferred over Wi-Fi. This method maintains the diagnostic coverage needed while creating a wearable form factor that is more comfortable than HSAT.

This prototype uses a hub and node style three ESP32 devices working together over Wi-Fi to collect, time-coordinate, and record physiological information as shown in figure 23. Wi-Fi stations ESP1 (the IMU node) and ESP3 (the microphone and thermistor node) provide sensor

data to ESP2, the hub, on a regular basis. ESP2 is chosen as hub as it validates and acknowledges each data packet and stores synchronised records on a microSD card at the same frequency as the data packets received.

There are two supported modes of data collection. The ESP3's microphone is enabled, and the nodes transmit at 2 Hz in Mode-1, in Mode-2, the rate of transmission is lowered to 1 Hz, and the microphone is turned off to conserve power. The two modes are intended for different applications as stated in project objectives in chapter 1. Mode-1 is intended for thorough diagnostics in which all signals oximetry, respiratory effort, airflow, and microphone acoustic data are collected at a higher frequency. In keeping with the system's function as a study and diagnostic tool, this mode offers the most comprehensive dataset for identifying and categorising apnoea and hypopnea episodes. Mode-2, on the other hand, is designed for general sleep monitoring, where the device uses less power due to a lower sample frequency and the removal of the microphone while still monitoring essential metrics like oxygen saturation, effort, and airflow.

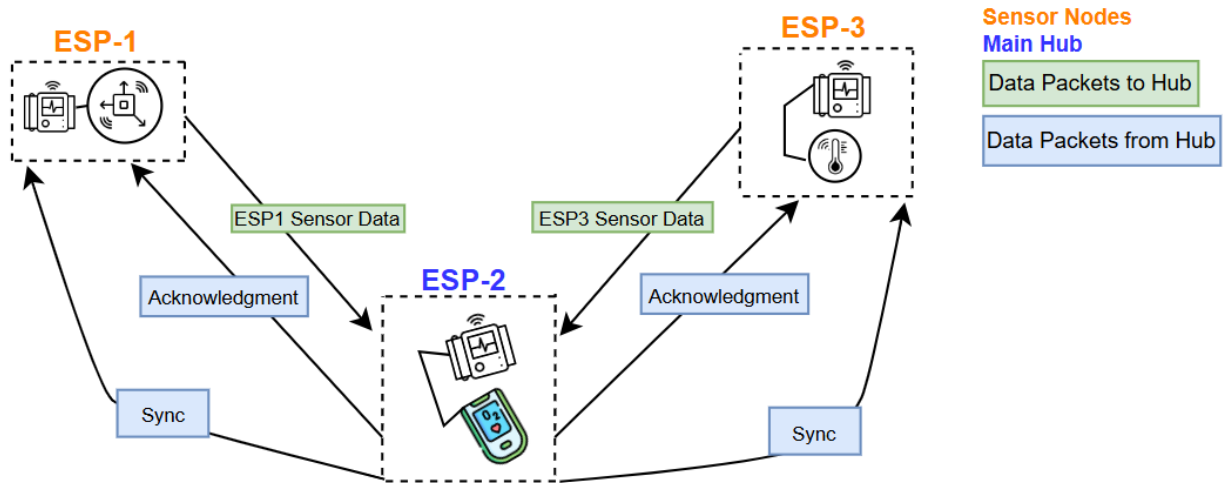


Figure 23. End-to-end communication link map for the three-ESP system: ESP1 and ESP3 send Data packets to the Hub (ESP2), the Hub returns per-packet ACKs, and broadcasts 1 Hz SYNC.

Three primary packet types are exchanged in this configuration as shown in figure 23 for time-aligned data collecting. Sensor data packets are transmitted from ESP-1 and ESP-3 to the hub (ESP-2). The hub replies with acknowledgement (ACK) packets after receiving these packets, confirming successful reception and requesting retransmission if not received. If an ACK is not received within 150 ms from hub, the sending node automatically retries transmission up to two times, if it fails, to mark the missing packet, -1 is written by default in the SD card csv log data rows. Additionally, the hub periodically broadcasts synchronisation (SYNC) packets to all nodes each second to update the mode of operation. To further reduce the chances of missing the packet reception (to avoid packet collision), a small random jitter is added before sending out data packets, so they always arrive at different times and hub can pick up all packets. The detailed communication, packet structure and other functions of the hub are discussed in section 2.4.

Power Management and Battery Strategy

Along with comfort and performance, battery life is an important measure of a wearable, at-home sleep apnoea testing device. Every ESP runs on a separate Li-ion battery, and the system's entire utility depends on its capacity to run continuously through the night. A detailed power

budget is created to guarantee this, taking into consideration of wireless connection in addition to the ESP32's and sensors' baseline usage.

The total current drawn by each ESP can be calculated by, $I_{ESP} = I_{WIFI} + I_{Baseline}$

Were, $I_{WIFI} = \sum f_{tx} t_{tx} I_{tx} + \sum f_{rx} t_{rx} I_{rx}$

From ESP32 Datasheet, for active wi-fi operation [51], $I_{tx} = 240mA$, $I_{rx} = 100mA$

From the previous section, it was established that four different packet types are used for wireless communication. The table 6 summarises the size of each packet, which is used to calculate the transmission and reception times according to the equation shown.

$$t_{tx/rx} = \frac{\text{No. of Bytes in packet} \times 8}{\text{Data rate}}$$

Theoretical maximum Wi-Fi speed for the ESP32 is 150 Mbps under the 802.11n (2.4 GHz) standard [51]. Assuming average *Data rate* = 6Mbps and the default headers of all the layer-2 and laye-3 protocol, headers combined 74 bytes

Packet Name	Packet Data size	Packet header size	IP+UDP+802.11 MAC protocol header	Total TX bytes
ESP1 Data (ESP1 → ESP2)	48	12	74	134
ESP3 Data (ESP3 → ESP2)	44	12		130
ACK (ESP2 → node)	8	0		82
SYNC (ESP2 broadcast)	12	0		86

Table 6. Breakdown of wireless packet size, showing data size, header size, and total transmission size.

The active time, frequency, and current consumption of wireless communication transmission and reception in both operational modes are summarised in the tables below. The hub (ESP-2) consumes the most because it manages both synchronisation and acknowledgement packets. According to this analysis, communication only accounts for a minor but quantifiable portion of total power consumption, with Mode-2 providing lower power consumption than Mode-1.

ESP	TX packet	Total size (B)	f_{tx} (Hz) – Mode 1	f_{tx} (Hz) – Mode 2	t_{tx} (ms)
ESP-1 (Node)	Data	134	2	1	0.179
ESP-2 (Hub)	ACK	82	4	2	0.109
	SYNC	86	1	1	0.115
ESP-3 (Node)	Data	130	2	1	0.173

Table 7. Wi-Fi transmission characteristics of the three ESPs

ESP	RX packet	Total size (B)	f_{rx} (Hz) – Mode 1	f_{rx} (Hz) – Mode 2	t_{rx} (ms)
ESP-1 (Node)	ACK	82	2	1	0.109
	SYNC	86	1	1	0.115
ESP-2 (Hub)	Data (ESP-1)	134	2	1	0.179
	Data (ESP-3)	130	2	1	0.173
ESP-3 (Node)	ACK	82	2	1	0.109
	SYNC	86	1	1	0.115

Table 8. Wi-Fi reception characteristics of the three ESPs

ESP	Mode-1 I_{WIFI} (mA)	Mode-2 I_{WIFI} (mA)
ESP-1 (Node)	0.119	0.065
ESP-2 (Hub)	0.203	0.115
ESP-3 (Node)	0.117	0.064

Table 9. Estimated Wi-Fi average current consumption for each ESP node in Mode-1 and Mode-2.

The baseline current consumption with exact settings and parameters used in this prototype are calculated below and summarised in table 10.

On the MAX30102, the LED current registers are 8-bit, with 0x00–0xFF mapping to 0–50 mA [40]. That implies each step is,

$$I_{step} = \frac{50mA}{255} = 0.196mA \text{ per LSB}$$

In the firmware, the MAX30102, LED current registers were set to 0x64,

$$I_{LED} = 100 \times 0.196 = 19.6mA$$

the Pulse width is set to 411 μ s and sampling rate is 100.

$$I_{Avg} \text{ per LED} = I_{LED} \times T_{PULSE} \times F_S = 19.6 \text{ mA} \times 411 \mu\text{s} \times 100 \text{ Hz} = 0.805 \text{ mA}$$

For 2 LEDs (Red and IR), it is 1.61mA, IC measurement supply (analogue front end and digital) is approximated to 0.6 mA, totalling to 2.21mA for this setup of MAX30102.

Using Ohm's law, current in thermistor divider is, $I_{Thermistor} = \frac{3.3V}{10 \text{ k}\Omega + 10 \text{ k}\Omega} = 0.165 \text{ mA}$

The difference between Mode-1 and Mode-2 is minimal in terms of Wi-Fi usage. The current draw is dominated by the ESP32 itself (30 mA) with the IMU adding a smaller contribution of 3.9 mA. Due to the combined load of the ESP32, MAX30102 pulse oximeter, DS3231 RTC, and screen + microSD module, the hub, ESP-2, has the highest consumption at 56.41 mA, with the display and storage module taking up the most amount among the sensors. In Mode-1, the microphone is active and draws 600 μ A. In Mode-2, the microphone is off and only draws 10 μ A, dropping the total down to 30.175 mA. The thermistor adds 0.165 mA in both cases.

The total combined current consumption of each ESP is shown in table 11, and expected battery runtime with a 2000mAh battery in both modes are shown in table 12.

ESP	Component(s)	Avg current	Total I(mA)
ESP-1	ESP32 CPU	30 mA[51]	33.9
	IMU: MPU-6050	3.9 mA[38]	
ESP-2	ESP32 CPU	30 mA[51]	56.41
	Pulse Oximeter: MAX30102	2.21mA	
	RTC: DS3231	200 μ A[47]	
	Screen + MicroSD Module	24 mA [45]	
ESP-3	ESP32 CPU	30 mA[51]	

	Microphone	Mode 1: 600 μ A Mode 2: 10 μ A [43]	Mode 1: 30.765 Mode 2: 30.175
	Thermistor	0.165 mA	

Table 10. Average current consumption of each ESP32 and its connected modules, showing per-component contributions and the resulting total current in Mode-1 and Mode-2.

ESP	Baseline Components	Mode-1 Wi-Fi (mA)	Total Mode-1 Current (mA)	Mode-2 Wi-Fi (mA)	Total Mode-2 Current (mA)
ESP-1 (Node)	33.9 mA	0.119	34.2	0.065	33.96
ESP-2 (Hub)	56.41 mA	0.203	56.6	0.115	56.5
ESP-3 (Node)	Mode1: 30.765 mA Mode2: 30.175 mA	0.117	30.9	0.064	30.2

Table 11. Final Average Current Consumption of Each ESP

ESP	Runtime - Mode1	Runtime - Mode2
ESP-1 (Node)	58.48h	58.9h
ESP-2 (Hub)	35.34h	35.4h
ESP-3 (Node)	64.72h	66.23h

Table 12. Expected battery runtime per ESP on 2,000 mAh

The estimated runtimes with a 2000 mAh battery, based on the computed totals, are approximately 35 hours for ESP2 (hub) and 65 hours for ESP3, and 58 hours for ESP1. With ESP-2 restricting overall duration because of the increased load of the SD card and display, this is equivalent to several nights of operation on a single charge. The difference in power consumption between Mode-1 and Mode-2 is small because the microphone and Wi-Fi contribute only a minor share compared to the constant baseline draw of the ESP32 and other sensors. As a result, disabling the microphone and halving the packet rate leads only a modest gain in runtime.

However, under real-world circumstances, runtimes will differ based on several variables, including temperature, battery health and age, packet transmission retries, and many more. Practical runtimes are usually a shorter than the theoretical predictions. The analysis, however, indicate that each node can operate comfortably through the night and can typically run for several nights in a row before needing to be recharged. The actual runtime test results would be reported in validation chapter.

2.4 Event Detection Algorithms

With the hardware architecture defined, the next step is to define the algorithms that process the acquired signals. While the sensors and system architecture assure consistent data collection, the signal processing and event detection algorithms ultimately determine how well apnoea, hypopneas, and other sleep characteristics may be recognised. This section illustrates how features from airflow, effort, oximetry, and acoustic signals are extracted and transferred to AASM scoring standards for automated analysis.

Breathing and effort estimation algorithms

The thermistor detects the temperature of inspired (cooler) and expired (warmer) air directly at the nostril, resulting in a cosine looking waveform as shown in figures 7,8,10 and 11 whose

absolute level wanders slowly with ambient temperature and are also sensitive to probe position, while the breath-to-breath swing contains airflow information. The accelerometer, which is placed on the abdomen, records the motion of the abdominal wall. Its trace is based on a relatively constant gravity offset by a tiny oscillation at the breathing rate, this also resulting in similar looking and varying signal as thermistor. These signals are complementary: the thermistor is close to airflow but sensitive to temperature drift, whereas the accelerometer is temperature-independent but sensitive to body motion.

To do controlled assessment of implemented algorithms, traces that mirror the signals can be created and utilised. For either thermistor absolute temperature or abdomen accelerometer values, a simple sample signal can be defined as, $x(t) = A(t) \sin(2\pi f_0 t + \phi) + D_0 + D_1 t + e(t)$ where f_0 is the breathing frequency, $e(t)$ is noise signal, $A(t)$ is the amplitude of the signal and D_0 and D_1 are constants to create drift effects. $A(t)$ is varied over time to mimic normal, reduce and no breathing or effort.

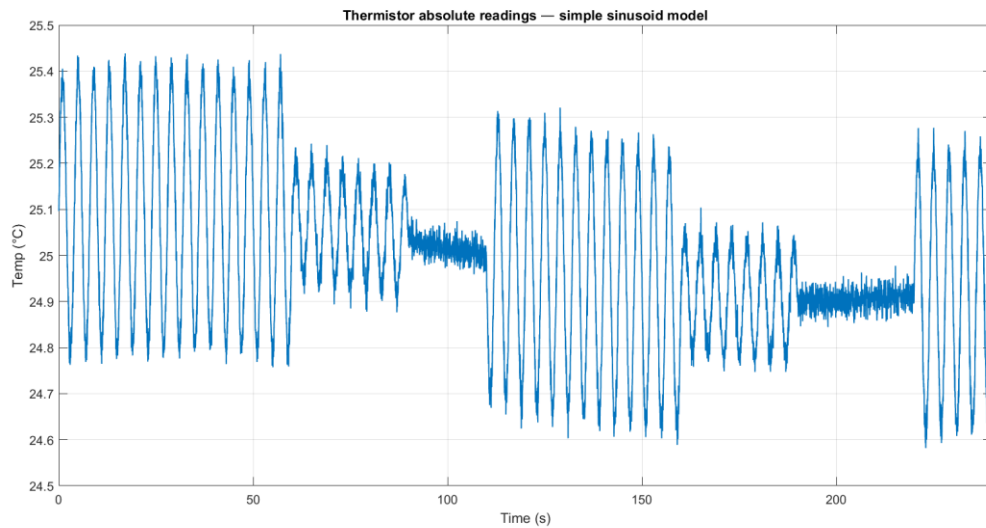


Figure 24. Simulated nostril-thermistor absolute temperature waveform generated with the simple sinusoid model with breathing frequency 0.25 Hz. The amplitude varies to mimic normal, reduced and no airflow. A very slow drift and small white noise were added to get close to real recordings.

Now for analysis, to get the AC signal from this thermistor absolute trace, IIR filtering is performed, for the IIR filter, $\alpha = 1 - e^{-2\pi f_{cutoff} / f_{sampling}}$. To smoothen the temperature signal and remove 50Hz and other high frequency noise, applying a simple low pass filter, if $x[n]$ is the input of the filter, the output is $y[n] = (1 - \alpha)y[n - 1] + \alpha x[n]$ [52]. Sampling frequency is 25Hz and the cutoff frequency is set to 0.8Hz. This is good enough for breathing signal (translates to $0.8 * 60 = 48$ breaths/min). After this filtering, most of the noise is removed and AC + DC + drift is present. The signal of interest is only AC as it indicates the actual change in airflow. To calculate the DC and drift signals, applying a simple low pass filter $d[n] = (1 - \alpha)d[n - 1] + \alpha x[n]$ with very low cutoff frequency of 0.02Hz, this ensures the filtered output contains only constant DC signal and very low frequency drifts. Then this signal is removed from the output of previous filter signal, that gives the AC signal, $a[n] = y[n] - d[n]$. The same can be achieved with a single bandpass filter, but this approach of 2 simple IIR filters are easy to implement in microcontroller and requires less computation. The outcome AC is the grey background waveform in the figure 25.

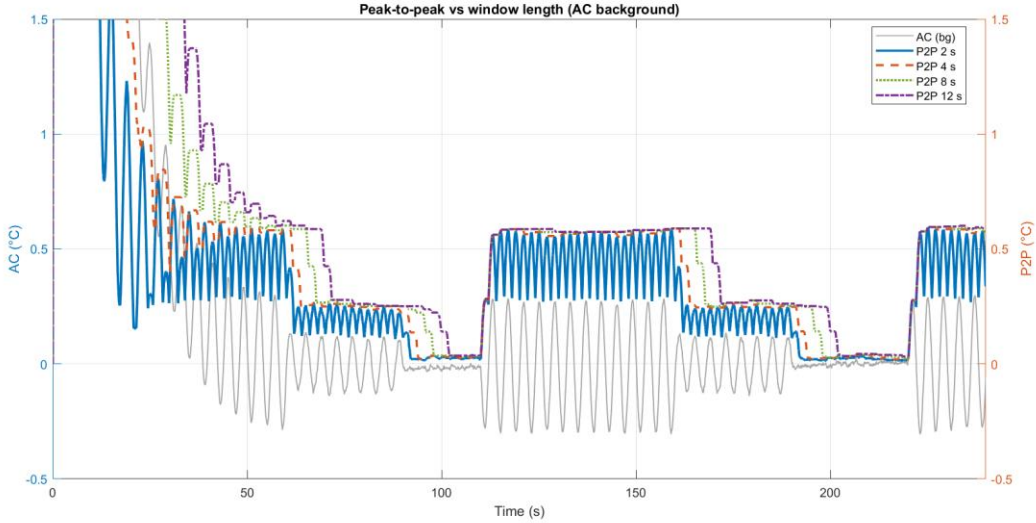


Figure 25. Peak-to-peak amplitude vs. window length for the band-limited thermistor AC signal. Grey trace: AC waveform (left axis). Moving P2P with 2, 4, 8, and 12 s windows (right axis). Short windows track changes quickly but are noisier; long windows are smoother but show delayed and smeared transitions

Peak-to-peak (P2P) is then calculated as a sliding window maximum minus minimum over the AC signal, with four window lengths (2, 4, 8, and 12 seconds). Shorter windows (2 s) respond almost rapidly to amplitude changes and closely track peaks, but they exhibit more ripple from cycle-to-cycle fluctuation. Longer windows (8-12 s) are smoother and produce stable peak values, but they lag at transitions and spread across segment boundaries since each estimate still contains samples from the past state, this is why the 12 s curve descends/ascends more slowly at 60 s, 90-110 s, 160 s, and so on. During no-effort periods (90-110 s and 190-220 s), all curves fall to zero, with the longer windows needing a few seconds to decay due to memory.

P2P is a good indicator of changes in airflow, another way to track the change is to plot the envelope of the signal, if the same simple 1-pole IIR filter is applied twice on the AC ($|a[n]|$) instead of raw signal once with a short time constant (0.8 s) and once with a long time constant (25 s), two envelopes with very different behaviours can be seen as shown in figure 26.

For the IIR filter, $\alpha = 1 - e^{-2\pi \frac{f_{cutoff}}{f_{sampling}}}$. The short or faster following envelope signal is expressed as $e_s[n] = e_s[n - 1] + \alpha_s(|a[n]| - e_s[n - 1])$ [52] and similarly the longer or slower following envelope signal is expressed as $e_l[n] = e_l[n - 1] + \alpha_l(|a[n]| - e_l[n - 1])$. This filter is also called as Exponential Moving Average (EMA) as it's a moving average whose weights decay exponentially with sample age, the newest sample has weight α , the one-before has $(1 - \alpha)\alpha$, the next $(1 - \alpha)\alpha^2$, and so on. The floor value is a lower bound imposed to the envelope so that the system does not interpret tiny, noise-dominated magnitudes to be actual breathing. If set too low it leads to false positives in quiet periods, if set it too high it leads to missed small efforts.

Within a breath or two, the short envelope (blue) collapses to near the floor with no effort. The lengthy envelope (orange) decays gradually, so it remains elevated for several seconds after a dip and slowly increases when effort is resumed. This dynamic distinction implies that immediately after effort returns, shorter envelope jumps but longer envelope remains low, resulting in a good short/long ratio, whereas throughout lengthy stable portions, both converge to same values. In comparison to the P2P plot, short can be viewed as the IIR analogue of a small P2P window (faster, noisier) and long as the analogue of a long window (slower, more

stable). The advantage here is that both come from the same filter form with only one parameter variation (τ).

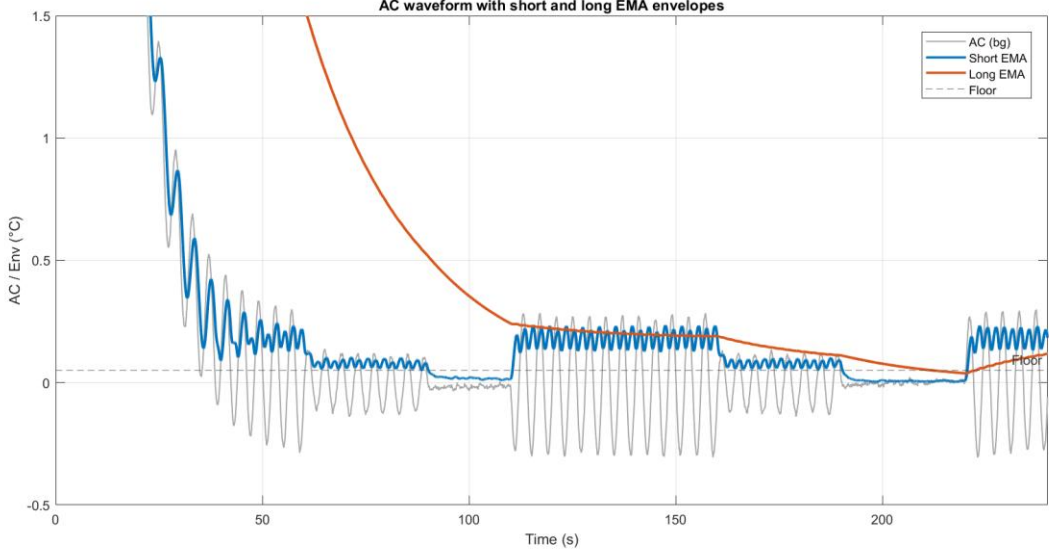


Figure 26. Thermistor AC (grey) with short and long envelopes of the rectified AC, computed using the same first-order low-pass with different time-constants. The dashed line marks the absolute-envelope floor ($0.05\text{ }^{\circ}\text{C}$). Short tracks breath-to-breath changes, long provides a slow baseline that lags at transitions.

A study by Varris et.al [53] used the difference of upper and lower envelopes to classify apnoea and hypopnea. In this study, ratio of smaller and longer envelopes is explored. Ratio = $\frac{e_s[n]}{e_l[n]}$, to avoid divide-by-near-zero in quiet periods, the denominator of the ratio is defined as, $base[n] = \max(e_l[n], 80\% \text{ of } floor)$, the alternate values 90 and 100% can also be used, the ratio becomes slightly tighter in that case. This ratio curve is shown in figure 27. To automate the effort classification, the state machine drawn in figure 28 can be used.

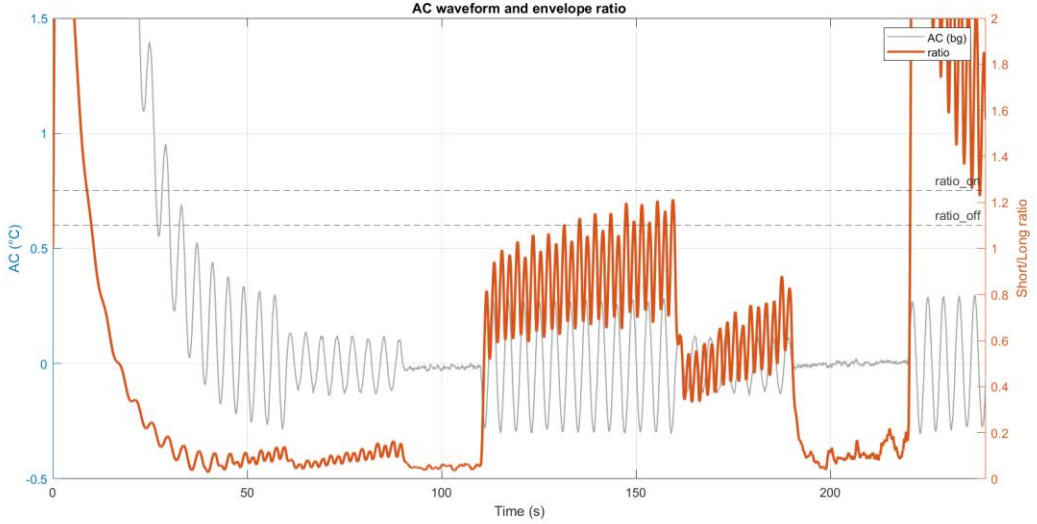


Figure 27. AC waveform (grey, left axis) and short/long envelope ratio (orange, right axis). The ratio on=1.25 and is ratio off= 1.10. The ratio falls in reduced/no-effort segments and spikes at effort resumption because the short envelope outruns the long baseline.

From figure 27, during continuous normal effort, the short and long envelopes track equally, thus the ratio is approximately 1.1-1.2. When effort is reduced, the short envelope declines

immediately while the long decays slowly, hence, the ratio progressively goes below 1 and approaches the off region. In no-effort segments, the short envelope sinks towards the floor while the long is clamped by the base term, causing the ratio to collapse towards zero, accurately reflecting the absence of oscillation. When breathing restarts, the short envelope jumps within a breath, but the long remains low, causing the ratio to spike above the on threshold before relaxing when the long baseline catches up.

A single threshold would turn on/off repeatedly if signal wobbles at threshold. To improve this, hysteresis can be used, once effort detected, it must drop further (≤ 1.10) to change as no effort, and once marked no effort, it must rise higher (≥ 1.25) to turn as effort label therefore produces stable labels. Short spikes can temporarily boost short envelope, so a confirmation time of at least few seconds can be added for better stability. Similarly, rapid drops do not drop below ratio off long enough to flip the label.

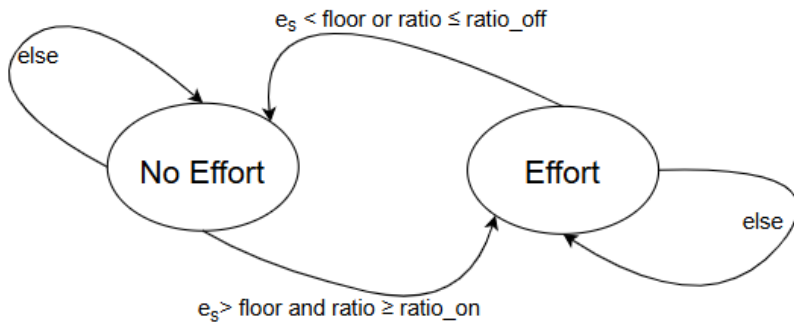


Figure 28. State machine diagram for respiratory effort classification using the short/long envelope ratio.

The disadvantage of this method is that ratio entirely depends on ac amplitude which itself is dependent on many factors. The thermistor AC swing is roughly proportional to $|exhaled - inhaled temperature| \times \text{airflow}$ and inversely proportional to distance from nostril. If the thermistor bead touches the skin, then skin temperature also comes into play. Therefore, whenever there is a decent ac amplitude, ratio of these envelopes is a good feature to classify the effort (IMU signal) or presence of breathing (Thermistor signal), but not reliable otherwise.

The other way to follow ac signal is the root-mean-square (RMS) amplitude, RMS computed over sliding windows of 2, 4, 8, and 12 seconds are shown in figure 29. It measures average signal energy and is never negative. Across the period, the RMS curves follow the same pattern as P2P, high flats during normal effort, lower flats at reduced effort, and collapse towards the RMS floor in zero-effort intervals. Short windows (2 s) respond quickly but have more ripple, long windows (8-12 s) are smoother but lag at transitions because they keep samples from prior states.

The final method explored for classifying respiratory effort in both the nostril-thermistor and abdominal-accelerometer signals that are independent from amplitude as shown in figure 30, the zero crossing methods were used as a complementary metric for classifying airflow signals in few studies [54,55], it transitions from amplitude to oscillation indications. Starting with the same AC signal (grey), residual DC can be eliminated by removing a short-time EMA (the same single pole IIR equation) at the preferred analysis rate (3 s in figure 30). This removes very-low-frequency wiggle, so the signal is centred at zero and crossings are counted. The result (blue dashed), which now oscillates around zero when breathing occurs. A 6 s window over the signal is implemented to count only sign changes that cross a small amplitude floor ($\pm 0.05^\circ\text{C}$ in figure 30), resulting in the orange step trace. The dashed horizontal line indicates

minimum zero crossings = 2 over a 6 second window, which is the threshold set to establish the presence of a breathing (thermistors signal AC) or effort (accelerometer signal AC).

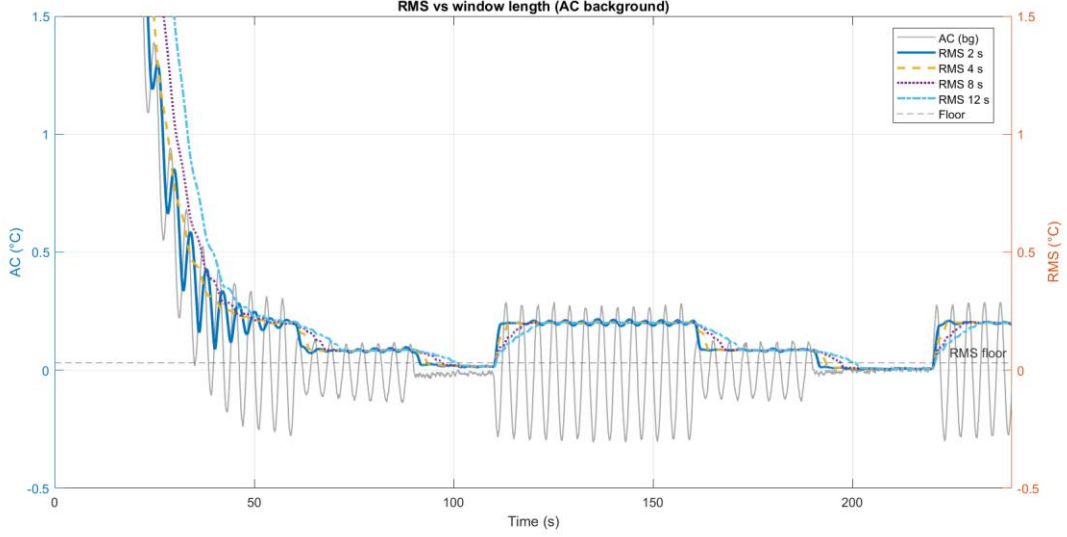


Figure 29. RMS vs window length for the thermistor AC signal. Grey: AC waveform (left axis). Sliding RMS with 2/4/8/12 s windows (right axis). Short windows are responsive, long windows are stable but lag at changes. The dashed line marks the RMS floor used to suppress noise-only intervals.

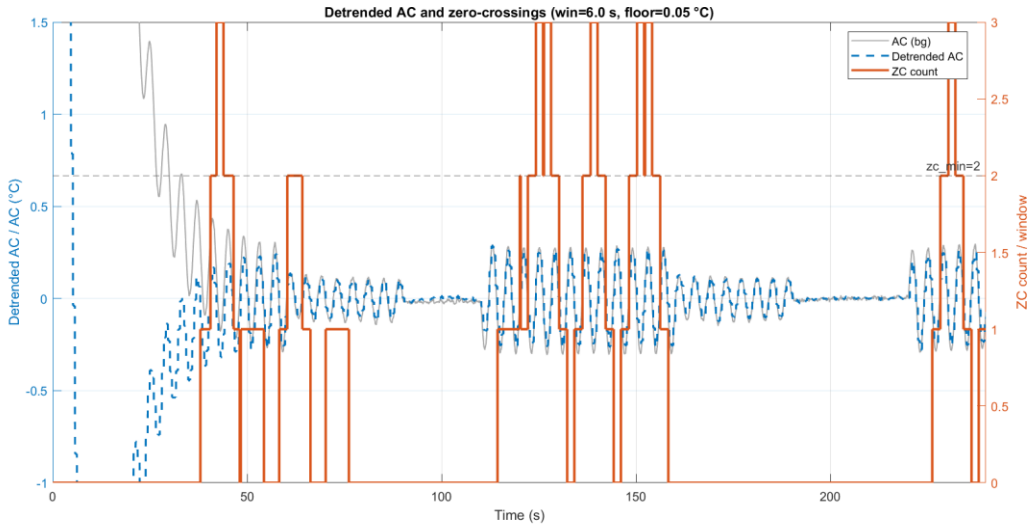


Figure 30. Detrended thermistor AC and zero-crossing (ZC) count. blue dashed: detrended AC after subtracting a short-time EMA baseline ($\tau=3$ s); orange: ZC count in a 6 s sliding window, counting only sign flips exceeding ± 0.05 °C.

Reading the plot from left to right, in normal-effort, the detrended signal has clear zero-centred waves, and the windowed count is around 2-3 crossings every 6 s. During reduced effort, amplitude decreases, and many cycles fail to exceed the floor. During no-effort intervals, the waveform remains near zero with no threshold crossings, resulting in a count of 0. This complements the envelope ratio. The detrend removes drifts, and only continuous oscillation results in counts ≥ 2 . It is useful if amplitude metrics are confusing or not effective, however, relying on zero crossings alone is not a good approach because it depends strongly on the chosen floor and window length.

There is no single parameter configuration or algorithm that works in all situations and every user. Real recordings are more complex than simple sinusoid model used in this section, with

irregular rates, posture changes, sensor position drift and motion artefacts. A better approach is to use multiple complimentary detectors.

For the final build, both envelope and oscillation detectors are used by the thermistor (ESP3) and IMU (ESP1) to determine the effort in real time. The IMU selects the posture-appropriate axis (X for supine/prone, Z for left/right), whereas the thermistor uses the same detectors on recorded nasal temperature. To summarise the implementation, each signal is first band-passed using basic first-order IIR filters to produce AC, the envelope detector watches both a rapid and a slow envelope and uses their ratio with a small absolute floor. After detrending the AC signal and maintaining a small buffer, the oscillation path verifies that zero-crossings surpass a minimum and RMS surpasses a floor.

When the signal is too low and steady, the samples are flagged quiet to prevent false positives. On the IMU, this is accomplished by using inertial quietness (low gyro RMS and small accel deviation) and envelope is very small, on the thermistor, it is accomplished by using the envelope alone.

Every sample is annotated with a reason code (0 = no conditions met, 1 = envelope), 2 = oscillation, 3 = both, 4 = quiet/no effort) indicating which detector turned effort on and a 0 to 1 confidence level derived from normalised envelope and oscillation thresholds, allowing to plot decisions and to demonstrate why and how strong a decision had been made.

$$Effort\ Confidence = \max (Confidence_{Envelope}, Confidence_{Oscillation})$$

$$Confidence_{Oscillation} = Magnitude_{oscillation} = \frac{RMS - RMS_{min}}{2RMS_{min}}$$

$$Confidence_{Envelope} = Magnitude_{env} \times Ratio_{env} = \frac{Env_{Short} - Env_{min}}{2Env_{min}} \times \frac{r - r_{off}}{r_{on} - r_{off}}$$

Where Env_{Short} is fast envelope, r = envelope ratio, RMS_{min} = RMS floor, RMS = RMS over the oscillation buffer and Env_{min} = absolute envelope floor.

Pulse oximetry algorithms

The SpO_2 and Heart rate are calculated from the PPG signal detected using MAX30102, The MAX30102 sensor samples at 100 Hz in dual-LED mode (IR/RED). Processing takes place on overlapping windows with a set length of N=256 samples (about 2.56s) that are moved every 500 ms to match the mode-2 output rate. In practice, the effective frequency is observed slightly varying from the sensor. Therefore, the effective sampling rate is calculated over every 10 s by calculating delta between samples.

As mentioned in section 2.3, the AC and DC signals from the PPG are used for SpO_2 and FFT is performed on IR signal for heart rate. The LED brightness set to 0x64 (from range 0x00 – 0xFF), pulse width 411 ns, and both IR/RED pulse amplitudes set to 0x24. With these settings, it is observed that a proper contact gives a substantial DC (above 30000) counts on both wavelengths, to prevent against no-finger or poor-contact if IR and RED DC < 20000, the samples are not considered for calculation and SpO_2 is suppressed to -1 by default to indicate invalidity at that sample.

SpO_2 and Heart rate are calculated for every window, within each window, the DC is the mean of the raw sensor readings, the AC is the RMS of the band-passed waveform, this band-pass is

implemented by combination of low pass and high pass for easier implementation on microcontroller, and SpO₂ is derived from the standard ratio of ratios (R).

$$R = \frac{(AC/DC)_{Red}}{(AC/DC)_{IR}}$$

$$SpO_2 = C1 + C2 \times R = 110 - 25R$$

FFT of the IR AC is used to detect HR. For an N-point FFT of a signal sampled at F_s, the complex values X[n] are obtained for n = 0 to N-1. Each index n is a bin that corresponds to a frequency, F_n = $\frac{n}{N} \times F_s$ and the frequency resolution is $\Delta f = \frac{F_s}{N} = \frac{100}{256} = 0.39\text{Hz}$. Heart rate (in bpm) from a frequency f is HR = 60f, So one bin equals $0.39 \times 60 = 23.4$ bpm. To reduce bpm per bin, N can be increased, with N = 2048, bpm per bin is 2.93 but window size needs to be $N \times F_s = 20.48$ seconds, which introduces significant latency. Instead, the peak is searched with N = 256 only in 0.6–3.0 Hz band (36–180 bpm), so $n_{min} = 0.6 \times \frac{N}{F_s} = 1.53 \approx 2$ and $n_{max} = 3 \times \frac{N}{F_s} = 7.68 \approx 8$. From these bins, around the tallest bin, the (windowed) FFT magnitude looks like a smooth curve.

Parabolic interpolation is used to find maximum value of the curve [56], by fitting a parabola to the three points (n-1, a), (n, b), (n+1, c) where b is the local maximum on FFT magnitude curve, the estimated true peak is at $\delta = \frac{1}{2} \times \frac{a-c}{a-2b+c}$ [56], taking a = |X[n - 1]|, b = |X[n]| and c = |X[n] + 1|. Therefore, $F_{est} = \frac{n+\delta}{N} \times F_s$, which gives $HR_{est} = 60F_{est} = 60 \times \frac{n+\delta}{N} \times F_s$. This fitting method helps turning a 23.4 bpm step into roughly 3 to 5 bpm without increasing N. To reject windows with negligible pulse, a threshold is set to AC to DC ratio of IR, and it should be at least 0.02%. If this condition is failed, -1 is returned indicating HR is not assessed. The final HR is smoothed with averaging current value with 50% weight and past 2 values with the other 50% weight to reduce spikes and dips.

Audio algorithm

The ESP3 uses a microphone and samples audio at 8 kHz. The microphone approach is specifically intended to detect snoring during sleep. Each analysis frame contains 1024 audio samples (about 128 ms at 8 kHz) that are buffered and passed through a window for spectral analysis with a Fast Fourier Transform (FFT).

The FFT output gives a magnitude spectrum ranging from 0 to 4 kHz (Nyquist). However, around 500-1500 Hz band is considered important for snoring, as literature [57] and 2 different snoring audio analysis (with higher sampling and analysis rate) shown in figures 31 and 32 show that snore sounds are often broadband with prominent components around this range. A peak-search is performed inside this band to extract features, maximum spectral magnitude, dominant frequency and averaged absolute amplitude. A snore decision is then made using a set of threshold rules applied on these frequency and time domain features. If spectral magnitude exceeds a fixed threshold, set at 15000, dominant frequency within expected snore band, average amplitude exceeds a fixed level, set at 10000, indicating the snore loudness, that frame is labelled as snore.

Snore Detection Features & Decision

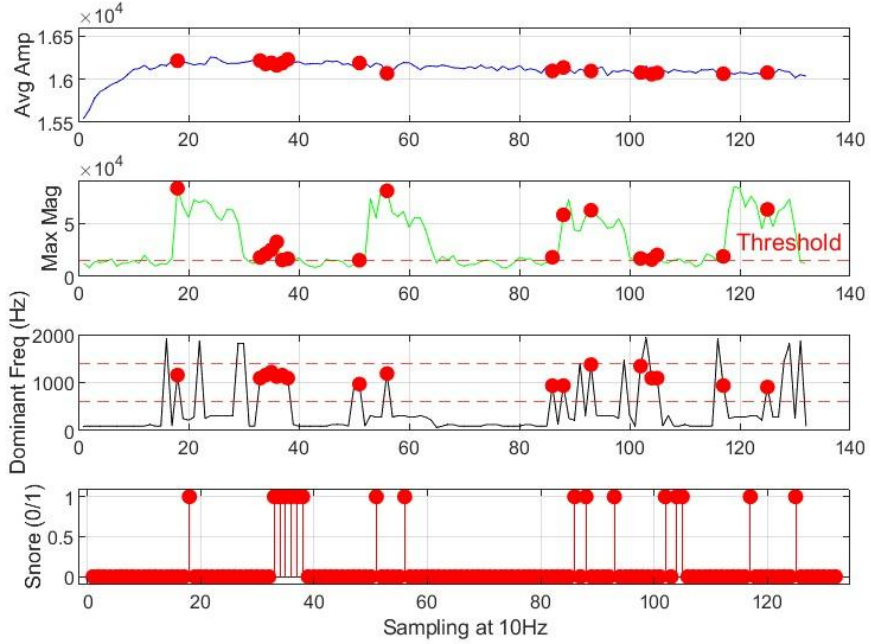


Figure 31. Snore detection features extracted from ESP3 microphone during playback of constant snoring (mic sample rate = 16 kHz, buffer = 512, frame = 100 ms, amplitude averaged for past 10 samples).

Snore Detection Features & Decision

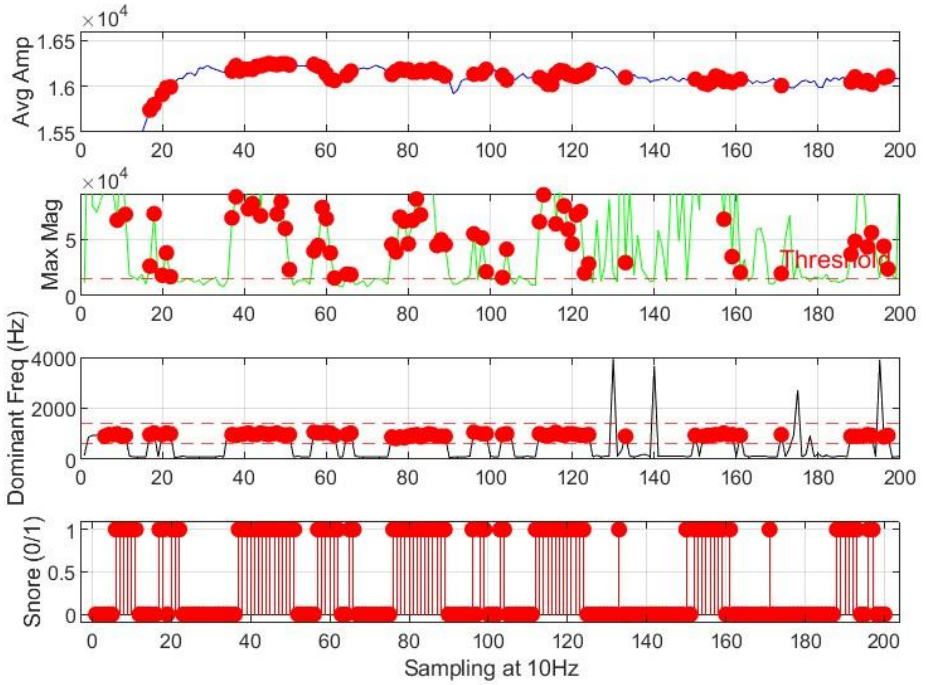


Figure 32. Snore detection features extracted from ESP3 microphone for a second constant snoring recording (mic sample rate = 16 kHz, buffer = 512, frame = 100 ms, amplitude averaged for past 10 samples).

The figures 31 and 32 shows that the system can detect snoring characteristics using a mix of amplitude, spectral magnitude, and dominant frequency criteria. Red marks indicate frames that fulfil the detection criteria, while the final binary output labels snoring portions.

From the first snoring audio plotted in figure 31 the average amplitude remains relatively stable, with intermittent frames exceeding the detection threshold (red markers). The maximum spectral magnitude has bursts in the 500–1500 Hz band, with several peaks clearly crossing the set threshold, corresponding to snore-like events. The dominant frequency mostly lies within the snoring band. The decision output (bottom) shows detected snore intervals, where all three conditions are simultaneously satisfied. The detection is consistent, with snoring events corresponding to the played recording.

In figure 32, another snoring audio recording is used, the average amplitude is higher and more stable than in the previous audio. The maximum spectral magnitude exhibits more fragmented bursts, although it still crosses the threshold regularly. The dominating frequency is again mostly confined within the snoring range. The final output shows extensive periods of continuous snore detection, indicating the persistence of acoustic energy and frequency content within the expected snoring range. Compared to Figure 31, the detections are more maintained. However, variations in amplitude (placement of microphone) can heavily affect detection.

Although the spectrum runs from 0 to 4 kHz, the peak search is restricted to 500-1500 Hz and expected to cross a magnitude threshold as this is range of interest for snoring. This band-limited search ensures fewer false positive but have an obvious side effect. The dominant frequency output will always be between 500-1500 Hz. If the dominant tone in a frame is less than 500 Hz, the strongest bin within the search window will line up along the bottom edge. If dominant tone exceeds 1500 Hz, it saturates towards the upper margin of the search band. Therefore, to prevent mislabelling these edge situations, detection uses a tighter acceptance band of 600-1400 Hz for dominant frequency to rise snoring flag. The features are still searched in 500-1500 Hz. The trade-off is this is counter measure although gets rid of false positives will also miss to catch true positive snores in bands below 600 and above 1400 Hz.

Sleep Posture detection algorithm

Sleep posture detection is based on the accelerometer outputs of the body-worn IMU (ESP1). The sensor is required to always orientated with the y-axis pointing from head to foot, the x-axis spanning left to right across the body, and the z-axis pointing vertically while supine as shown in figure 33. Using this as a stable reference frame, multiple sleep postures are inferred directly from the accelerometer's observed gravity vector.

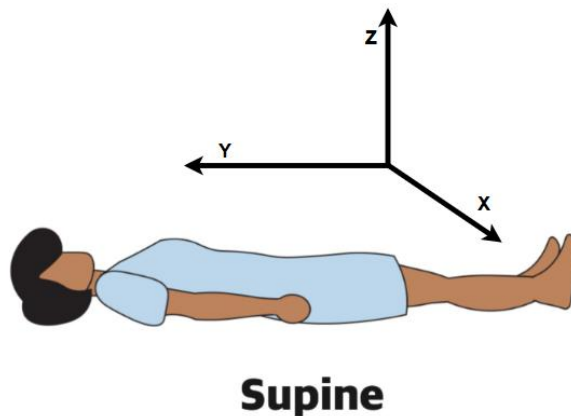


Figure 33. Reference orientation of the IMU axes when worn on the body. The y-axis is aligned along the head-to-feet direction, the x-axis spans left-right, and the z-axis points upward when supine. This orientation was used as the basis for posture classification (sleeping human icon adapted from [58])

The classification was based on the main axis of gravity compared to a threshold (set at 70% of g). If the z-axis was close to +g, the user was lying on their back (supine) as shown in figure

33, if $-z$ dominated, they were prone. Similarly, a large $+x$ denoted right lateral position, whereas a $-x$ indicated left lateral position. A significant y -axis component was regarded as standing or upright seating. If none of these criteria were met (during transition between postures), the posture was labelled unknown. Additionally, to record user movement during sleep each sample is labelled as still if the gyro-RMS is less than 0.3 rad/s and the acceleration deviation from constant g is less than 1.2 m/s^2 , otherwise as moving.

Wireless Communication Setup and Data Logging

All ESPs run in Wi-Fi station (STA) mode and must join the same access point (phone hotspot or home router). Although devices are on same network, IP addresses change over time and across reconnections. To make devices discoverable regardless of IP changes, all the 3 ESPs uses mDNS (ESPmDNS library) so they can be reached by name: esp1.local, esp3.local, and sleep-hub.local.

ESP1 (the IMU node) and ESP3 (the microphone and thermistor node) transmit sensor data to the hub over port 5005 (initiated using WiFiUpd library). Every data packet begins with a header, which makes each message self-describing and useful for ordering. The header packet structure is shown in table 13, dev_id indicates which node produced the data (1 for ESP1, 3 for ESP3), mode identifies the sender's current mode, payload_len allows the receiver to validate the number of bytes that arrive. seq is a continuously increasing counter used for ACK/duplicate detection, and t_ms records the sender's local millisecond timestamp at send time. This header enables the hub to accept data from different nodes on the same port without ambiguity, detect fails or resends based on sequence number, and align data using timestamps.

Field	Type	Size	Description
dev_id	uint8_t	1 byte	Device ID: 1=ESP1 (IMU), 2=Hub 3=ESP3 (Mic + Thermistor)
mode	uint8_t	1 byte	Operating mode (1=Mode-1 (2 Hz), 2=Mode-2 (1 Hz))
payload_len	uint16_t	2 bytes	Length of the data in bytes
seq	uint32_t	4 bytes	Sequence number, incremented for each transmission (used for acknowledgment, /retry)
t_ms	uint32_t	4 bytes	Device's local timestamp in milliseconds

Table 13. Details of Common Packet Header, all data packets start with this header.

After the header follows the node-specific structured data as shown in table 14 for ESP1 and table 15 for ESP3. For ESP1, the packet contains raw IMU data (ax , ay , az , gx , gy , and gz) as well as breathing effort features. For ESP3, the packet contains audio information from the 8 kHz/1024-point FFT and the thermistor data and features, and an apnoea event indicator. Keeping these data fixed size allows packets to easily appended to the CSV log.

Field	Type	Size	Description
ax , ay , az	float	12 B	Accelerometer values (m/s^2) in X, Y, Z.
gx , gy , gz	float	12 B	Gyroscope values (rad/s) in X, Y, Z.
env	float	4 B	Envelope magnitude of the filtered breathing effort signal.
ratio	float	4 B	Ratio of short-term vs. long-term envelope (effort detection feature).
rms	float	4 B	RMS of detrended acceleration values (breathing strength).
zc	uint8_t	1 B	Zero-crossing count in oscillation buffer
posture	uint8_t	1 B	Posture classification: 1=Prone, 2=Right, 3=Left, 4=Supine, 5=Sit/Stand, 0=unknown

motion	uint8_t	1 B	0=Still, 1=Moving
effort	uint8_t	1 B	0>No effort, 1=Effort detected (respiratory effort).
why	uint8_t	1 B	Detector reason: 0=no conditions met, 1=A (envelope), 2=B (oscillation), 3=A+B(both), 4=Q (quiet/no effort).
conf	float	4 B	Confidence score (0–1), based on envelope/oscillation strength, discussed in validation section.

Table 14. Details of data packet from ESP1(IMU).

Field	Type	Size	Description
avgAmplitude	int32_t	4 B	Average absolute microphone amplitude (loudness).
maxMagnitude	float	4 B	Maximum spectral magnitude in FFT (dominant peak strength).
dominantFreq	float	4 B	Frequency (Hz) corresponding to the spectral peak (snore band detection).
snoring	uint8_t	1 B	0>No snore, 1=Snore detected (if peak within 600–1400 Hz band).
tempC	float	4 B	Absolute thermistor-derived temperature (°C).
env	float	4 B	Envelope of filtered thermistor breathing signal.
ratio	float	4 B	Ratio of short-term vs. long-term thermistor envelope.
rms	float	4 B	RMS of detrended thermistor signal (breathing effort strength).
zc	uint8_t	1 B	Zero-crossing count in thermistor oscillation.
effort	uint8_t	1 B	0>No effort, 1=Effort detected.
why	uint8_t	1 B	Detector reason: 0=no conditions met, 1=A (envelope), 2=B (oscillation), 3=A+B(both), 4=Q (quiet/no effort).
conf	float	4 B	Confidence score (0–1), based on envelope/oscillation strength, discussed in validation section.
apnea	uint8_t	1 B	1=Apnoea episode (no effort for >10 s), 0=Normal.

Table 15. Details of data packet from ESP3(Mic and Thermistor).

At the hub, this received data packets is used in three ways. the hub instantly returns a small acknowledgement packet as shown in table 16 to the sender via port 5006. Each node waits up to 150 milliseconds for this confirmation and can retry transmission up to twice in case of failure. Second, rows are appended to a CSV file on the microSD card for storage. Each row has 36 different parameters (data from all 3 ESPs) stored in 36 columns. Description of each column logged in SD is given in table 18. Each row is written only if the node's data arrived within a 3 s else the corresponding fields are written as -1 placeholders. Third, the hub sends the same data row across port 8000 for remote capture or live plotting. This path is intended for a PC program rather than a microcontroller, and any desktop tools like MATLAB, Python, or a custom dashboard connected to same Wi-Fi network can be used to listen, save this data and plot any of those 36 parameters in real time. In this project MATLAB is used collect data from port 8000.

Field	Type	Size	Description
dev_id	uint8_t	1 B	Device ID of the sender being acknowledged.
seqAck	uint32_t	4 B	Sequence number being acknowledged (matches seq in original packet).

Table 16. Details of acknowledgment packet from hub to nodes.

A different port 5007 and small packet as shown in table 17 is used to handle system-wide time synchronisation and mode control. Once per second, the hub broadcasts this SYNC so any device on the network can listen.

Field	Type	Size	Description
msgType	uint8_t	1 B	1=SYNC (time), 2=MODE_SET.
targetDev	uint8_t	1 B	Target device (0=all, or specific device ID).
epoch_ms	uint32_t	4 B	Hub's system time in ms (for aligning timers).
mode	uint8_t	1 B	Current operating mode (1=Mode-1 (2 Hz), 2=Mode-2 (1 Hz)).

Table 17. Details of sync packet from hub to nodes. To sync mode and time.

To avoid drifts in time, every data packet header in this system contains t_ms, the sender node's own millisecond clock (since boot), which is captured when the measurement was taken. This allows the hub to analyse actual time independently of Wi-Fi delays or retries, order samples correctly. In the meantime, the hub's SYNC messages that includes epoch_ms, the hub's millisecond clock (since boot) at send time. Nodes use this information to estimate their time offset and drift in relation to the hub, align their time with the hub's timeline for driftless communication.

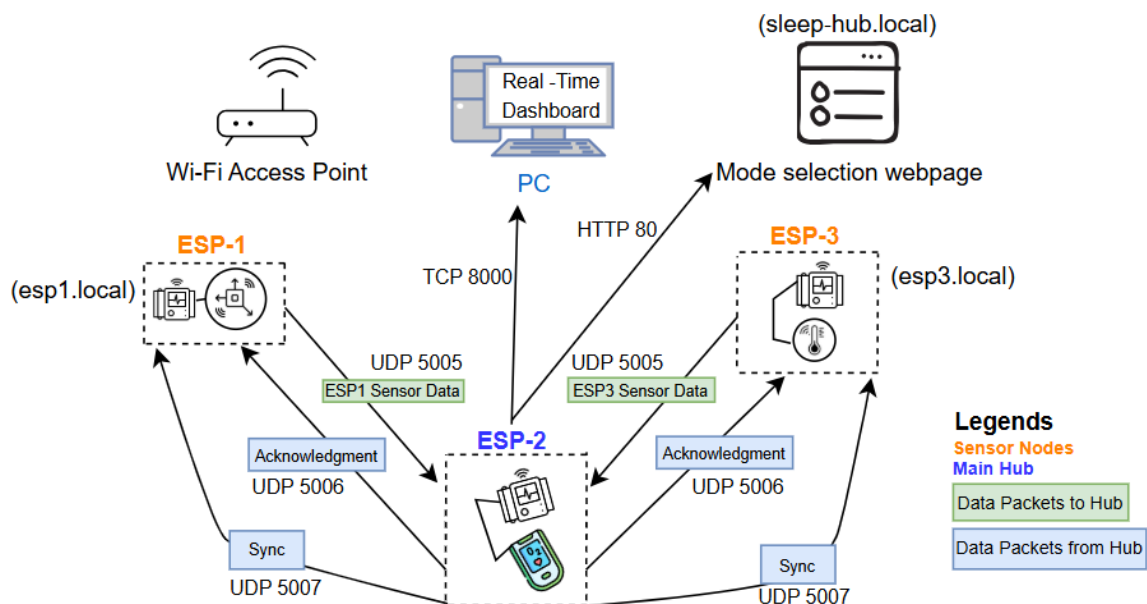


Figure 34: System-level communication architecture of the sleep monitoring setup. Data is bridged to a PC client over TCP port 8000 for real-time dashboard, while a web interface for mode switching is over HTTP port 80. All devices connect through a common Wi-Fi access point and are discoverable using mDNS (esp1.local, esp3.local, sleep-hub.local).

Finally, the hub on port 80 serves a very simple web interface implemented with the ESP32 WebServer library serving a simple HTML page with two buttons for mode selection. For all ESPs to have to the same mode, when button clicked the hub updates its mode and sends out a SYNC message with new mode, this html page can be assessed at IP address or mDNS of hub, at sleep-hub.local in a browser. The complete wireless setup with data packets, ports and services are summarised in figure 34.

Column Number	Column Name	Description (units / values)
1	Date	dd-MM-yyyy (RTC)
2	Time	HH:mm:ss (RTC)

3	Mode	Mode: 1=2 Hz, 2=1 Hz
4,5,6	ax, ay, az	Acceleration X, Y, Z (m/s ²)
7,8,9	gx, gy, gz	Gyro X, Y, Z (rad/s)
10	Posture	0–5 (Unknown/Prone/Right/Left/Supine/Stand)
11	Motion	0/1 (excess motion)
12	Env	IMU envelope magnitude (m/s ²)
13	Ratio	IMU fast/slow envelope ratio (unitless)
14	RMS	IMU RMS of band-passed signal (m/s ²)
15	ZC	IMU zero-crossings (count)
16	Effort	IMU breathing effort (0/1)
17	Why	IMU reason: “A”, “B”, “A+B”, “Q”, “-”
18	Conf	IMU confidence 0–1
19	TempC	Nostrils air temperature (°C, smoothed)
20	EnvT	Thermistor envelope (°C)
21	RatioT	Thermistor fast/slow ratio (unitless)
22	RMST	Thermistor RMS (°C)
23	ZCT	Thermistor zero-crossings (count)
24	EffortT	Thermistor effort 0/1
25	WhyT	Thermistor reason: “A”, “B”, “A+B”, “Q”, “-”
26	ConfT	Thermistor confidence 0–1
27	Snore	Mic snore flag 0/1
28	DFreq	Dominant mic frequency (Hz)
29	Mag	Peak FFT magnitude
30	Amp	Mean abs mic amplitude
31	Apnea	Apnoea pulse from ESP3 0/1 (instant)
32	IRdc	PPG IR level (ADC counts)
33	REDdc	PPG RED level (ADC counts)
34	SpO ₂	Oxygen saturation (%)
35	HR	Heart rate (bpm)
36	ApneaCount	Running apnoea counter

Table 18. Column map for each row in the SD card CSV log file, numbered fields with units and meanings. One row is written per sample (Mode-1: 2 Hz; Mode-2: 1 Hz), stale or missing or invalid data are recorded as -1.

2.5 Events to Signal features mapping

The system correlates collected signals and features to clinically relevant sleep events. The microcontroller detects breathing effort (normal vs quiet/no-effort), generates an apnoea pulse when thermistor effort is low for ≥ 10 s, detects snoring episodes, identifies motion/arousal, posture changes, and continuously estimates HR and SpO₂. It also displays the cumulative apnoea counter, HR, and SpO₂ on the screen. The real time mapping of these targeted sleep events to the recorded signals and features are summarised in table 19.

Real-Time Analysis on Microcontroller		
Sleep event	Signals watched	Rule / Trigger
Normal breathing	IMU (ax/az), Thermistor	Envelope (Short envelope \geq floor and ratio \geq ratio on) or Oscillation (ZC \geq minimum zero crossings and RMS \geq rms floor) detector ON and not Quiet:

		IMU: floor = 0.008, ratio on = 1.35, minimum zero crossings = 2 in 6 second window, rms floor = 0.006. Thermistor: floor = 0.050 °C, ratio on = 1.25, minimum zero crossings = 2, rms floor = 0.030 °C.
Quiet / No effort	IMU gyro RMS, acceleration deviation, envelope	Quiet: gyro RMS < 0.05, acceleration deviation < 0.20, and Short envelope < 1.3×floor (IMU) or short envelope < 1.2×floor (Thermistor).
Apnoea event	Thermistor effort state	Effort turns OFF and stays low ≥ 10 s
Snoring episode	I2S mic FFT (8 kHz, N=1024)	Dominant frequency is in 600–1400 Hz, spectral magnitude > 15000, and time-domain average amplitude > 10000.
Motion / Arousal	IMU gyro RMS, acceleration deviation	Motion flag when gyro RMS > 0.3 or acceleration deviation > 1.2, do not trust effort in this interval.
Posture change	IMU DC gravity alignment	Change in DC gravity axis orientation

Table 19. Real-time sleep event detection on the microcontrollers, signals monitored and the rule that triggers each event.

In addition, MATLAB is used for postprocessing following complete sleep recording. Using the fraction of IMU effort during the apnoea-occurred time window, each apnoea event is classified as central, obstructive, or mixed. Session-level summaries are then generated (SpO_2 minima and desaturations, HR extrema, postural time spending) as summarised in table 20.

The algorithms and sensing used in current setup do not quantify airflow, instead, they estimate effort based on IMU and thermistor envelopes/oscillations and cannot accurately differentiate between shallower than usual breaths and normal variability, since clinical hypopnea necessitates a quantifiable reduction in airflow ($\geq 30\%$ for ≥ 10 s with desaturation/arousal). Hypopneas were therefore excluded from the event counts.

Type of Apnoea: Post-Processing Analysis in MATLAB		
Sleep Event	Signals watched	Rule
Central apnoea	Apnoea event + IMU Effort	In the apnoea window, IMU effort present < 30% of samples.
Obstructive apnoea	Apnoea event + IMU Effort	In the apnoea window, IMU effort present > 70% of samples.
Mixed apnoea	Apnoea event + IMU Effort	In the apnoea window, IMU effort present between 30% to 70% of samples.
Additional reported post-processing measures in MATLAB		
Sleep Event	Signals watched	Data
Maximum and Minimum SpO_2	SpO_2	Maximum and Minimum SpO_2 during entire sleep recording
Number of <4% SpO_2 drops	SpO_2	Number of <4% SpO_2 drops in a 30 second window
Maximum and Minimum HR	Heart Rate	Maximum and Minimum heart rate during entire sleep recording

Sleep Posture (duration and percent of recording)	IMU DC gravity alignment	Each Sleep Posture duration and percent of recording
--	-----------------------------	--

Table 20. Off-device post-processing in MATLAB. Apnoea typing logic (central/obstructive/mixed) using IMU effort around each apnoea event, plus additional summary metrics.

2.6 Microcontroller Process Outline

The three ESP modules were divided into defined functional blocks, as shown in the flowcharts for ESP1, ESP2, and ESP3 below. Each node operates its own sensor and processing pipeline while maintaining synchronised connection with the hub.

ESP1 handles inertial measurements at 25 Hz and updates the effort detector at 2 Hz, performing posture classification, motion detection, and effort confidence estimation before transmitting packets as shown in figure 35.

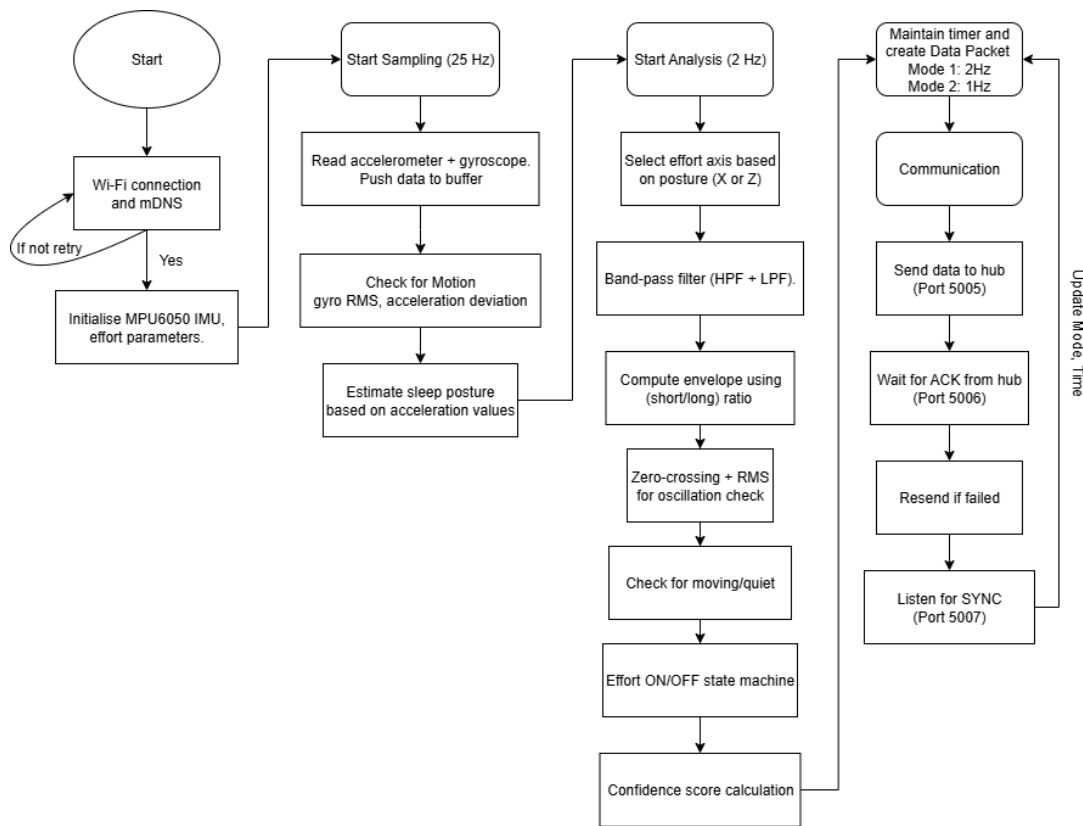


Figure 35. Flowchart of ESP1 operations

ESP3 combines thermistor-based breathing analysis (25 Hz sampling, 2 Hz analysis) with microphone-based snore detection (8 kHz audio, 1024-point FFT), reporting breathing features, effort, apnoea events and snoring episodes as shown in figure 36.

The main hub, ESP2, manages Wi-Fi, SD card logging, and the MAX30102, as well as UDP/TCP/HTTP ports, data, acknowledgements, and synchronisation packets. The flowcharts demonstrate the system's modular yet coordinated design, in which each ESP extracts local features while the hub consolidates data streams for real-time display, logging, and wireless access.

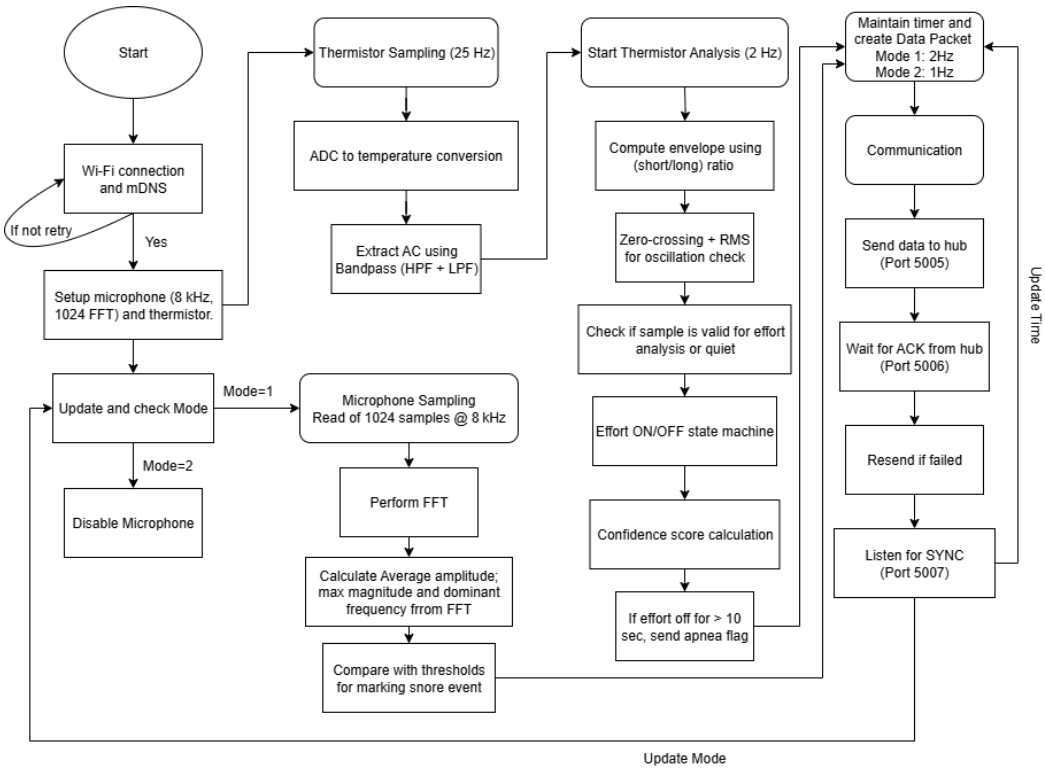


Figure 36. Flowchart of ESP3 operations.

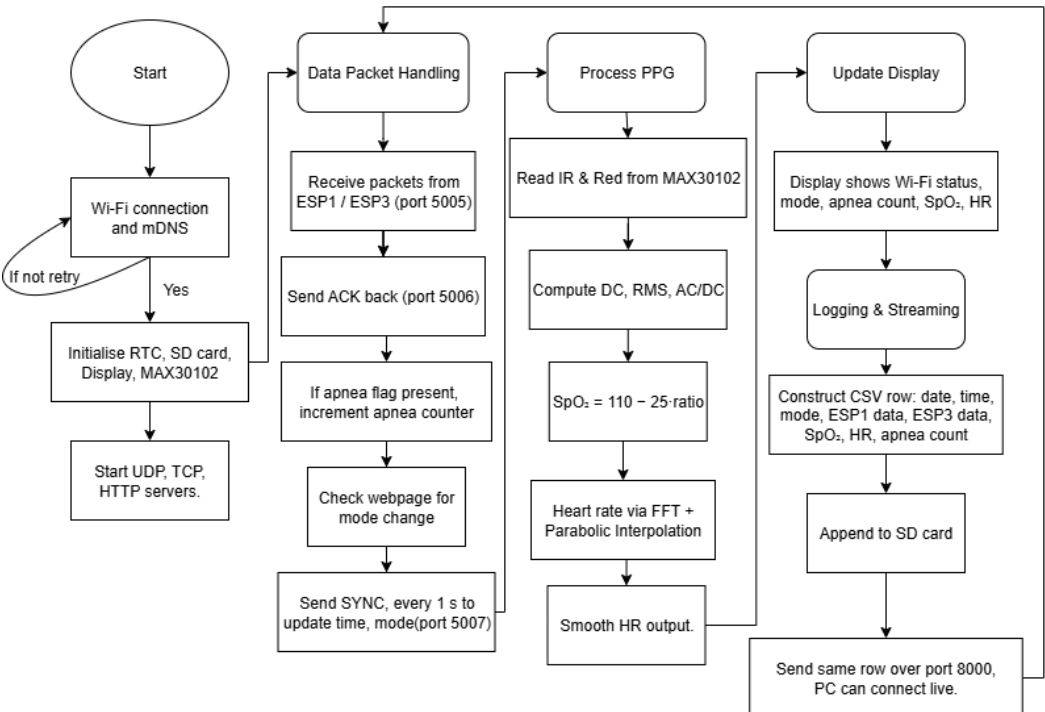


Figure 37. Flowchart of ESP2 operations

2.7 Wearable Design

Three custom enclosures were designed and 3D printed, one for each ESP, to ensure that the electronics may be worn safely and updated conveniently. All three have the few common

features in the layout, a 19 mm side hole for a panel power switch wired in series with the battery, a rectangular USB-C slot that allows the ESP32 to be charged and programmed / read over serial without opening the box, and a small top pilot hole aligned with the charger's indicator LED to show charging status. Each device includes an ESP32 and sensors on a prototyping board of approximately 70 × 60 mm. The lid and base close with four snap joints (one at each corner), allowing the assembly to be securely locked without the need of fasteners. The enclosure has an interior clear height of 40 mm and an external height of 43 mm due to the 1.6 mm top and bottom shells. While this maintains the package durable, it is not suitable for prone sleeping.

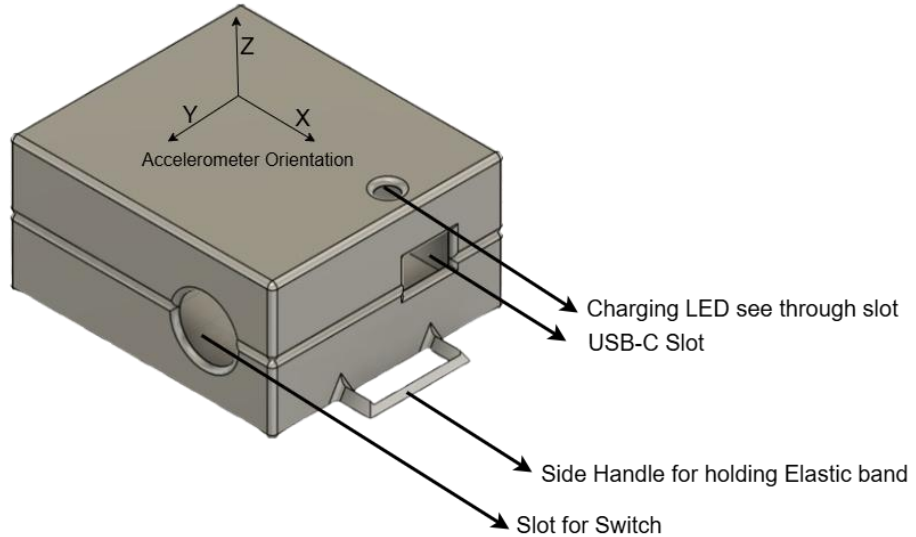


Figure 38. ESP1 (IMU) enclosure. Top shows the X-Y-Z reference used for accelerometer/posture orientation.

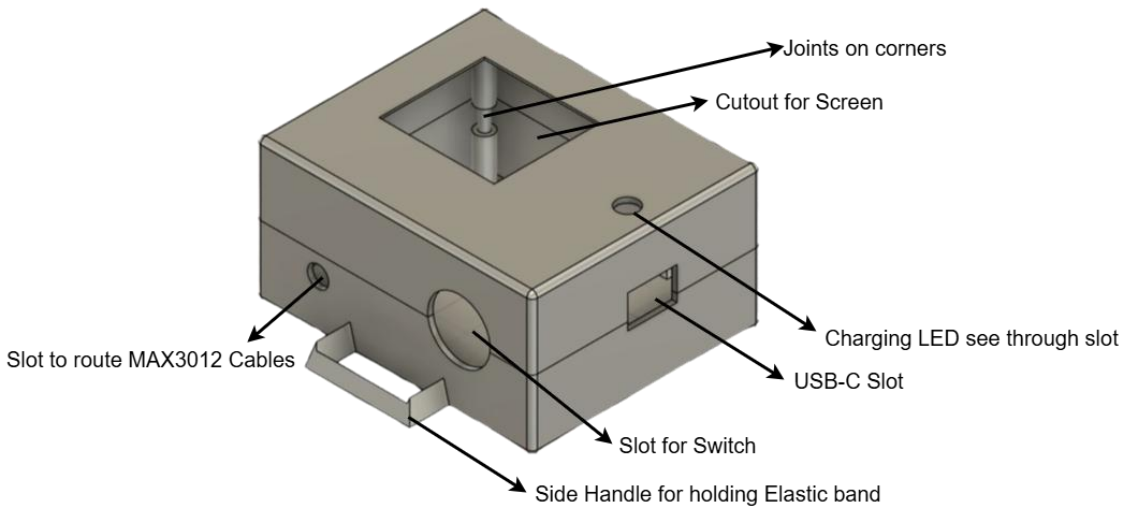


Figure 39. ESP2 (Hub) enclosure. Top cut-out for the display, internal standoffs on all 4 corners, side notch on the switch side to route the MAX30102 PPG cable

Device-specific apertures are only added where necessary as marked in figures 38, 39 and 40 for ESP-1,2,3 respectively. The ESP2 includes a top cutout for the display module and a small relief on the switch side for routing the MAX30102 leads. ESP3 (mic + thermistor) includes a top acoustic window centred over the microphone and a thin side notch next to the switch to

allow the thermistor leads to leave cleanly. ESP1 (IMU) uses a standard layout with no additional apertures. Each enclosure has strap handles on the left and right walls, an elastic band threads through these and secures with Velcro at both ends, allowing the units to be tightened to the desired body location, with length adjustable to accommodate varying body sizes. The MAX30102 finger clip is additionally 3D-printed from an existing open-source CAD model [59] and then assembled with screw and spring. It retains the sensor board, routes the short cable to ESP2 via the side release, and delivers consistent finger pressure without obstructing blood flow.

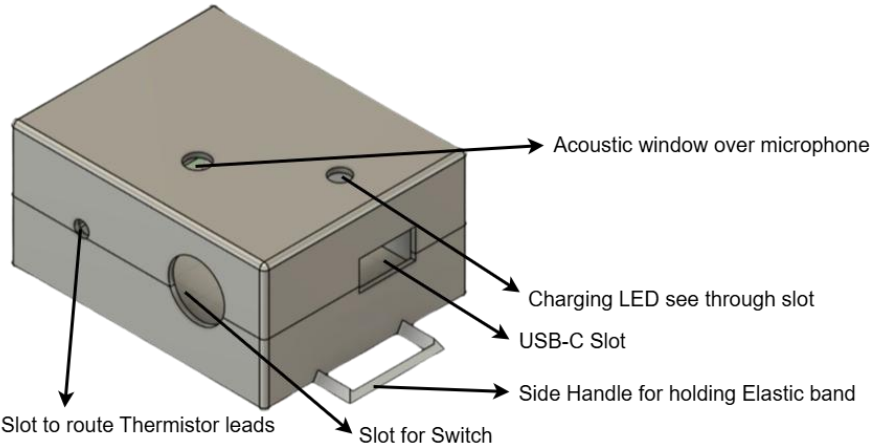


Figure 40. ESP3 (Mic + Thermistor) enclosure. Top acoustic port aligned above the IIS microphone and a small side relief next to the switch for the thermistor lead to exit.

Each enclosure has its own 2000 mAh Li-ion battery (JST-PH 2.0 connector) to power the ESP32 and associated sensors. A side-mounted power switch allows the user to simply turn the unit on and off without unplugging the battery or opening the casing. The wireless communication process, signal-processing algorithms, and mechanical design have now been laid out, the following chapter assesses and validates the entire system in operation.

Chapter 3 – System Validation and Results

The validation for this study was planned as an end-to-end system check rather than a clinical experiment. The goal was to validate that the chosen sensing modalities can reliably gather usable signals in real time, and that the on-device algorithms, wireless data communication, live data tracking and logging function together under real conditions. Validation is performed in two stages, an initial pre-validation on microphone for snoring detection and MAX30102 to check the ppg, and an overall system validation in lab-controlled settings with 10 participants, and results are discussed in this chapter. All participants were healthy adults, there was no sleep apnoea diagnosis, and apnoea incidents were not clinically validated. The findings thus show capability and readiness for future, clinical validation rather than diagnostic performance.

3.1 Pre-Validation

Snoring True Positives Pre-Validation

To test the on-device snore detector, 50 different one-second snore recordings from the dataset by T. H. Khan [60]. Each file is 1 second long, 50 different recordings were concatenated to create a 50-second clip and played it via a speaker. ESP3 calculated audio features dominant frequency (Hz), maximum magnitude (FFT peak magnitude between 500 and 1500 Hz), average amplitude (per 1024-samples), and the snore flag if conditions met. In MATLAB, the

same audio waveform was plotted, and the resulting dominant frequency and peak magnitude (500-1500 Hz), average amplitude and snore flag from ESP3 log are shown in figure 41.

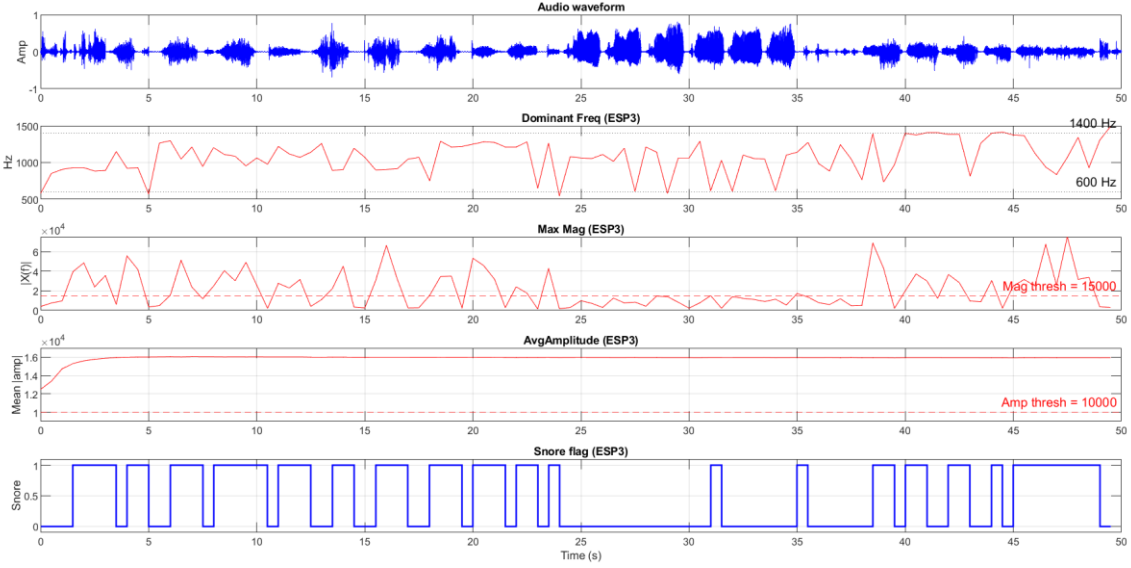


Figure 41. Snoring validation on ESP3 (8 kHz, 1024-sample frames). 50-s waveform made by concatenating fifty second long snore clips [60] and ESP3 features computed in real time.

Many snore episodes were caught, however a cluster lasting 25-35 seconds was missed or just slightly indicated. Maximum Magnitude fell below fixed thresholds, with 1024-point FFT at 8KHz sampling, only 128ms of audio is captured and used out of every 500ms analysis window. The tight 600-1400 Hz decision band and fixed thresholds are conservative, it is good for limiting false alarms, but they will miss lower frequency and quieter snores, such as those near 25-35 seconds. It can be enhanced by slightly broadening the decision band and increasing the FFT length to use more audio. The false positives of snoring are discussed in later section with help of real-time audio data. This simple, fixed-threshold detector is only good to confirm the snoring in a less background noise environment (expected during sleep). More advanced features and, ideally, a trained machine learning classifier, would be required to count snores and handle varying loudness and backgrounds.

Heart Rate and SpO₂ Pre-Validation

To pre-validate the MAX30102, raw RED and IR readings were recorded at 20 Hz for 30 s in two separate instances, then processed in MATLAB with the same approach used on the hub, a 12.8 s (256-sample) window sliding every 0.5sec, band-pass 0.6-3.0 Hz to obtain AC PPG, heart-rate by FFT peak + parabolic interpolation (valid 36-180 bpm), and SpO₂ = 110 – 25·R. Windows are only accepted if IR AC/DC $\geq 0.02\%$, otherwise held.

As shown in the figure 42, IR and RED AC have a comparable phase. Brief disturbances, such as finger pressure, motion, are prone to appear in AC. HR/SpO₂ values are calculated from past 256 samples (12.8 s window at 20 Hz), therefore the first and last 6.4 s of displayed data reflect a partially filled and zero padded buffer. Estimates settle only after the window fills, resulting in less trustworthy points at start and end of the recording causing the sudden jumps seen in HR and SpO₂ in the start and end of the plots.

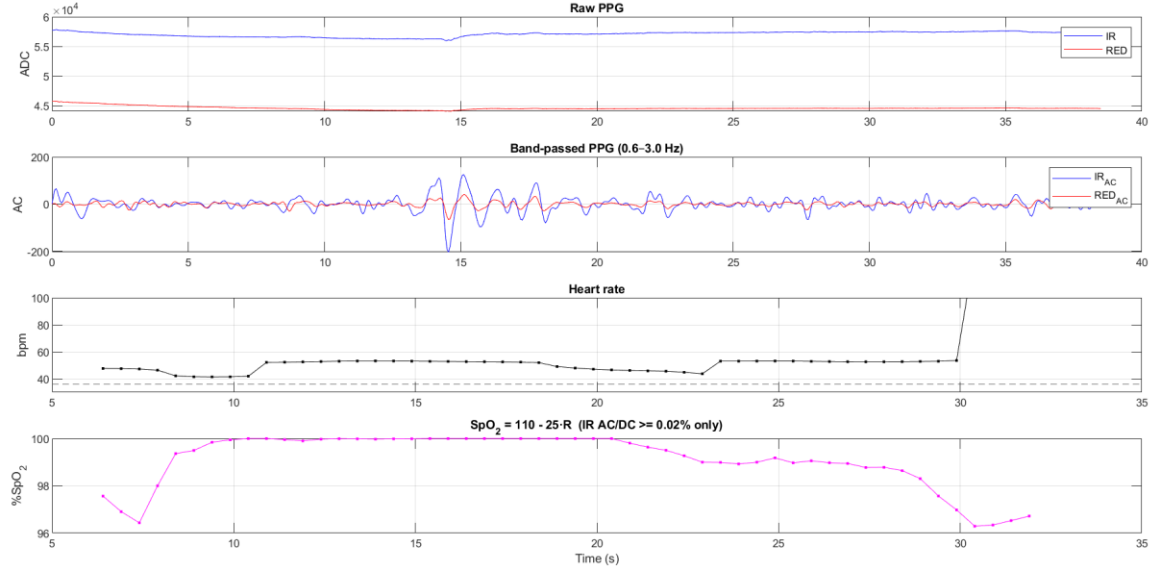


Figure 42. MAX30102 PPG analysis for 30 s, 20 Hz recording. Plots with raw IR/RED (DC), band-passed AC (0.6–3.0 Hz), heart rate from a 12.8 s FFT with parabolic interpolation and SpO_2 .

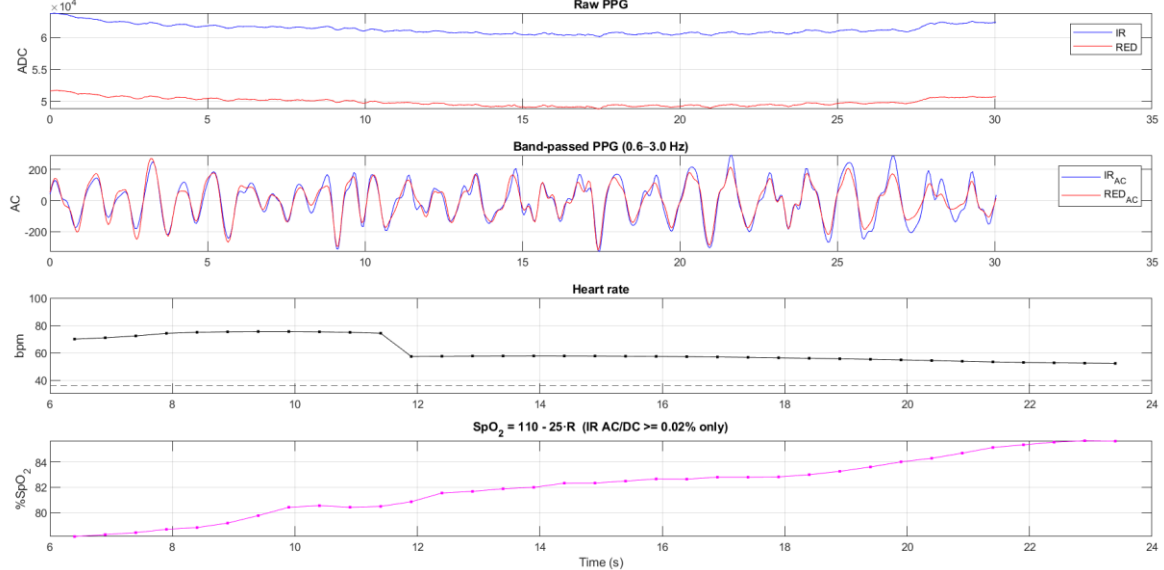


Figure 43. MAX30102 PPG analysis for 30 s, 20 Hz recording with brighter LEDs. Plots with raw IR/RED (DC), band-passed AC (0.6–3.0 Hz), heart rate from a 12.8 s FFT with parabolic interpolation and SpO_2 .

In figure 43, with increased LED current drive, both channels have a larger ADC range than in the previous figure. This has better pulsations (± 200 counts) and in-phase IR/RED oscillations. This increases the IR AC/DC ratio significantly above 0.02%. Because of the usage of large windows, HR is steadier and gradually declining, making it appear physiological (slowing) rather than an artefact. Stronger AC leads to more consistent R and a steady increase in SpO_2 throughout the plot, the longer signal recording could give better indication of HR and SpO_2 performance. The ESP2 calculates the values with similar thresholds over 256 samples but at higher sensor sampling rate of 100, therefore taking only 2.56 seconds to fill the buffer.

3.2 Test Setup

To validate the system in real conditions, 10 healthy adult volunteers (above 18 years, male and female) were recruited primarily from PhD and Master students to participate in the study. Recruitment and assessment followed the University of Nottingham's criteria for human-

participant studies.

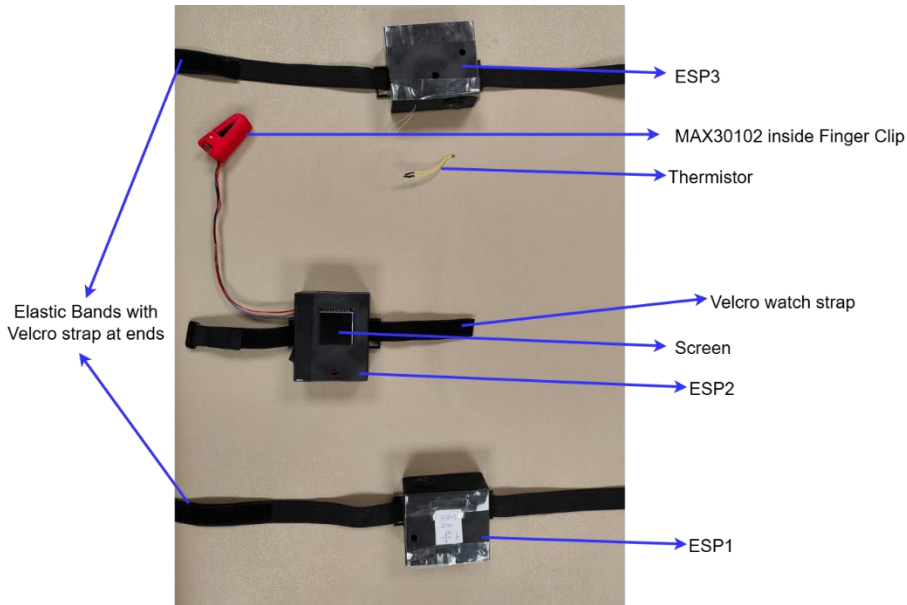


Figure 44. Prototype wearable with three strap-mounted enclosures, on top: ESP3 (mic + thermistor; mic port and thermistor lead), middle: ESP2 hub (screen window; MAX30102 finger-clip and cable), bottom: ESP1 (IMU). Each box has a side power switch and USB-C slot.

The image above shows the three wearables prepared for each session, the IMU node (ESP1), the hub (ESP2) and the mic + thermistor node (ESP3). Each enclosure is mounted on an elastic strap with Velcro so the modules can be secured to the body and adjusted for different sizes. The MAX30102 finger clip connects to ESP2 via a short cable.

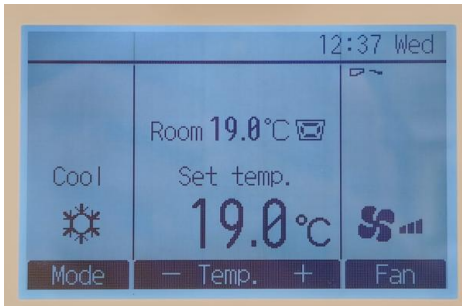


Figure 45. Controlled test environment, thermostat showing room temperature fixed at 19 °C during volunteer data collection.

All recordings were carried out in an air-conditioned lab on an examination bed, the room temperature was held at 19 °C throughout (figure 45).

Participants wore all 3 components as shown in figure 46, each participant then asked to rest for 30 minutes to emulate rest/light sleep, for most of this time they were lying prone and breathing naturally, then short posture blocks couple of minutes each, where they were asked to switch between left, and right and finally, few breaths of mouth-breathing and deep-breathing. This procedure allowed to record real-time signals, test the algorithms across various postures and breathing patterns to evaluate system performance.

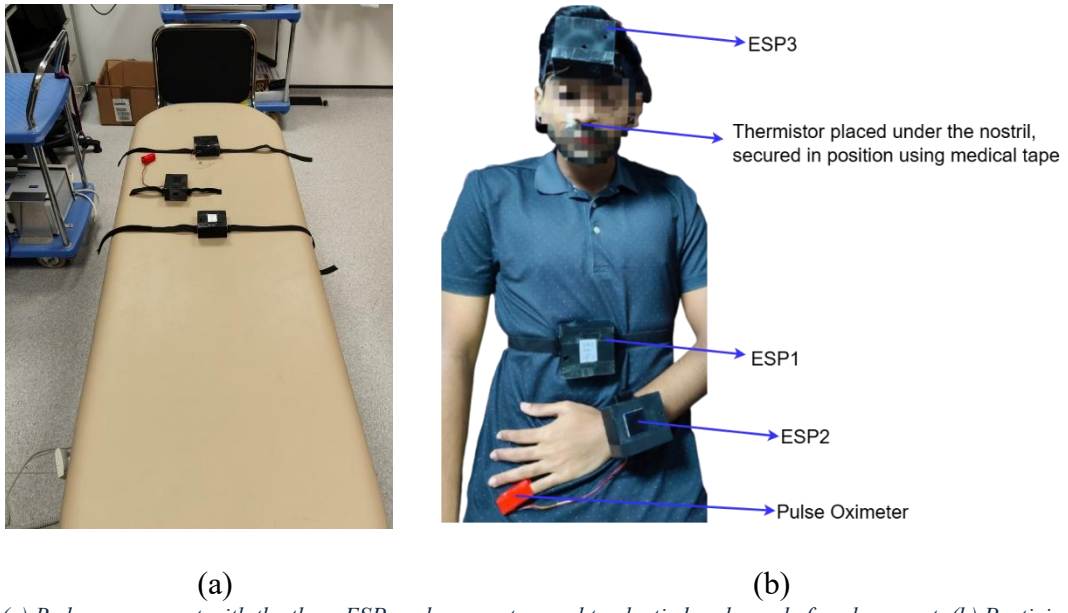


Figure 46. (a) Bed arrangement with the three ESP enclosures strapped to elastic bands ready for placement. (b) Participant wearing the full system, ESP3 on the head with the thermistor taped under the nostril, ESP1 on the abdomen, and ESP2 on the wrist with the MAX30102 pulse-oximeter clip on the finger.

During the volunteer sessions, thermistor airflow and IMU effort/posture were logged at 2 Hz from all 10 participants. The on-board microphone (ESP3) was enabled for a subset of 5 participants to collect snore-related features at same rate. The pulse-oximeter (MAX30102) module was not used in this study because its protective cover glass cracked, to avoid unreliable readings and any risk to participants, SpO₂ and HR measurements were excluded. The detailed results are discussed in next section.

3.3 Results

IMU based Results

The IMU summary over the full recording of a participant is shown in figure 47, except for small movements, the gyroscope stays at or near zero. The Posture and Motion panel accurately records the different motion bursts and posture changes that occur between 1,200 and 1,400 seconds. The envelope and ratio are low and consistent during still moments, both rise and generate peaks when the person moves or their breathing effort increases, with ratio more sensitive than envelope which is expected. The oscillation panel illustrates the RMS (blue, left axis) and zero-crossings (orange, right axis), ZC counts cyclical sign changes, whereas RMS indicates signal amplitude.

An important observation for this recording is that the zero crossings were only seen lateral positions and were practically flat in supine due to low RMS, but in supine position, the ratio feature tracked continuous effort this indicates persistent but minimal effort.

Another observation is that, whenever there is a huge change in envelope due to increased effort or movement/posture change, the ratio goes flat for next few seconds before it starts to mirror the effort again. Bigger the changes, longer time it takes to recover. However, ZC takes over during these periods to track effort. This shows the complementary nature and advantages of using both detectors together.

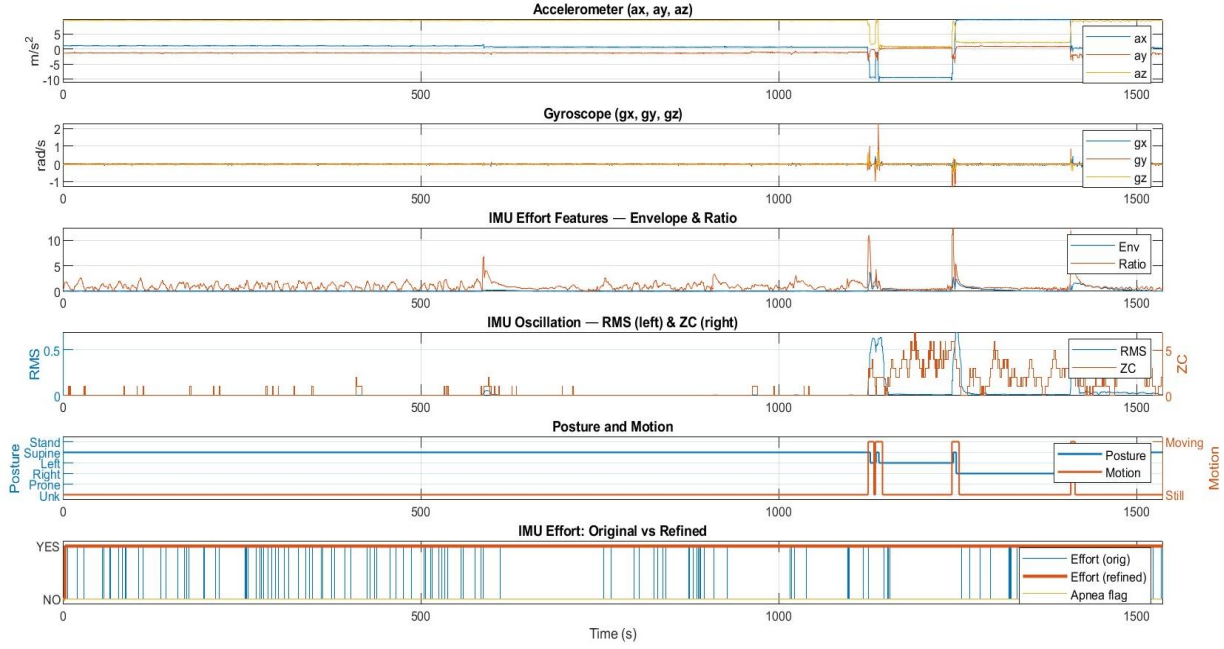


Figure 47. ESP1 IMU summary over the full recording. From top: (1) 3-axis accelerometer; (2) 3-axis gyroscope; (3) IMU effort features (short-window envelope and ratio); (4) IMU oscillation features with dual y-axes—RMS (left, blue) and zero-crossing count (right, orange); (5) sleep posture (left axis) and motion flag (right axis); (6) respiratory effort state from the device versus the refined , with apnoea pulses from ESP3 overlaid for reference.

Figure 48 and 49 summarises IMU data of different participants, posture panel accurately records every posture change and compared to previous participant, movement is visible throughout. Oscillation features (RMS/ZC) are present in all postures here indicating consistent effort. In supine position, the ratio feature accurately monitors effort but fails to follow in lateral orientations due to spikes in envelope caused by posture change.

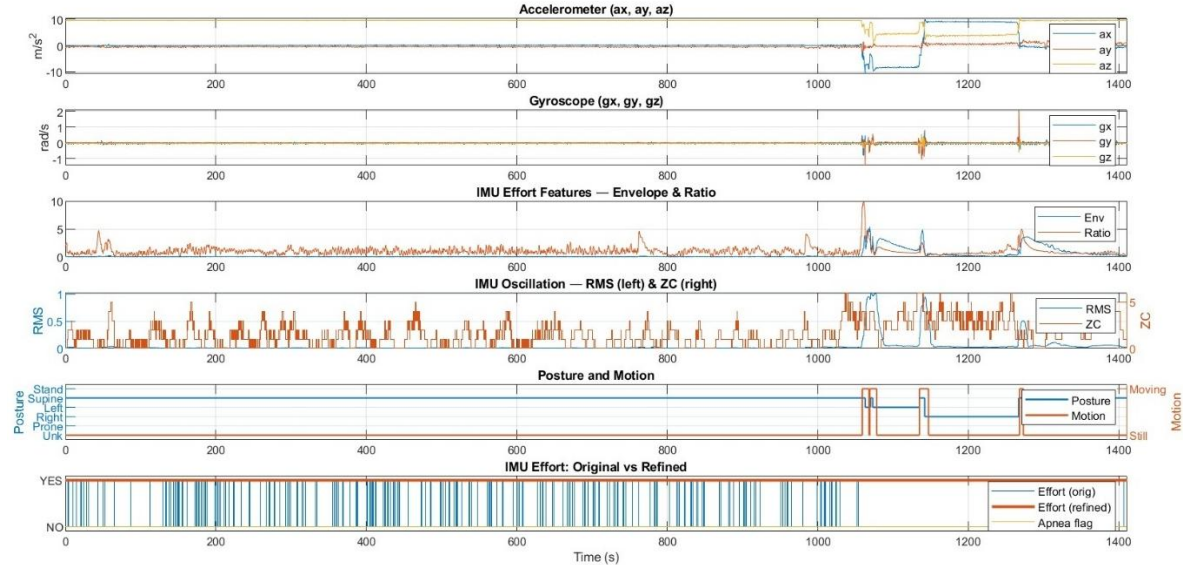


Figure 48. IMU summary of full recording from another participant. Accelerometer & gyroscope, effort features (envelope/ratio), oscillation metrics (RMS & ZC), posture/motion, and original vs. refined effort.

In all the IMU summarises, the improved IMU effort turns the noisy, binary Effort into stable event by a 2-step post processing. First, a 2 second moving average of the confidence output indicates likely effort, whenever confidence score ≥ 0.9 . Second, a debounce is used with at

least 1-s ON and 2-s OFF pause to prevent small losses from disrupting actual episodes and short spikes from creating fake ones. As a result, the thick refined trace eliminates single-sample flips while preserving effort and providing a cleaner look for logic as apnoea events.

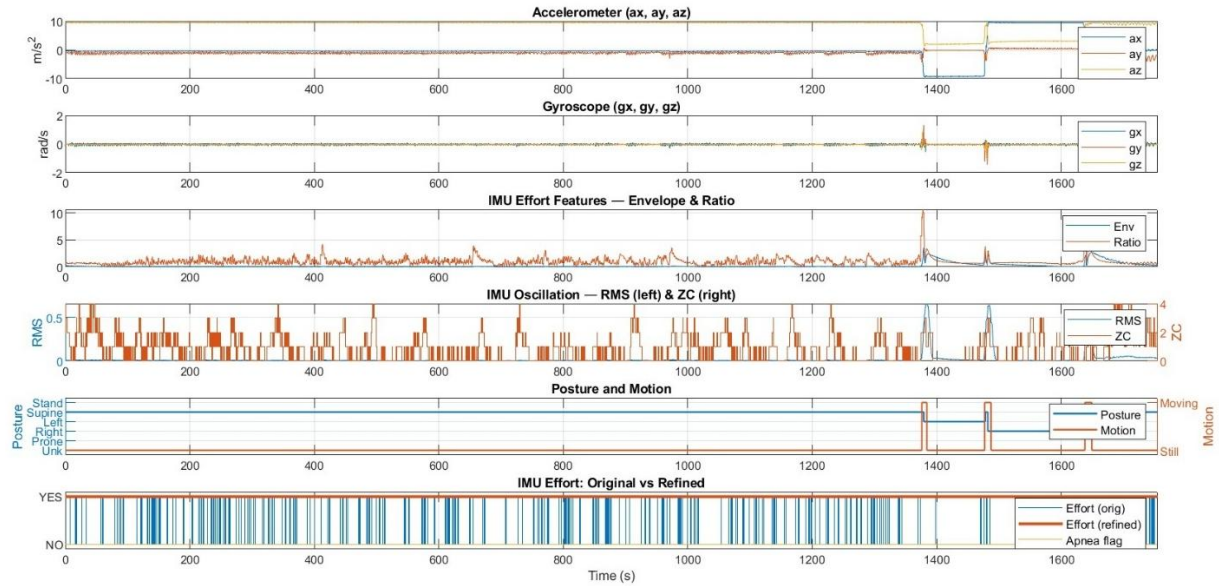


Figure 49. IMU summary of full recording from another participant. Accelerometer & gyroscope, effort features (envelope/ratio), oscillation metrics (RMS & ZC), posture/motion, and original vs. refined effort.

In the magnified plot showing only initial 50 seconds of recording from previous plot in supine as shown in figure 50, the accelerometer, displays gradual, repetitive up-then-down ramps as the abdomen lifts on inhaling and falls as it settles on exhale.

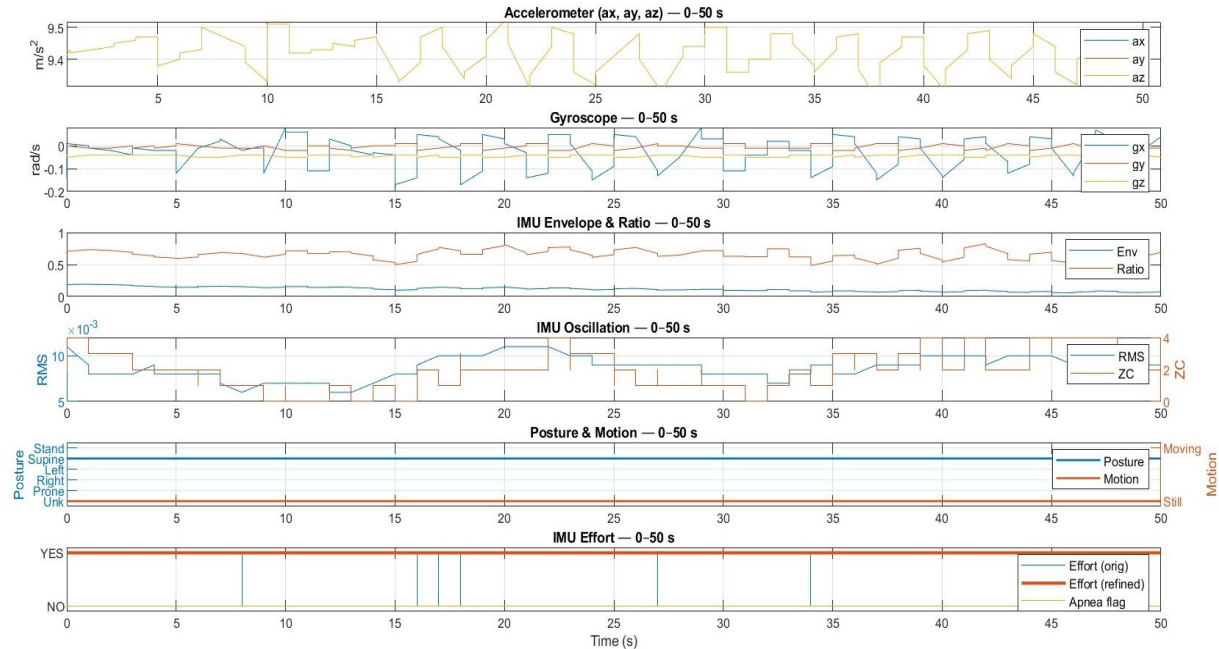


Figure 50. IMU summary of full recording from same participant as figure 49 with only 50 seconds of data in supine.

When the unit is placed flat on a table, there is no motion. Accelerometer traces are almost constant, the envelope is flat, and the oscillation metrics are at zero. Posture is consistently

supine (only gravity orientation), and motion is still. When there is no movement, both original and refined effort remain OFF throughout.

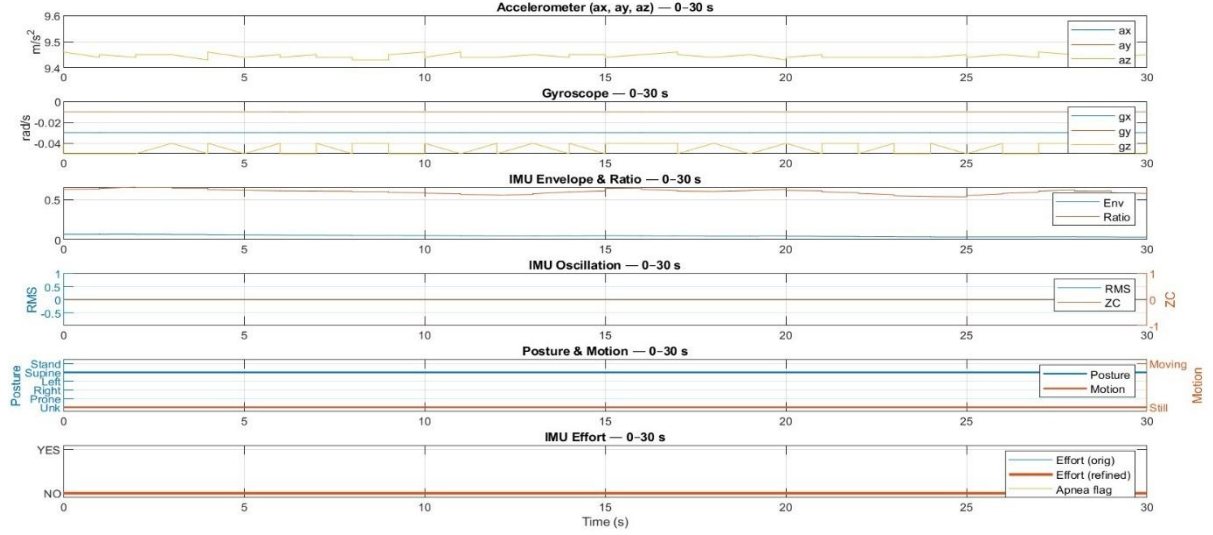


Figure 51. IMU summary of ESP1 resting on table without subject to any motion.

Thermistor based Results

The temperature-based summary over the full recording of a participant is shown in figure 52. The nasal thermistor captures depth and timing well when breathing through the nose, envelope/RMS is a good indicator for depth with ZC reflecting breath timing, periodic ZC spikes observed in figure 52 corresponding to brief quicker breaths. The penultimate window displays deeper, slower breathing (higher envelope/RMS, lower ZC), followed by mouth breathing in the last seconds, where nasal features fade.

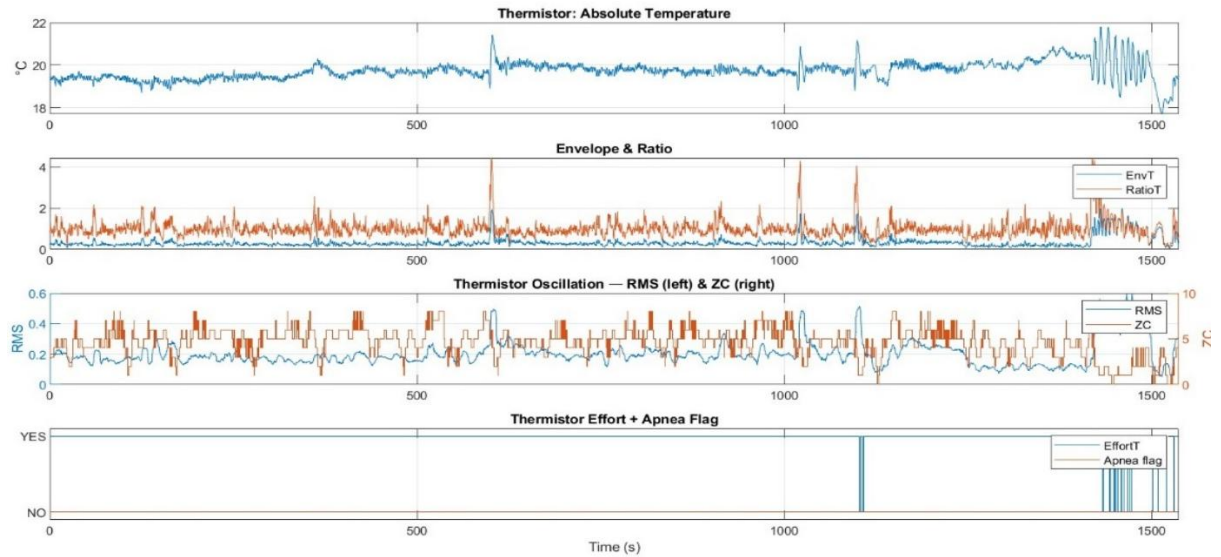


Figure 52. Thermistor summary of a full recording plotting absolute nasal temperature (top), envelope & ratio of the breathing band, oscillation metrics (RMS & ZC), and thermistor-derived effort + apnea flag.

Another recording is shown in figure 53, temperature drifts slowly, with occasionally steps (small repositioning of thermistor with posture changes). Again, envelope/RMS rise in the penultimate seconds, while ZC dips, indicating deep, slower breaths. Switching to mouth

breathing in the last few seconds causes nasal flow to collapse at the end, envelope/RMS and ratio decrease towards baseline, and thermistor-only effort reduces, this results in apnoea flags even though the individual was still breathing through the mouth (sensor blind to oral flow).

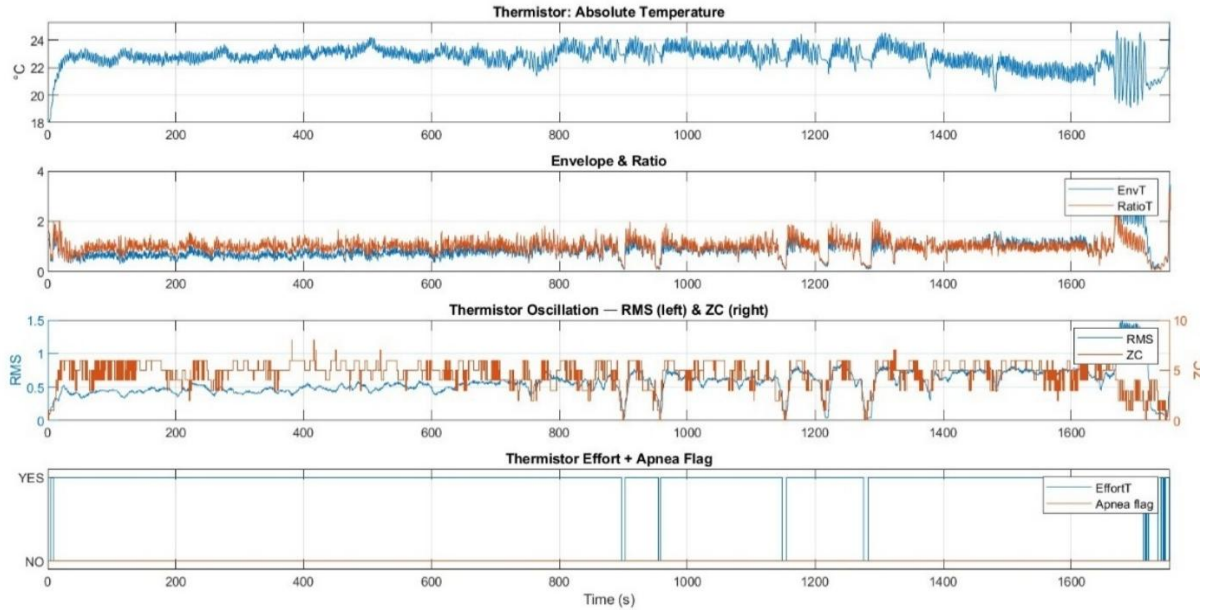


Figure 53. Thermistor summary of another recording in same layout.

The same plot zoomed from 1100 to 1300 seconds are plotted in figure 54. While inhaling the temperature readings goes low and rise during exhalation. During steady breaths, the temperature trace oscillates often, the envelope and RMS are at moderate levels, and ZC (zero-crossings) ticks per breath. During short intervals between 1144-1146 s, 1278-1282 s, the nasal temperature flattens, the envelope collapses, the RMS falls near zero, and the ZC temporarily lowers to zero (no crossings). The Effort switches off in these windows, then returns to ON as Envelope/RMS rebound and ZC continues stepping. Around 1218-1226 s, the characteristics fall, but ZC does not totally drop out, indicating few shallow breaths in that window rather than a complete halt. Although these episodes are brief (<10 s), the feature set resolves each micro-pause. Envelope/RMS capture depth, ZC captures time, and the derived effort translates those cues into brief OFFs. This zoom shows the thermistor reliably catches brief breathing pauses.

In another recording as shown in figure 55, early (0-100 s) signal shows small, noisy deviations and the effort flickers. From 100-300 s, the trace is essentially flat, which is typical for a probe located outside the nostrils. After repositioning, around 320 seconds, there is an obvious step change, temperature baseline shifts, Envelope and Ratio climb with visible breath-to-breath modulation, RMS increases, and ZC starts regular stepping. The sensor is properly situated from 330-500 s, allowing for clean tracking of breathing cycles. Overall, the panel illustrates how misplacement suppresses all features, and how restoring the probe to the nostril immediately brings back thermistor-based breathing detection.

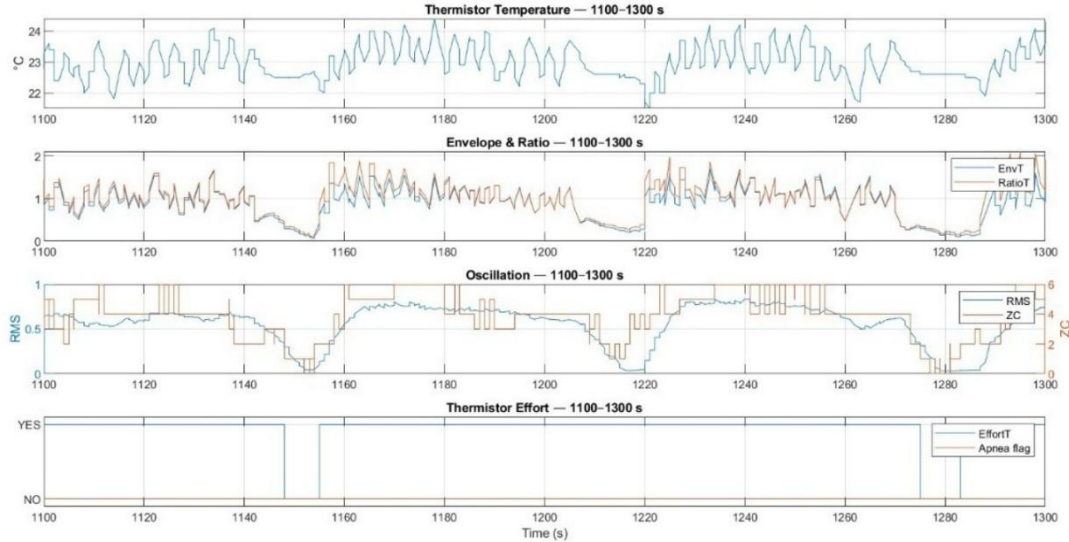


Figure 54. Thermistor summary zoom (1100–1300 s) on same plot, nasal temperature, envelope/ratio, oscillation (RMS left, ZC right), and thermistor-derived effort.

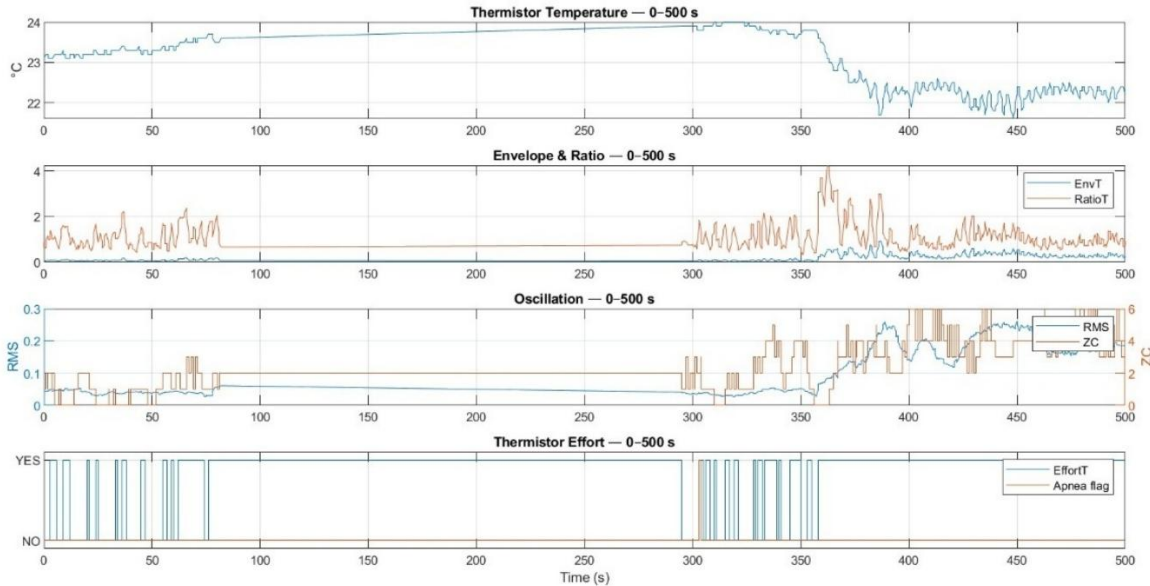


Figure 55. Thermistor summary (0–500 s), initially mis-placed, then corrected around 320 s

Audio based Results

Figure 56 depicts the microphone output for the whole session, plotting average amplitude, maximum spectral magnitude, dominating frequency, and the snore choice against time. The trace is relatively quiet for whole recording. The few snore flags grouped around second half coincide with background talk, not snoring. Speech temporarily satisfies the present criteria (high energy with a dominant frequency in the 600–1400 Hz area), leading to false positives, these are observed other recordings as well. Outside of these spoken sections, the detector remains off. Voice activity can be seen as sudden surges in spectral magnitude and grouped dominant-frequency spikes, which occur when the researcher cues postural changes or deep/mouth breathing.

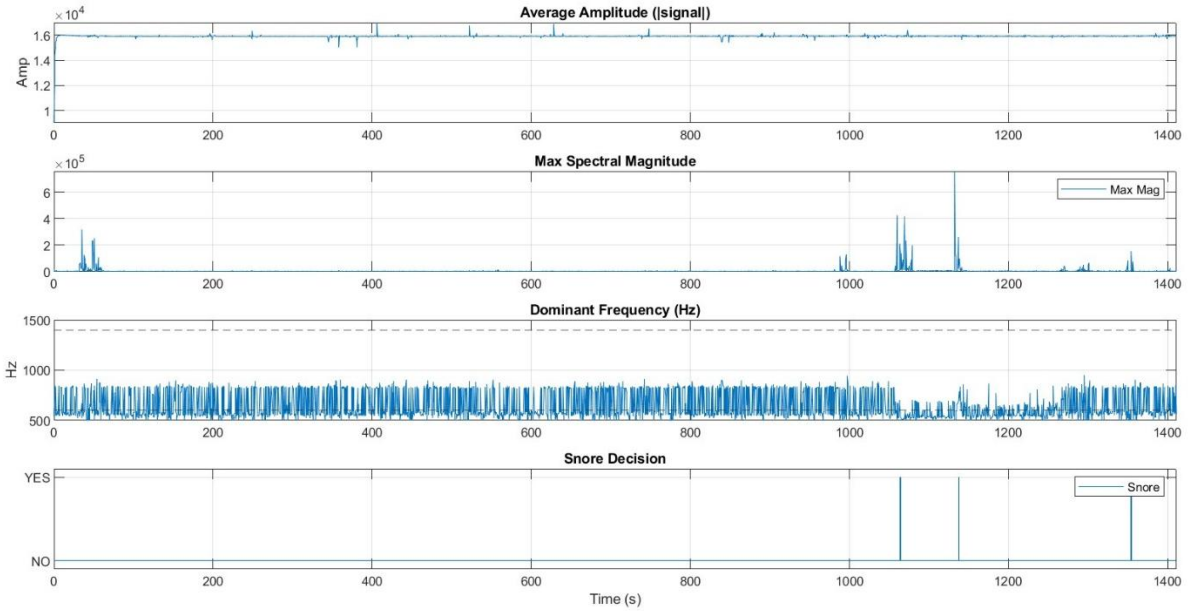


Figure 56. Microphone snoring features summary of a recording

3.4 Specification Validation

Battery Life Validation

A battery life test was performed with 2000 mAh battery, the system streamed sensor data at 2Hz (Mode-1) via Wi-Fi and logged it constantly to the microSD card for 20 h 24 min 8 s (20:24:08) without intervention. At that point, the hub (ESP2) was turned off, this result shows an adequate energy budget for overnight use and can comfortably support at least two full nights on a single charge.

Weight and Comfort

The overall on-body mass of entire wearable is around 360 g, with ESP1 weighing 120 g, ESP2 weighing 150 g, and ESP3 weighing 90 g. In use, the chest unit feels acceptable, the wrist unit is the heaviest but still doable, and the 90-gram head unit is noticeable after a while but comfortable with a soft strap. Compared to a standard HSAT and PSG configuration, which includes multiple belts, a nasal cannula, and long wires to a bedside box, this prototype is less cumbersome and cable-free between nodes. The users can sleep in supine, lateral left or right postures as shown in figure 57, except prone, existing enclosures are 4 cm tall, making prone sleeping impractical. Additionally, the stiff shells can cause pressure points if you roll across them.



Figure 57. User wearing the complete system in a lateral-sleep posture

Overall comfort is decent during supervised sessions and short naps, for all-night use, the system would benefit from smaller casings, softer padding, and a lighter head unit. The setup is quick compared to HSAT. It takes a few seconds to strap ESP1 and ESP2 and check the hub screen. However, the thermistor is the time-sink, centimetre-level placement of the bead beneath the nostril is necessary to provide consistent airflow from ESP3, if too distant signal drops.

Real Time Dashboard

A MATLAB client makes a TCP connection to the ESP2 hub TCP port and once joined, writes every incoming CSV line to file while plotting the most recent samples in real time. Each packet has 36 columns, the script indexes these fields and can plot any variable by specifying its column index and including a trace in the charting section.

This live view is great for real-time inspection and event monitoring. A smooth, periodic nasal temperature waveform shows proper thermistor placement, while a flat trace implies misplacement. The dashboard shows breathing effort (IMU and thermistor), apnoea/snore flags, SpO₂, and heart rate, allowing to spot any events like apnoea, brief pauses, deep/slow breaths, snoring or motion as they happen. The layout can be readily customised by selecting the columns of interest. The plot is made of most recent 500 samples (250 s at 2 Hz) by default. The window duration can be adjusted by the user.

Because the data is timestamped and saved, the precise data viewed live can be replayed and analysed later. The figure 58 shows the live plot setup used during the study, with both IMU and thermistor plotted on same plot and thermistor reading monitored in a separate plot.

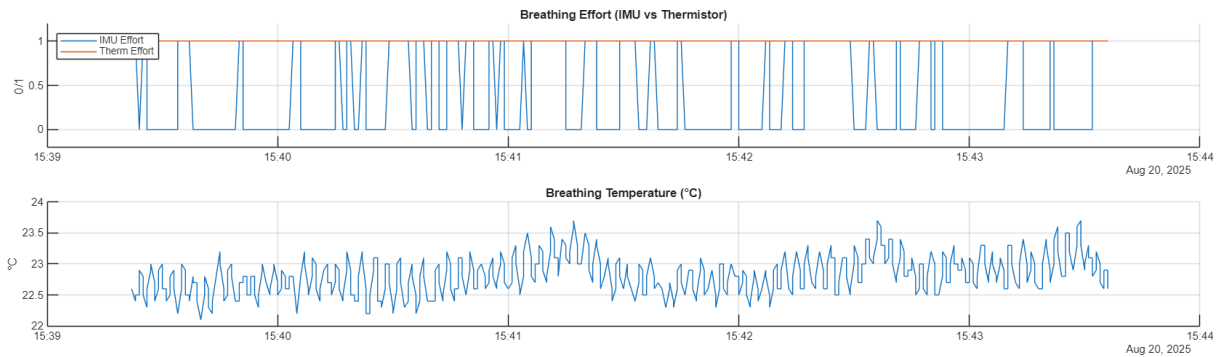
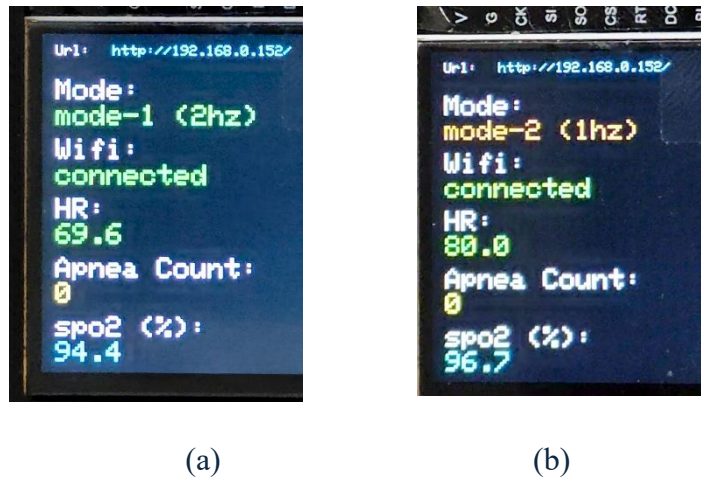


Figure 58. Live data stream from ESP2 plotted in MATLAB, IMU vs Thermistor Effort and Nasal Temperature

Screen and Mode Updates

Besides the MATLAB dashboard for remote viewing and logging, users can view a limited live data on the ESP2 screen. The screen prints Wi-Fi connectivity, current HR and SpO₂ levels, total number of apnoea occurrences since power-on, and active mode (mode-1: 2 Hz logging with mic on, mode-2: 1 Hz logging without mic) as shown in figure 59. The blue URL at the top represents the device's IP address, which can be entered into any browser to access the Mode Control webpage as shown in figure 60. The same page is accessible using the mDNS name sleep-hub.local. The homepage includes two buttons for selecting the desired mode, and the "Current mode" indication refreshes quickly after switching.



(a)

(b)

Figure 59. Displayed screen on ESP32 (a) operates in Mode-1, screen refresh twice every second (b) operates in Mode-2, screen refresh every second, displaying Wi-Fi status, Current Mode, HR, SpO₂, Apnoea count and ESP2 IP address for mode selection.

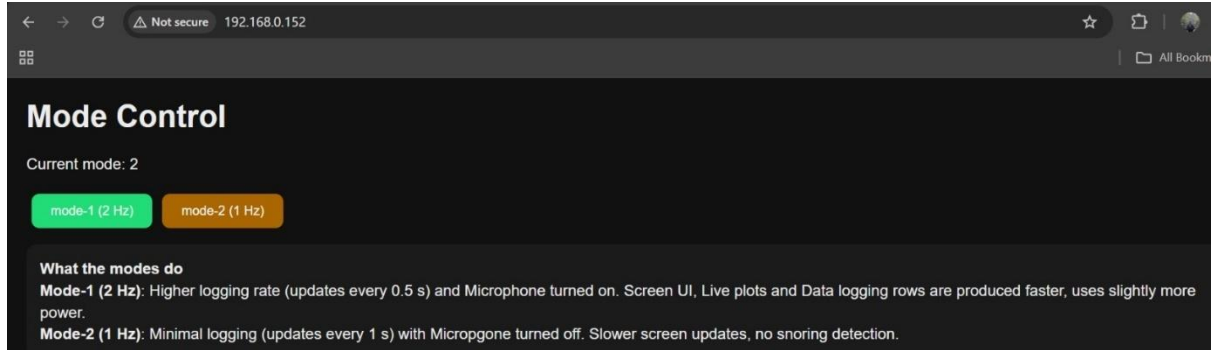


Figure 60. Browser view via the device IP address showing the same Mode Control page and current mode.

Test Summary

```

SLEEP SUMMARY
=====
Start time   : 2025-08-20 15:36:41
Stop time    : 2025-08-20 16:05:56
Total time   : 00:29:15 (0.49 h)

Respiratory Events
-----
Apneas       : 0 (Central=0, Obstructive=0, Mixed=0)
Apnea timestamps:
  (none)
Snoring      : 1 episodes
Snore timestamps:
  - 2025-08-20 15:57:00

Sleep Posture (duration and percent of recording)
-----
Unknown     : 00:00:00 ( 0.0%)
Prone       : 00:00:00 ( 0.0%)
Right        : 00:05:02 ( 8.8%)
Left         : 00:03:11 ( 5.6%)
Supine      : 00:49:00 ( 85.6%)
Stand        : 00:00:00 ( 0.0%)

```

Figure 61. Summary report generated for one session with apnoea typing from IMU-effort (10 s window before each flag), snore events, and posture distribution.

To summarise the findings in each sleep section, post processing of recorded data to report number of apnoea events and classifying the apnoea type, along with posture classification and

snoring events with timestamps of occurrence were generated in MATLAB. The typing of apnoea is done as stated previously in table 20 based on the extent of presence of IMU effort during breathing pauses lasting at least 10 seconds. Other physiological features listed in table 20 related to heart rate and SpO₂ were not computed here because the MAX30102 PPG data were not collected during these runs. Report generated for an entire recording is shown in figure 61.

Chapter 4 – Conclusion

The purpose of this research was to make sleep-apnoea screening easier, less expensive, and more comfortable than current practice. A prototype was designed and developed for a feasible sensor grouping with minimum wire, including an abdominal IMU for respiratory effort and posture monitoring, a nose thermistor for airflow depth and timing, a microphone for snoring, and a wrist PPG for SpO₂/HR. All data is transferred to a compact hub in real-time for data logging. The event criteria and reporting were linked with AASM standards (e.g., ≥ 10 -s respiratory episodes), and the analysis logic was developed to mirror standard scoring whenever possible.

There were intentional deviations from the standard recommended sensor types, most notably the use of an IMU instead of inductance belts for effort and the reliance on a thermistor rather than nasal pressure for airflow, to try reducing cost and burden while maintaining clinically useful information. A side-by-side comparison of the gold standard PSG, commercial home sleep apnoea testing devices and the built prototype can be seen in the figure 62.

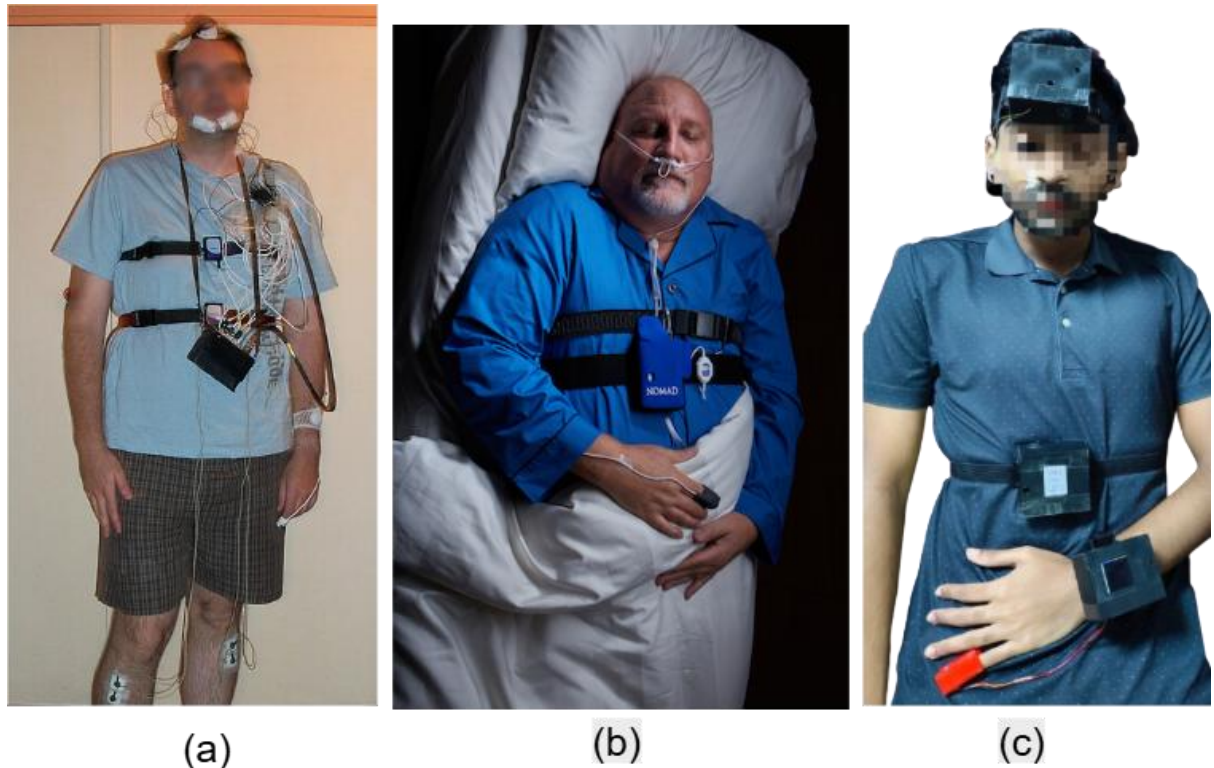


Figure 62. Devices for sleep–apnoea assessment (a) In-lab polysomnography (PSG) with multiple wired sensors [61] (b) Home Sleep Apnoea Test (HSAT) belt-mounted recorder with nasal cannula and oximetry [62] (c) Prototype device, wireless nodes (abdomen IMU effort, nasal thermistor airflow, microphone for snore, wrist PPG for SpO₂/HR).

Far fewer wires were present, and the setup is comparatively quick and tolerable for home use. Wireless communication implemented is very reliable. During standard in-lab tests, a technologist supervises and ensure proper positioning of sensors and data capture, and for most commercial home sleep testing devices there are no data quality control option during study, if user doesn't wear the sensors properly, it may affect scoring and data quality can be assessed only post recording. For this prototype, live plots feature allows instant verification of placement and signal quality, reducing unusable studies. With a single charge this prototype can work for at least 2 overnight sleep recordings.

Despite these advantages, the prototype has a few significant limitations. First, there is no direct quantitative way to track airflow changes, therefore difficult to track hypopneas. Second, the thermistor is blind to mouth breathing, therefore airflow may be underestimated during oral breathing. Third, the IMU is motion-sensitive, motions might temporarily imitate or disguise effort. Furthermore, the snoring algorithm can create speech-related false positives, the packaging is still bulky and research-grade, and evaluation sample is small. These constraints point to clear next steps outlined in future development.

4.1 Future Work

Hardware miniaturisation

Although each sensor is small, the prototype used prototype boards, pin headers, and extra tolerance for 3D-printed enclosures, which increased the enclosure height, most notably the head-mounted ESP3. A custom PCBA with processor and sensors on a single board can be designed to cut down both volume and weight. Additionally, the hard and stiff shells 3d printed enclosures can be replaced with softer foamed padded enclosures.

Airflow sensing beyond thermistor

The nasal thermistor was convenient and almost weightless and reliably detected pauses, but it cannot quantify airflow and is location-sensitive, hypopneas are therefore harder to score. A secondary quantitative airflow sensor like a differential pressure transducer, or an FBG pressure sensing unit integrated in a mask to cover both nasal and oral breathing can be explored. The threshold based breathing detector worked well in controlled condition for small sample size, it can be replaced with an adaptive machine learning classifier trained to label breath/no-breath for better performance under different setups and conditions.

IMU effort labelling and alternative sensing

IMU tracked posture and motion well, but on-device labels for effort estimation were noisy and due to the smaller feature magnitude, they are extremely threshold dependent, post-processing over-smoothed missing to detect smaller pauses, thresholds were user and setup dependent. Adaptive thresholding algorithms using per-session calibration, more advanced features can be explored along with training a supervised model for effort segmentation. Apart from MEMS based IMU, Fiber Bragg grating sensors can be used for abdomen tracking, to monitor respiratory movements, by detecting the strain caused by the expansion and contraction of the abdomen during breathing. Integration of these sensors, into wearable textiles or belts, to convert physical movement into a shift in their reflected light's wavelength, allowing for continuous monitoring of breathing effort can be explored.

Snore detection Improvement

The current energy and dominant-frequency rule are fast but misses low-frequency and quiet snores and shows speech false positives. Alternate mic placements can be tested a machine learning classifier can be used to detect snoring in varying backgrounds.

SpO₂ and HR

The strongest missed opportunity was correlating events with SpO₂ and HR, limited by no PPG data in this study. In future validation, with synchronised PPG data along with IMU and thermistor signals can be explored and studied for any trends or correlations during different sleep events.

Wireless Communication

In the current build, all ESPs connect to a single external Wi-Fi access point (such as a home router or Mobile hotspot) and works seamlessly, but the communication entirely relies on external Wi-Fi. A reasonable next step would be to relocate primary storage (SD card) to a lower-power consuming node (e.g., the IMU node) and have that ESP operate as its own access point, allowing ESPs and PC to connect directly as long as powered without a router dependency.

Data logging format

While CSV is convenient for prototyping and quick plotting, A more accepted standard for sleep data is the European Data Format (EDF/EDF+) and commonly used for PSG and HSAT. Future builds can explore logging in this format.

Hypopnea and AHI estimation

The current prototype reports only apnoea event counts and classify them, but a widely used severity indicator for disordered breathing is AHI (events per hour of sleep) and hypopnea grading is required to calculate it which is limited by airflow measured mainly by a thermistor. To make it a better screening tool and report these indicators, a secondary quantitative airflow channel is a must. Next validation tests can be done with the new build and commercial HSATs simultaneously to compare the measurements, detection accuracy and performance.

Implementing these steps would improve the sensitivity and closing the gap to gold standard measurements and improving user comfort leading to a better screening tool.

4.2 Societal Fit

Health and Safety

This prototype is both low-risk and non-invasive. All sensors are external and battery-powered, no skin penetration or high voltages are required. Enclosures can be made of biocompatible plastics with smooth edges to reduce any skin irritation. The nasal thermistor is attached under nostril with hypoallergenic medical tape. All status LEDs are covered by enclosure so that they do not shine into the eyes while asleep and cause strain when looked over for longer duration. The microphone does not record or store raw audio, instead it computes and saves non-reconstructable metrics to protect privacy. All the rechargeable batteries used have an in-built battery protection ICs.

Diversity, inclusion

This prototype uses elastic bands to hold the enclosures in position, this ensure it fits different face and body sizes, The setup is easy, and screen UI is simple with plain language and large font.

Societal Impact

Obstructive sleep apnoea is prevalent and underdiagnosed, a comfortable, low-cost system at home with real-time quality control can increase access and reduce waitlists. This design's bill of materials consists primarily of off-the-shelf components that are suitable for low-cost production.

4.3 Reflection

Project Reflection

The initial project meetings, literature survey and AASM standards review were helpful and provided clear directions for sensor and implementation choices. The original design planned called for a wired system, however, the design changed midway through to a wireless architecture seeing an opportunity to build a better wearable prototype. The change ultimately improved usability and enabled a mode-based configuration system (user-selectable sampling/sensor sets), but it took a significant amount of time to setup, debug and test different communication channels and protocols (ESP-NOW, Wi-Fi, Node RED), implement retries and acknowledgements to reduce data loss significantly. This integration effort overloaded the schedule and reduced the amount of time available for event-scoring algorithms, particularly IMU-based effort detection and ended up using same algorithms that worked for thermistor. Despite noticed limitations from the literature [31], the attempt to detect and score partial airflow reductions using thermistor-only airflow was time-consuming and resulted in a dead end.

The prototype built could have been more compact and comfortable with allocating more time better CAD design of enclosures. Lack of spare resulted in missed opportunities for SpO₂/HR data collection. A few lessons learnt were, validation should have been planned earlier, so any sensor or system failures identified would have enough time to replace hardware, rework and recollect data. Limit the scope changes midway through. Better risk planning and maintaining a spare set for critical hardware as a risk mitigation. This would have avoided the PPG data gap and enabled like-for-like replacement during the study.

Time managed well to finish most of the planned tasks, could be improved with implementing tasks in parallel. Regular meetings were helpful to establish weekly goals and progress, minutes were maintained to summarise the discussion, suggestions, and track action items. They were effective for documenting, communicating modifications and highlighting blockages and seek guidance.

Personal Reflection

This project felt truly problem-driven, the potential of making sleep apnoea screening more comfortable and accessible kept it motivating. The scope of this project also enabled me to draw on and integrate many modules of the year's learning. The IT Infrastructure module provided immediate insights on the wireless architecture, including access-point selection, DNS, networking, client-server communication, retries/ACKs. Learnings from temperature sensing methods, ADCs from Instrumentation module, State machines and de-bouncing from

HDL module, Digital signal-processing lectures and coursework on filtering, FIR/IIR filters paid off when constructing filters on a microcontroller, and while developing the respiration features (envelope, band-limits) that support the algorithms in this thesis.

The project also enabled a significant learning curve in system level thinking, approaching new libraries and its documentation, reading header files, handling conflicts between multiple libraries and programming with reusable functions and modules with configurable parameters, data visualisation in MATLAB. I also learnt the essentials of CAD to design and iterate the enclosures for 3D printing. Overall, the experience was beneficial as it produced a functioning prototype, identified clear areas for development, and taught me valuable lessons in planning, validation that I will use to future projects.

Reference List

- [1] D. Desai, A. Momin, P. Hirpara, H. Jha, R. Thaker, and J. Patel, “Exploring the Role of Circadian Rhythms in Sleep and Recovery: A Review Article,” *Cureus* (Palo Alto, CA), vol. 16, no. 6, pp. e61568-, 2024, Accessed: Apr. 30, 2025. [Online]. Available: doi: <http://dx.doi.org/10.7759/cureus.61568>
- [2] B. Lechat et al., “Multi-night measurement for diagnosis and simplified monitoring of obstructive sleep apnoea,” *Sleep medicine reviews*, vol. 72, pp. 101843–101843, 2023, Accessed: Apr. 30, 2025. [Online]. Available: <https://doi.org/10.1016/j.smrv.2023.101843>
- [3] A. V. Benjafield et al., “Estimation of the global prevalence and burden of obstructive sleep apnoea: a literature-based analysis,” *The Lancet Respiratory Medicine*, vol. 7, no. 8, pp. 687–698, 2019. Accessed: Apr. 30, 2025. [Online]. Available: [https://doi.org/10.1016/s2213-2600\(19\)30198-5](https://doi.org/10.1016/s2213-2600(19)30198-5)
- [4] Gerstenslager, B., & M. Slowik, J. (2025, January 1). Sleep study. PubMed. Accessed: Apr. 30, 2025. [Online]. Available: <https://pubmed.ncbi.nlm.nih.gov/33085294/>. PMID: 33085294.
- [5] L. C. Markun and A. Sampat, “Clinician-Focused Overview and Developments in Polysomnography,” *Current sleep medicine reports*, vol. 6, no. 4, pp. 309–321, 2020, Accessed: Apr. 30, 2025. [Online]. Available: <https://doi.org/10.1007/s40675-020-00197-5>
- [6] R. Skomro, M. Fenton, E. Penz, S. A. Stewart, and J. D. Leuppi, “Investigating Cost Implications of Incorporating Level III At-Home Testing into a Polysomnography Based Sleep Medicine Program Using Administrative Data,” *Canadian respiratory journal*, vol. 2017, no. 2017, pp. 1–7, 2017, Accessed: Apr. 30, 2025. [Online]. Available: <https://doi.org/10.1155/2017/8939461>
- [7] M. Braun, M. Stockhoff, M. Tijssen, S. Dietz-Terjung, S. Coughlin, and C. Schöbel, “A Systematic Review on the Technical Feasibility of Home-Polysomnography for Diagnosis of Sleep Disorders in Adults,” *Current sleep medicine reports*, vol. 10, no. 2, pp. 276–288, 2024, Accessed: Apr. 30, 2025. [Online]. Available: <https://doi.org/10.1007/s40675-024-00301-z>
- [8] M. T. Smith et al., “Use of Actigraphy for the Evaluation of Sleep Disorders and Circadian Rhythm Sleep-Wake Disorders: An American Academy of Sleep Medicine Systematic Review, Meta-Analysis, and GRADE Assessment.,” *Journal of clinical sleep medicine : JCSM: official publication of the American Academy of Sleep Medicine*, vol. 14, no. 7, pp. 1209–1230, Jul. 2018, Accessed: Apr. 30, 2025. [Online]. Available: <https://doi.org/10.5664/jcsm.7228>
- [9] E. D. Chinoy et al., “Performance of seven consumer sleep-tracking devices compared with polysomnography,” *Sleep (New York, N.Y.)*, vol. 44, no. 5, 2021, Accessed: Apr. 30, 2025. [Online]. Available: <https://doi.org/10.1093/sleep/zsaa291>.
- [10] M. de Zambotti, N. Cellini, L. Menghini, M. Sarlo, and F. C. Baker, “Sensors Capabilities, Performance, and Use of Consumer Sleep Technology,” *Sleep Medicine Clinics*, vol. 15, no. 1, pp. 1–30, Mar. 2020, Accessed: Apr. 30, 2025. [Online]. Available: <https://doi.org/10.3390/iot3020018>
- [11] Frost & Sullivan. (2016). Hidden health crisis costing America billions. In Frost & Sullivan. American Academy of Sleep Medicine. Retrieved April 29, 2025, from <https://aasm.org/resources/pdf/sleep-apnea-economic-crisis.pdf>
- [12] J. M. Marin, S. J. Carrizo, E. Vicente, and A. G. Agusti, “Long-term cardiovascular outcomes in men with obstructive sleep apnoea-hypopnoea with or without treatment with continuous positive airway pressure: an observational study,” *The Lancet (British edition)*,

- vol. 365, no. 9464, pp. 1046–1053, 2005, Accessed: Apr. 30, 2025. [Online]. Available: [https://doi.org/10.1016/S0140-6736\(05\)71141-7](https://doi.org/10.1016/S0140-6736(05)71141-7)
- [13] O. Bestsennyy, G. Gilbert, A. Harris, and J. Rost, “Telehealth: A quarter-trillion-dollar post-COVID-19 reality?,” McKinsey & Company, Jul. 09, 2021. Accessed: Apr. 30, 2025. [Online]. Available: <https://www.mckinsey.com/industries/healthcare/our-insights/telehealth-a-quarter-trillion-dollar-post-covid-19-reality>
- [14] M. H. Chyad, S. K. Gharghan, and H. Q. Hamood, “A Survey on Detection and Prediction Methods for Sleep Apnea,” IOP Conference Series: Materials Science and Engineering, vol. 745, no. 1, p. 012102, Mar. 2020, Accessed: Apr. 30, 2025. [Online]. Available: <https://doi.org/10.1088/1757-899X/745/1/012102>
- [15] S. Javaheri et al., “Sleep Apnea,” Journal of the American College of Cardiology, vol. 69, no. 7, pp. 841–858, Feb. 2017, Accessed: Apr. 30, 2025. [Online]. Available: <https://doi.org/10.1016/j.jacc.2016.11.069>
- [16] A. M. O’Mahony, J. F. Garvey, and W. T. McNicholas, “Technologic advances in the assessment and management of obstructive sleep apnoea beyond the apnoea-hypopnoea index: a narrative review.,” Journal of thoracic disease, vol. 12, no. 9, pp. 5020–5038, Sep. 2020, Accessed: Apr. 30, 2025. [Online]. Available: <https://doi.org/10.21037/jtd-sleep-2020-003>
- [17] L. S. Gaspar et al., “Peripheral biomarkers to diagnose obstructive sleep apnea in adults: A systematic review and meta-analysis.,” Sleep medicine reviews, vol. 64, p. 101659, Aug. 2022, Accessed: Apr. 30, 2025. [Online]. Available: <https://doi.org/10.1016/j.smrv.2022.101659>
- [18] M. H. Chyad, S. K. Gharghan, H. Q. Hamood, A. S. H. Altayyar, and S. L. Zubaidi, “A sleep apnea system based on heart rate and SpO₂ measurements: Performance validation,” 2023, p. 040001. Accessed: Apr. 30, 2025. [Online]. Available: <https://doi.org/nottingham.idm.oclc.org/10.1063/5.0157203>
- [19] A. Tiwari, M. K. Baghel, and V. Kumar, “A multimodal approach for sleep apnea detection: SpO₂ and force sensitive sensors in a flexible 3D-printed wearable.,” Mikrochimica acta, vol. 192, no. 3, p. 150, Feb. 2025, Accessed: Apr. 30, 2025. [Online]. Available: <https://doi.org/10.1007/s00604-025-07001-7>
- [20] R. . A. Alhamad, S. A. Mohammed, M. A. Abdullah, F. H. Mohammed, and T. Bonny, “Sleep Apnea Detecting and Monitoring System (SADMS),” in 2021 14th International Conference on Developments in eSystems Engineering (DeSE), IEEE, Dec. 2021, pp. 265–268. Accessed: Apr. 30, 2025. [Online]. Available: doi: 10.1109/DeSE54285.2021.9719432.
- [21] Ranjitha. Bs, “Non-invasive sleep apnea detection and monitoring system,” International Research Journal of Engineering and Technology, 2016, Accessed: Apr. 30, 2025. [Online]. Available: <https://www.irjet.net/archives/V3/i6/IRJET-V3I6225.pdf>
- [22] T. Sangeetha, D. Kumutha, M. D. Bharathi, and R. Surendran, “Smart mattress integrated with pressure sensor and IoT functions for sleep apnea detection,” Measurement: Sensors, vol. 24, p. 100450, Dec. 2022, Accessed: Apr. 30, 2025. [Online]. Available: doi: 10.1016/j.measen.2022.100450.
- [23] Y. J. Jeon, S. H. Park, and S. J. Kang, “Self-x based closed loop wearable IoT for real-time detection and resolution of sleep apnea,” Internet of Things, vol. 22, p. 100767, Jul. 2023, Accessed: Apr. 30, 2025. [Online]. Available: doi: 10.1016/j.iot.2023.100767.
- [24] A. H. Yüzer, H. Sümbül, and K. Polat, “A Novel Wearable Real-Time Sleep Apnea Detection System Based on the Acceleration Sensor,” IRBM, vol. 41, no. 1, pp. 39–47, Feb. 2020, Accessed: Apr. 30, 2025. [Online]. Available: doi: 10.1016/j.irbm.2019.10.007.
- [25] Apple Inc., “Estimating Breathing Disturbances and Sleep Apnea Risk from Apple Watch,” 2024. Accessed: Apr. 28, 2025. [Online]. Available:

- https://www.apple.com/health/pdf/sleep-apnea/Sleep_Apnea_Notifications_on_Apple_Watch_September_2024.pdf
- [26] A. Abd-Alrazaq et al., "Detection of Sleep Apnea Using Wearable AI: Systematic Review and Meta-Analysis," *Journal of medical Internet research*, vol. 26, no. 1, pp. e58187-, 2024, Accessed: Apr. 30, 2025. [Online]. Available: doi: 10.2196/58187.
- [27] S. Javaheri, D. M. Rapoport, and A. R. Schwartz, "Distinguishing central from obstructive hypopneas on a clinical polysomnogram," *Journal of clinical sleep medicine*, vol. 19, no. 4, pp. 823–834, 2023, doi: 10.5664/jcsm.10420. Accessed: Aug. 30, 2025. [Online].
- [28] Haddad, F.L.M., Bittencourt, L.R.A., Stefanini, R., Villaça, D.S., Togeiro, S.M.G.P. (2022). Obstructive Sleep Apnea: An Overview. In: Frange, C., Coelho, F.M.S. (eds) *Sleep Medicine and Physical Therapy*. Springer, Cham. https://doi.org/10.1007/978-3-030-85074-6_14 . Accessed: Aug. 30, 2025. [Online].
- [29] Sharma, S., Mishra, V.M. Development of Sleep Apnea Device by detection of blood pressure and heart rate measurement. *Int J Syst Assur Eng Manag* 12, 145–153 (2021). <https://doi.org/10.1007/s13198-020-01041-3> . Accessed: Aug. 30, 2025. [Online].
- [30] Berry RB, Brooks R, Gamaldo CE, et al. for the American Academy of Sleep Medicine. The AASM Manual for the Scoring of Sleep and Associated Events: Rules, Terminology and Technical Specifications. Darien, IL: American Academy of Sleep Medicine; 2017. Version 2.4. <https://pulmo-ua.com/wp-content/uploads/2021/12/AASM-sleep-scoring-2017.pdf>. Accessed: Aug. 30, 2025. [Online].
- [31] R. Farre, J. M. Montserrat, and D. Navajas, "Noninvasive monitoring of respiratory mechanics during sleep," *The European respiratory journal*, vol. 24, no. 6, pp. 1052–1060, 2004, doi: 10.1183/09031936.04.00072304. Accessed: Aug. 30, 2025. [Online].
- [32] Glos M, Sabil A, Jelavic KS, Schöbel C, Fietze I, Penzel T. Characterization of Respiratory Events in Obstructive Sleep Apnea Using Suprasternal Pressure Monitoring. *J Clin Sleep Med*. 2018 Mar 15;14(3):359-369. doi: 10.5664/jcsm.6978. PMID: 29458696; PMCID: PMC5837837. Accessed: Aug. 30, 2025. [Online].
- [33] A. Sabil, C. Marien, M. Levaillant, G. Baffet, N. Meslier, and F. Gagnadoux, "Diagnosis of sleep apnea without sensors on the patient's face," *Journal of clinical sleep medicine*, vol. 16, no. 7, pp. 1161–1169, 2020, doi: 10.5664/jcsm.8460. Accessed: Aug. 30, 2025. [Online].
- [34] S. Kontaxis, F. Kanellos, A. Ntanis, N. Kostikis, S. Konitsiotis, and G. Rigas, "An Inertial-Based Wearable System for Monitoring Vital Signs during Sleep," *Sensors (Basel, Switzerland)*, vol. 24, no. 13, Art. no. 4139, 2024, doi: 10.3390/s24134139. Accessed: Aug. 30, 2025. [Online].
- [35] Y. S. Bahgat, Y. M. Khalil, R. A. El Maghraby, E. El Sayed Mohamed, and M. M. A.-N. Elsayed, "The use of overnight pulse oximetry and phoniatrics parameters in the screening protocol of obstructive sleep apnea," *The Egyptian journal of chest diseases and tuberculosis*, vol. 61, no. 4, pp. 459–468, 2012, doi: 10.1016/j.ejcdt.2012.08.017. Accessed: Aug. 30, 2025. [Online].
- [36] Crivello, Antonino & Barsocchi, Paolo & Girolami, Michele. (2019). The Meaning of Sleep Quality: A Survey of Available Technologies. *IEEE Access*. PP. 10.1109/ACCESS.2019.2953835. Accessed: Aug. 30, 2025. [Online].
- [37] S. D. Clinic, "Sleep Study - Snoring&Sleep Apnoea - 2 night," Sleep Disorders Clinic. <https://thesleepdisordersclinic.com/collections/sleep-study/products/home-sleep-study-snoring-sleep-apnoea-2-night>. Accessed: Aug. 30, 2025. [Online].
- [38] InvenSense Inc., "MPU-6000 and MPU-6050 product specification," Aug. 2013. [Online]. Available: <https://invensense.tdk.com/wp-content/uploads/2015/02/MPU-6000-Datasheet1.pdf>. Accessed: Aug. 30, 2025. [Online].

- [39] Analog Devices, Inc., “Accelerometer and Gyroscopes Sensors: Operation, sensing, and applications,” Analog Devices, May 14, 2025. <https://www.analog.com/cn/resources/technical-articles/accelerometer-and-gyroscopes-sensors-operation-sensing-and-applications.html>. Accessed: Aug. 30, 2025. [Online].
- [40] Maxim Integrated, MAX30102 High-Sensitivity pulse oximeter and Heart-Rate sensor for wearable health. 2018. [Online]. Available: <https://www.analog.com/media/en/technical-documentation/data-sheets/max30102.pdf>. Accessed: Aug. 30, 2025. [Online].
- [41] Whaleteq (2025). A Comprehensive Guide to Conducting Accurate Tests for ECG, PPG, PWTT, and Respiration Rate | WhaleTeq. [online] WhaleTeq. Available at: https://www.whaleteq.com/data/download/files/whaleteq%20webinar_a%20comprehensive%20guide%20to%20conducting%20accurate%20tests%20for%20ecg,%20ppg,%20pwtt,%20and%20respiration%20rate_updated.pdf Accessed: Aug. 30, 2025. [Online].
- [42] RS. Thermistor ICs RS PRO Thermistor, 10k Ω Resistance, NTC Type, 2.4 x 63.5mm. [online] Available at: <https://docs.rs-online.com/fb5f/A700000010296043.pdf>. Accessed: Aug. 30, 2025. [Online].
- [43] Adafruit Industries. SPH0645LM4H-B Rev B Datasheet I2S Output Digital Microphone Typical Applications • Small portable devices: wearables • Set-top boxes: TV, gaming, remote controllers • Smart home devices, Internet of Things, Connected equipment. [online] Available at: <https://cdn-shop.adafruit.com/product-files/3421/i2S+Datasheet.PDF>. Accessed: Aug. 30, 2025. [Online].
- [44] Adafruit Industries. Adafruit I2S MEMS Microphone Breakout. [online] Available at: <https://cdn-learn.adafruit.com/downloads/pdf/adafruit-i2s-mems-microphone-breakout.pdf>. Accessed: Aug. 30, 2025. [Online].
- [45] DFRobot (2020). 1.54” IPS TFT LCD Display with MicroSD Card Breakout Wiki - DFRobot. [online] Dfrobot.com. Available at: https://wiki.dfrobot.com/1.54%20Inches%2020240_240_IPS_TFT_LCD_Display_with_MicroSD_Card_Breakout_SKU_DFR0649. Accessed: Aug. 30, 2025. [Online].
- [46] Adafruit Industries. Adafruit DS3231 Precision RTC Breakout [online] Available at: <https://cdn-learn.adafruit.com/downloads/pdf/adafruit-ds3231-precision-rtc-breakout.pdf>. Accessed: Aug. 30, 2025. [Online].
- [47] Maxim Integrated, “DS3231 Extremely accurate I2C-Integrated RTC/TCXO/Crystal.” [Online]. Available: <https://www.analog.com/media/en/technical-documentation/data-sheets/DS3231.pdf>. Accessed: Aug. 30, 2025. [Online].
- [48] Espressif, “ESP32-WROOM-32 Datasheet,” 2023. Available: https://www.espressif.com/sites/default/files/documentation/esp32-wroom-32_datasheet_en.pdf. Accessed: Aug. 30, 2025. [Online].
- [49] dfrobot.com, “FireBeetle 2 ESP32-E: Unleash IoT Potential with Dual-Core Power!,” dfrobot.com, Aug. 14, 2025. <https://www.dfrobot.com/product-2195.html>. Accessed: Aug. 30, 2025. [Online].
- [50] RS, “SKU:DFR0654 (<https://www.dfrobot.com/product-2195.html>).” Accessed: Sep. 01, 2025. [Online]. Available: <https://docs.rs-online.com/308c/A70000008916343.pdf>. Accessed: Aug. 30, 2025. [Online].
- [51] Espressif, “ESP32 Series Datasheet Including,” 2024. Available: https://www.espressif.com/sites/default/files/documentation/esp32_datasheet_en.pdf. Accessed: Aug. 30, 2025. [Online].
- [52] T. R, “Low-Pass Single-Pole IIR Filter | TomRoelandts.com,” [tomroelandts.com](https://tomroelandts.com/articles/low-pass-single-pole-iir-filter). <https://tomroelandts.com/articles/low-pass-single-pole-iir-filter>. Accessed: Aug. 30, 2025. [Online].

- [53] M. Varis, T. Karhu, T. Leppänen, and S. Nikkonen, "Utilizing envelope analysis of a nasal pressure signal for sleep apnea severity estimation," *Diagnostics*, vol. 13, no. 10, p. 1776, May 2023, doi: 10.3390/diagnostics13101776. Accessed: Aug. 30, 2025. [Online].
- [54] Drzazga, J., Cyganek, B. (2021). An LSTM Network for Apnea and Hypopnea Episodes Detection in Respiratory Signals. *Sensors*, 21(17), 5858. <https://doi.org/10.3390/s21175858>. Accessed: Aug. 30, 2025. [Online].
- [55] D. Khodadad et al., "Optimized breath detection algorithm in electrical impedance tomography," *Physiological measurement*, vol. 39, no. 9, Art. no. 094001, 2018, doi: 10.1088/1361-6579/aad7e6. Accessed: Aug. 30, 2025. [Online].
- [56] D. Belega and D. Petri, "Unbiased Sine-wave Frequency Estimation by Parabolic Interpolation of DTFT Samples," 2021 IEEE International Instrumentation and Measurement Technology Conference (I2MTC), Glasgow, United Kingdom, 2021, pp. 1-5, doi: 10.1109/I2MTC50364.2021.9459910. Accessed: Aug. 30, 2025. [Online].
- [57] Qualickuz Zanan NH, Azman M, Zainuddin K, Wan Puteh SE, Mohamed AS, Mat Baki M. Sound frequency spectra of snore in relation to the site of obstruction among snorers. *Acta Otorhinolaryngol Ital.* 2021 Aug;41(4):348-355. doi: 10.14639/0392-100X-N1202. PMID: 34533538; PMCID: PMC8448177. Accessed: Aug. 30, 2025. [Online].
- [58] R. Bailey, "Anatomical Position: Definitions and illustrations," ThoughtCo, May 28, 2024. <https://www.thoughtco.com/anatomical-position-definitions-illustrations-4175376>. Accessed: Aug. 30, 2025. [Online].
- [59] Thingiverse.com, "Pulse Oximeter Finger Clip (MAX30102 module) by mobi_electronik," Thingiverse, May 25, 2020. <https://www.thingiverse.com/thing:4395147/makes>. Accessed: Aug. 30, 2025. [Online].
- [60] Snoring Dataset: Mpwlolle, "Snoring wav," Kaggle, Aug. 21, 2023. <https://www.kaggle.com/code/mpwlolle/snoring-wav/input>. Accessed: Aug. 30, 2025. [Online].
- [61] Image credits, Wikipedia contributors, "Polysomnography," Wikipedia, Aug. 04, 2025. <https://en.wikipedia.org/wiki/Polysomnography>. Accessed: Aug. 30, 2025. [Online].
- [62] Image Credits, "Nomad: Portable Home Sleep Testing | Nihon Kohden." <https://us.nihonkohden.com/products/nomad/>. Accessed: Aug. 30, 2025. [Online].